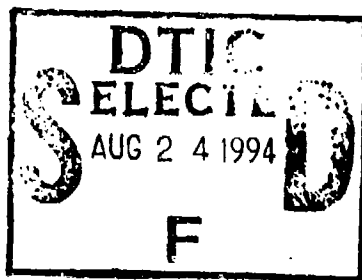


NAVAL POSTGRADUATE SCHOOL  
Monterey, California

AD-A283 610



THESIS

INTERMEDIATE DESIGN AND ANALYSIS OF  
THE PANSAT ELECTRICAL POWER SUBSYSTEM

by

Gregory F. Hand

March, 1994

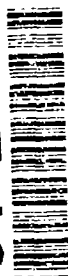
Thesis Advisor:

Robert Ashton

Approved for public release; distribution is unlimited.

DTIC QUALITY INSPECTED 1

94-26833



94 8 23 027

# REPORT DOCUMENTATION PAGE

Form Approved OMB No. 0704

Public reporting burden for this collection of information is estimated to average 1 hour per response, including the time for reviewing instruction, searching existing data sources, gathering and maintaining the data needed, and completing and reviewing the collection of information. Send comments regarding this burden estimate or any other aspect of this collection of information, including suggestions for reducing this burden, to Washington Headquarters Services, Directorate for Information Operations and Reports, 1215 Jefferson Davis Highway, Suite 1204, Arlington, VA 22202-4302, and to the Office of Management and Budget, Paperwork Reduction Project (0704-0188) Washington DC 20503.

1. AGENCY USE ONLY (Leave blank)		2. REPORT DATE March 1994	3. REPORT TYPE AND DATES COVERED Master's Thesis
4. TITLE AND SUBTITLE INTERMEDIATE DESIGN AND ANALYSIS OF THE PANSAT ELECTRICAL POWER SUBSYSTEM			5. FUNDING NUMBERS
6. AUTHOR(S) Gregory F. Hand			
7. PERFORMING ORGANIZATION NAME(S) AND ADDRESS(ES) Naval Postgraduate School Monterey CA 93943-5000			8. PERFORMING ORGANIZATION REPORT NUMBER
9. SPONSORING/MONITORING AGENCY NAME(S) AND ADDRESS(ES)			10. SPONSORING/MONITORING AGENCY REPORT NUMBER
11. SUPPLEMENTARY NOTES The views expressed in this thesis are those of the author and do not reflect the official policy or position of the Department of Defense or the U.S. Government.			
12a. DISTRIBUTION/AVAILABILITY STATEMENT Approved for public release; distribution is unlimited.			12b. DISTRIBUTION CODE A
13. ABSTRACT (maximum 200 words) This thesis examined three primary components of the electrical power subsystem (EPS) for the Petite Amateur Navy Satellite (PANSAT): (1) the solar array; (2) the power conditioning and control subsystem (PCCS); and (3) the batteries. The emphasis of this thesis was to analyze the output performance of the solar array. Additionally, the derivation of the hybrid PCCS proposed for the EPS was examined and the use of Nickel-Cadmium batteries as a candidate for the secondary power source was discussed. The investigation of the solar array's output performance led to PANSAM (PANSAT Solar Array Model), a computer model which simulates the power output of the solar array. The user can specify the sun's declination, the orbit's inclination, and the satellite's orientation and rate of rotation about each of its three axes. Once a simulation is complete, PANSAM provides the effective surface area illuminated by the sun, and the output current and power. The average effective area determined by PANSAM was 17.6% less than the 1259 cm <sup>2</sup> originally proposed by the PANSAT staff. This contributed to a substantial reduction in predicted power. A preliminary transient thermal analysis of PANSAT was also conducted to provide temperature data for PANSAM.			
14. SUBJECT TERMS PANSAT; Electrical Power System; Solar Array Output Performance Analysis; Power Conditioning and Control Subsystem			15. NUMBER OF PAGES 157
			16. PRICE CODE
17. SECURITY CLASSIFICATION OF REPORT Unclassified	18. SECURITY CLASSIFICATION OF THIS PAGE Unclassified	19. SECURITY CLASSIFICATION OF ABSTRACT Unclassified	20. LIMITATION OF ABSTRACT UL

NSN 7540-01-280-5500

Standard Form 298 (Rev. 2-89)

Prescribed by ANSI Std. Z39-18

Approved for public release; distribution is unlimited.

Intermediate Design and Analysis of  
the PANSAT Electrical Power Subsystem

by

Gregory F. Hand  
Lieutenant, United States Navy  
B.S., University of Florida

Submitted in partial fulfillment  
of the requirements for the degree of

MASTER OF SCIENCE IN ELECTRICAL ENGINEERING

from the

NAVAL POSTGRADUATE SCHOOL

March 1994

Author:

*Gregory F. Hand*  
\_\_\_\_\_  
Gregory F. Hand

Approved by:

*Robert W. Ashton*  
\_\_\_\_\_  
Robert Ashton, Thesis Advisor

*Sherif Michael*  
\_\_\_\_\_  
Sherif Michael, Second Reader

*Michael A. Morgan*  
\_\_\_\_\_  
Michael Morgan, Chairman  
Department of Electrical and Computer Engineering

Accession For	
NTIS CRA&I	<input checked="" type="checkbox"/>
DTIC TAB	<input type="checkbox"/>
Unannounced	<input type="checkbox"/>
Justification	
By	
Distribution /	
Availability Codes	
Dist	Avail and/or Special
A-1	

## ABSTRACT

This thesis examined three primary components of the electrical power subsystem (EPS) for the Petite Amateur Navy Satellite (PANSAT): (1) the solar array; (2) the power conditioning and control subsystem (PCCS); and (3) the batteries. The emphasis of this thesis was to analyze the output performance of the solar array. Additionally, the derivation of the hybrid PCCS proposed for the EPS was examined and the use of Nickel-Cadmium batteries as a candidate for the secondary power source was discussed. The investigation of the solar array's output performance led to PANSAM (PANSAT Solar Array Model), a computer model which simulates the power output of the solar array. The user can specify the sun's declination, the orbit's inclination, and the satellite's orientation and rate of rotation about each of its three axes. Once a simulation is complete, PANSAM provides the effective surface area illuminated by the sun, and the output current and power. The average effective area determined by PANSAM was 17.6% less than the 1259 cm<sup>2</sup> originally proposed by the PANSAT staff. This contributed to a substantial reduction in predicted power. A preliminary transient thermal analysis of PANSAT was also conducted to provide temperature data for PANSAM.

## TABLE OF CONTENTS

I.	INTRODUCTION . . . . .	1
A.	PURPOSE . . . . .	1
B.	PANSAT PROJECT DESCRIPTION . . . . .	2
1.	Mission Description . . . . .	2
a.	Store-and-Forward Communications . . . . .	3
b.	Spread Spectrum Modulation . . . . .	4
2.	Spacecraft Configuration . . . . .	6
a.	Overview . . . . .	6
b.	Communications Subsystem (CS) . . . . .	7
c.	Digital Control Subsystem (DCS) . . . . .	8
d.	Electrical Power Subsystem (EPS) . . . . .	9
II.	SOLAR ARRAY CHARACTERISTICS . . . . .	10
A.	INTRODUCTION . . . . .	10
B.	ELECTRICAL CHARACTERISTICS . . . . .	11
1.	I-V Curve . . . . .	11
2.	Effects of Light Intensity . . . . .	14
3.	Effects of Temperature . . . . .	18
4.	Effects of Radiation . . . . .	19
C.	GENERAL CONSTRUCTION . . . . .	22
1.	Solar Array Cells/Panels . . . . .	22
a.	Power Analysis . . . . .	22
b.	General Characteristics . . . . .	23

2.	Substrate . . . . .	25
3.	Coverglass . . . . .	25
4.	Adhesives . . . . .	26
a.	Coverglass to Solar Cell . . . . .	26
b.	Solar Cell to Substrate . . . . .	26
III.	EPS SOLAR ARRAY: PERFORMANCE ANALYSIS . . . . .	27
A.	INTRODUCTION . . . . .	27
B.	EFFECTIVE AREA OF PANSAT WITH RESPECT TO THE SUN .	28
1.	Frames of Reference . . . . .	28
2.	Orientation with Respect to the Sun . . . . .	32
3.	Computation of the Effective Area . . . . .	38
C.	THERMAL ANALYSIS OF PANSAT . . . . .	41
1.	Software Program Objective and Overview . . .	42
2.	Transient Thermal Analysis for PANSAT . . . .	43
D.	DETERMINATION OF THE SOLAR CELL AND ARRAY I-V	
	CURVES . . . . .	46
1.	Bare Cell Characteristics . . . . .	47
2.	Radiation Damage . . . . .	47
3.	Glassed Solar Cell I-V Curve . . . . .	48
4.	Effects of Intensity Change on Solar Cell I-V	
	Curve . . . . .	49
5.	Solar Cell I-V Curve at Operating	
	Temperature . . . . .	51
6.	Degraded Solar Cell I-V Curve . . . . .	53

a.	Assembly Factors . . . . .	53
b.	Ultraviolet and Micrometeorite Losses . .	54
7.	Total Change of the Solar Cell I-V Curve . . .	55
E.	DETERMINATION OF THE SOLAR ARRAY OUTPUT POWER . . .	56
1.	The Solar Cell Array Model . . . . .	57
2.	Development of the PANSAT Solar Array Model (PANSAM) . . . . .	59
3.	Investigation of the Worst Case . . . . .	66
IV.	POWER CONDITIONING and CONTROL SUBSYSTEM (PCCS) . . . .	73
A.	INTRODUCTION . . . . .	73
B.	POWER BUS . . . . .	74
1.	Regulation Topologies . . . . .	74
a.	Regulated Bus . . . . .	75
b.	Partially Regulated Bus . . . . .	76
c.	Unregulated Bus . . . . .	76
2.	Centralized Versus Decentralized . . . . .	78
C.	DESIGN CONSIDERATIONS FOR THE PANSAT PCCS . . . . .	78
1.	Overview . . . . .	78
2.	Dissipative and Nondissipative PCCSs . . . . .	79
a.	Dissipative PCCS . . . . .	79
b.	Nondissipative PCCS . . . . .	80
3.	Types of Regulators . . . . .	81
a.	Dissipative Regulators . . . . .	82
b.	Nondissipative Regulators . . . . .	84
4.	PCCS Topology Selection for PANSAT . . . . .	87

D.	DESCRIPTION OF OPERATION . . . . .	88
V.	BATTERIES . . . . .	92
A.	INTRODUCTION . . . . .	92
B.	SELECTION OF THE NICKEL-CADMIUM (Ni-Cd) BATTERY . .	93
C.	BATTERY CONCEPTS AND CONSTRUCTION . . . . .	94
1.	Primary vs Secondary . . . . .	95
2.	Nickel-Cadmium Battery Fundamentals . . . . .	95
3.	Capacity . . . . .	96
4.	Depth of Discharge (DOD) . . . . .	97
5.	Performance Characteristics . . . . .	97
a.	Energy Density . . . . .	98
b.	Discharge Properties . . . . .	98
c.	Charge Characteristics . . . . .	99
d.	Charge Retention . . . . .	100
e.	Life . . . . .	101
	(1) Temperature Effects . . . . .	101
	(2) Depth of Discharge Effects . . . . .	103
	(3) Effect of overcharge . . . . .	103
f.	Mechanical Stability . . . . .	104
VI.	RECOMMENDATIONS . . . . .	105
A.	SOLAR ARRAY . . . . .	105
B.	PCCS . . . . .	106
C.	BATTERY . . . . .	106
D.	CLOSING . . . . .	107



APPENDIX A - ORBIT PARAMETER CALCULATIONS . . . . .	109
A. ORBIT PERIOD CALCULATIONS . . . . .	109
B. FOOTPRINT CALCULATION . . . . .	110
1. Size of Footprint . . . . .	110
2. Time in Field of View of Satellite . . . . .	112
APPENDIX B - SOLAR ARRAY . . . . .	114
A. ANALYTICAL COMPUTER MODEL FOR I-V CURVE GENERATION . . . . .	114
B. SOFTWARE CODE FOR GENERATING I-V CURVES . . . . .	118
APPENDIX C - PANSAM AND RELATED PROGRAMS . . . . .	124
APPENDIX D - BATTERY DESIGN . . . . .	132
LIST OF REFERENCES . . . . .	140
INITIAL DISTRIBUTION LIST . . . . .	142

## ABBREVIATIONS

A	ampere
Ag	silver
Ah	ampere-hour
Al	aluminum
AM0	air mass zero
BCC	battery conditioning circuit
BCR	battery charge regulator
BDR	battery discharge regulator
BJT	bipolar junction transistor
BOL	beginning of life
BSR	back surface reflector
BSF	back surface field
C&DH	control and data handling
CAP	complex autonomous payload
cm	centimeter
CS	communication subsystem
DC	direct current
DCS	digital control subsystem
DOD	depth of discharge
EPS	electrical power subsystem
EOL	end of life
$F_A$	assembly factor (solar cell power output degradation)

$F_{TC}$	solar cell array power output degradation due to temperature cycling
GAS	get-away special
GFM	Government Furnished Material
in	inches
$I_{mp}$	maximum power point current
$I_{sc}$	short-circuit current
Kb	kilo-bytes
Kg	kilo-grams
Kbps	kilo-bytes per second
Km	kilometers
KW	kilo-watts
lbs	pounds
LEO	low earth orbit
mA	milliamp
mm	millimeters
MM	micrometeorites
MPP	maximum power point
mV	millivolt
Mb	mega-bytes
MOSFET	metal-oxide silicon field effect transistor
Ni-Cd	nickel cadmium
Ni-H <sub>2</sub>	nickel hydrogen
Ni-MH	nickel metal hydride

nmi	nautical miles
NPS	Naval Postgraduate School
P	power
PCB	primary control board
Pd	palladium
$P_{mp}$	maximum power point power
PANSAM	PANSAT Solar Array Model
PANSAT	Petite Amateur Navy Satellite
PCCS	power conditioning and control sub-system
PWM	pulse width modulated
S	solar constant (1353 W/m <sup>2</sup> )
S'	effective solar intensity
SCB	secondary control board
Si	silicon
SR	shunt regulator
SSAG	Space Systems Academic Group
SSCP	small self-contained payload
SSM	spread spectrum modulation
$T_0$	reference temperature
$T_{op}$	operating temperature
Ti	titanium
UV	ultraviolet
V	volts
Vdc	direct current voltage
$V_{mp}$	maximum power point voltage

$V_{oc}$	open-circuit voltage
W	watts
$\beta_i$	temperature coefficient for current
$\beta_v$	temperature coefficient for voltage
$\mu m$	micrometer
$\Omega$	ohm

### ACKNOWLEDGEMENTS

I would like to thank the following people for the assistance they provided:

- Professor Ashton, my advisor, for his time, patience, and valuable help.
- My CO, CDR Duym, who was always more than generous with his time and who made my last months in the Navy rewarding ones.
- My wife, Teri, whose love, support, encouragement, and understanding gave me light and hope in the darkest moments.
- Professor Kraus, for his gracious time, refreshing wit, and invaluable assistance on the thermal analysis portion of the thesis.
- My great family: Mom and Wayne; Dad and Peggy, Nanny and Grandaddy; Rick; Keith and Jule; Mark and Diane; and all the others, too numerous to mention. Thanks for all your support and encouragement from afar; rarely a phone call where it did not come up at least once.
- My great, new family: Mary Lou and Bill; Karyn and Jeff; Sharyn and Joey; Debi and Al; and Ed and Papa. Your support and encouragement were always appreciated.
- My bestman/roomie, Mark, who was always willing to listen to my complaining, go for a workout, and/or take a break at the Trident Club.

Thank you all.

## I. INTRODUCTION

### A. PURPOSE

The purpose of this thesis was to analyze and design the electrical power subsystem (EPS) for the Naval Postgraduate School's low earth orbit (LEO) Petite Amateur Navy Satellite (PANSAT) scheduled for launch in 1996. The battery selection and the power conditioning and control subsystem (PCCS) initially proposed in the preliminary design [Ref. 1] was changed. This thesis addresses these changes and scrutinizes the solar array power output initially suggested by the Space Systems Academic Group (SSAG).

This study continued to design a functional EPS capable of supplying necessary power requirements to the PANSAT subsystems. The EPS design and functionality depended heavily on power output capabilities of PANSAT's solar array. Therefore, this thesis places considerable emphasis on the solar array's performance analysis.

Some PANSAT subsystems are still in design, implementation, and/or testing phases. Consequently, not all power requirements are known or completely defined. Certain assumptions were made to allow the EPS implementation to progress. This study provided the foundation for the required follow-on work once power requirements of the PANSAT subsystems are defined. However, regardless of these power

requirements, the EPS must be constrained by the amount of power available from the solar array. Therefore, it was imperative to investigate the solar array output performance during a typical orbit and a worst case scenario.

## **B. PANSAT PROJECT DESCRIPTION**

The PANSAT project was proposed by the Naval Postgraduate School's Space System Academic Group (SSAG) to: (1) allow students an opportunity to obtain hands-on experience in a space systems design project; (2) provide a low earth orbit (LEO) SSM communications platform for the amateur radio community; (3) provide a space-based platform for conducting experiments; and (4) investigate the concept of LEO, store-and-forward digital communications for possible military application.

### **1. Mission Description**

Current plans call for the NASA space shuttle to act as the primary launch vehicle for PANSAT. PANSAT is configured as a complex autonomous payload (CAP) ejectable that will be carried aloft in a get-away special (GAS) canister located in the shuttle payload bay. A small self-contained payload (SSCP) ejection mechanism will inject PANSAT into its orbit.

PANSAT will be placed in a circular LEO, whose altitude can range from 250 to 350 nautical miles (nmi) (approximately 460 to 650 Km), with a possible inclination



ranging from 28° to 90°. Variations in altitude and inclination are dependent upon (a) the primary mission of the shuttle, and (b) whether an alternate launch vehicle, such as PEGASUS, is used. [Ref. 2] With PANSAT in a LEO of approximately 480 Km for a planned minimum 2 year mission life, it will act as a platform capable of providing store-and-forward digital communications for amateur radio users with SSM.

*a. Store-and-Forward Communications*

Using a single, high altitude, communication satellite, real-time communication between two ground stations is possible. This assumes satellite orbit parameters allow both ground stations to be within its footprint simultaneously. For a LEO satellite with an altitude of 480 Km, a calculation using liberal assumptions yields a footprint of 2590nmi (4790km) [Appendix A]. With this footprint, ground stations located on the U.S. east and west coasts would be unable to communicate with one another. For global coverage, this problem could be overcome by deploying a network of LEO satellites to relay digital communications. This method would be complex, expensive, and time consuming to implement. Another alternative, utilizing one LEO satellite, would be to incorporate a store-and-forward method for relaying digital signals. As illustrated in Figure 1, this method is accomplished by a user at one geographical location establishing a communication up-link with PANSAT while the

user is within its communication footprint. This user then transmits the desired data, which is received and stored in PANSAT's memory. Once PANSAT is in view of the user for whom the data is intended, at the second geographical location, PANSAT will establish a communication down-link with the second user, sending the data from its memory to the receiver.

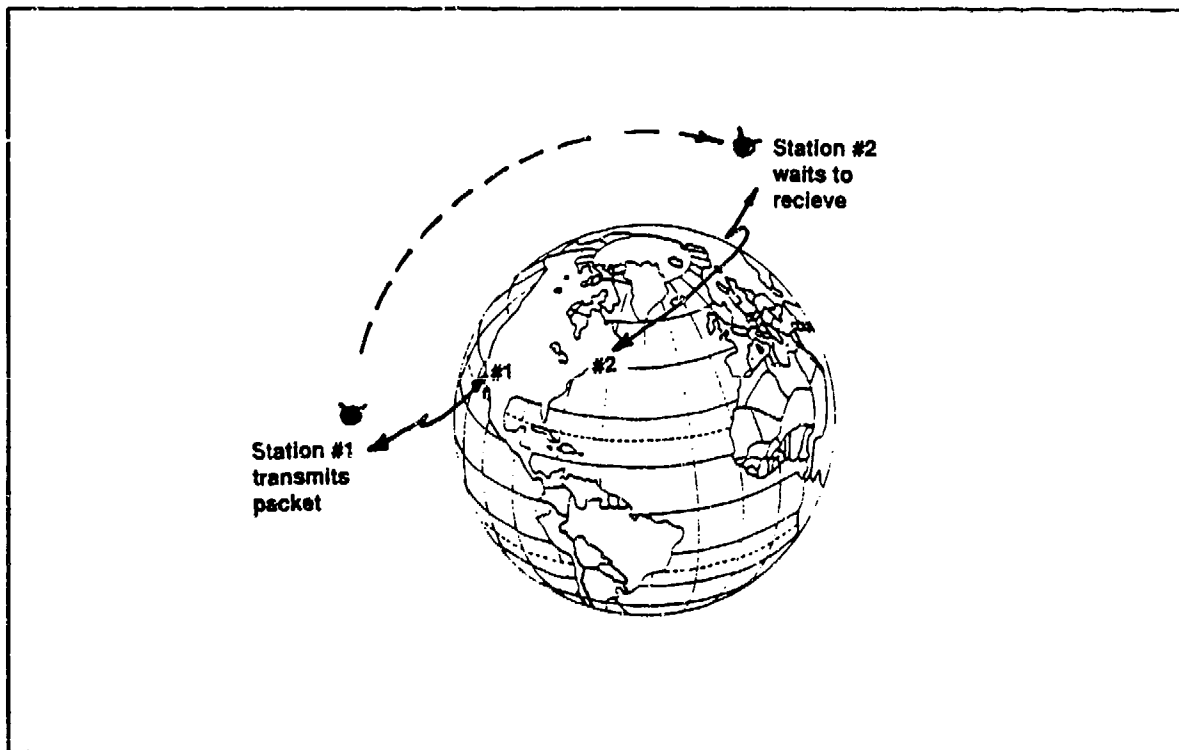


**Figure 1.** Illustration of the Concept of Store-and-Forward Satellite Communications

#### ***b. Spread Spectrum Modulation***

Spread-spectrum modulation is an attractive alternative to other modulation forms because it decreases the effects of interference without substantially increasing power needed for signal transmission. This includes intentional interference such as jamming. Additional benefits from using

SSM include:

- Low probability of intercept
- Multiple user random communications with selective addressing capability
- High resolution ranging
- Accurate universal timing

A minimum bandwidth is required to transmit information. SSM spreads information over a bandwidth greater than this minimum. Figure 2 depicts the contrast between the power spectrum of a typical narrowband waveform with the power spectrum of a spread waveform. Note that spread-spectrum is

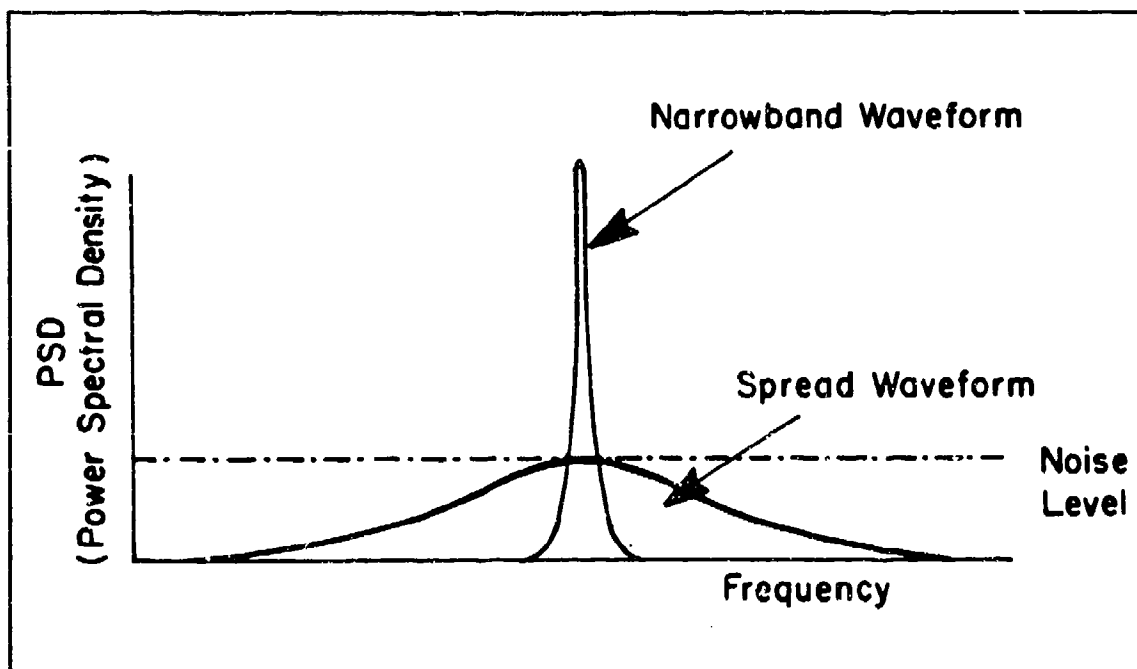


Figure 2. Power Spectral Density of a Typical Narrowband Waveform Compared to the Power Spectral Density of a Spread Waveform

capable of operating below the noise level. Spreading is performed by using a pseudo-random code, independent of the

data. Despreading and subsequent data recovery is achieved by incorporating synchronized reception with the code at the receiver.

Although SSM transmission utilizes a large frequency band, bandwidth cost is offset by reduced interference without an accompanying increase in power cost. This permits many users to share the same spectral band. [Ref. 3:p. 885]

A user on the earth's surface can view PANSAT for a maximum of approximately 11.3 minutes [Appendix A] if it passes directly overhead at an altitude of 480 Km. Due to this limited access time, the attributes associated with SSM are a great advantage to PANSAT. Also, the added immunity to interference does not increase the burden placed on PANSAT's electrical power subsystem (EPS).

## **2. Spacecraft Configuration**

### **a. Overview**

PANSAT is an octahedron structure, as shown in Figure 3, that fits within a spherical envelope of approximately 19 inches (48.26 cm). The satellite, constructed of aluminum, will weigh approximately 150 lbs (68.04 Kg). It is designed to be an autonomous spacecraft requiring no commands from the supervisory ground station at the NPS in order to function properly. PANSAT will be a tumbling satellite because it contains neither a propulsion system nor active attitude stabilization control.

PANSAT is an octahedron structure having 18 square panels externally. Seventeen are solar cell panels which

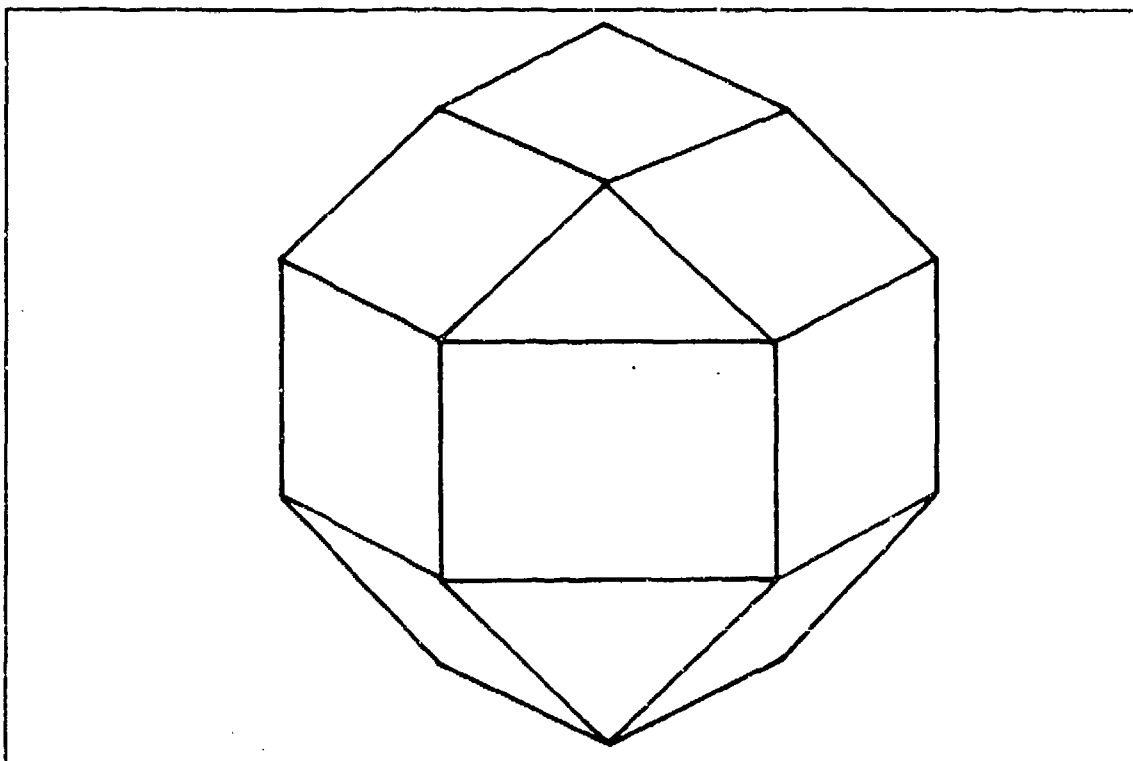


Figure 3. An External View of PANSAT Illustrating Its Octahedron Shape

comprise the solar array. The remaining panel is the base plate for mounting PANSAT to the SSCP ejection mechanism. Also, there are four dipole antennas in a tangential turnstile configuration. Internally, PANSAT consists primarily of three subsystems: communications, digital control, and electrical power. Accommodations can be made to include experiments, however none have been established as of yet. [Ref. 2]

*b. Communications Subsystem (CS)*

Since PANSAT will be a tumbling satellite, the communications payload must operate at any attitude. The CS

will consist of a transmitter and receiver utilizing direct sequence spread spectrum binary-phase-shift-keying (BPSK) modulation. Operating at a center frequency of 436.5 MHz, the PANSAT CS will have a 3 MHz bandwidth, and a data rate of 9.84 Kbps. Additionally, the CS will have a data storage capacity of approximately 4 Mb. [Ref. 2]

The CS is still in the design phase, therefore, a reliable value for the power consumption has not been established. However, based on the preliminary design, the continuous power usage per cycle (orbit) is predicted to be approximately 7 W.

#### *c. Digital Control Subsystem (DCS)*

The DCS is comprised of a primary and secondary control board (PCB and SCB). With respect to their composition and operations these control boards are practically identical. If the SCB suspects a failure of the PCB a control board switching procedure is invoked .

The design requirements for the control boards call for a multitasking environment capable of:

- Monitoring telemetry
- Transmitting messages to ground stations
- Receive, store, and forward mail from ground stations
- Receive commands from master ground station and respond in a predetermined manner
- Provide real time response to telemetry inputs associated with the electrical power subsystem
- Perform any tasks associated with on-board experiments.

The DCS design is currently based on a 10 MHz Intel® M80C186, 16-bit microprocessor. The memory section of the DCS is comprised of 256 Kb of switchable read only memory (ROM), 640 Kb of switchable system random access memory (RAM), and 4.0 Mb of user RAM. Additionally, the DCS will utilize analog to digital (A/D) control, a real-time clock, and digital I/O.

*d. Electrical Power Subsystem (EPS)*

PANSAT's EPS must supply adequate power to the CS, DCS, any experiments requiring power, and to itself. The EPS must also interact with the DCS by providing telemetry data that the DCS will use to establish control parameters for the subsystems of the EPS.

The remainder of this paper focuses on concepts and various options upon which the design of the PANSAT EPS is based. This study addresses the solar array with emphasis placed on analysis of its output performance. Next, there will be an investigation of battery types and requirements. Finally, this thesis discusses the power control and conditioning unit (PCCS).

## II. SOLAR ARRAY CHARACTERISTICS

### A. INTRODUCTION

General requirements of the solar array state that it shall be capable of providing 21.5 W of electrical power, at 15.2 Vdc, at a temperature of 28°C, after two years in a circular orbit. It will have an altitude of approximately 430 nmi (800 Km), and an inclination of 0°. [Ref 4:p. 2]

The solar array is comprised of 17 panels, each containing 32 series connected solar cells, for a total of 544 cells. Each cell is an n/p type, K6700, silicon solar cell with the dimensions: 1.92 cm x 4.0 cm x 0.02 cm. The contract for the construction of PANSAT's solar array panels was awarded to Spectrolab, Inc. Their power analysis indicates that each solar cell will provide 459 mV and 282 mA at summer solstice, at 28°C, after two years in orbit [Ref. 5:p. 10]. With the information provided by the SSAG, the contractor estimated an average effective area of 1209 cm<sup>2</sup>. Using this value, the contractor calculated the solar array should supply approximately 21.67 W and 15.27 V at EOL [Ref. 5:p. 10]; which will meet the general requirements stated above. Additionally, each panel is isolated from the bus with a steering diode. The steering diodes prevent current from illuminated panels from entering the circuitry of non-illuminated panels.

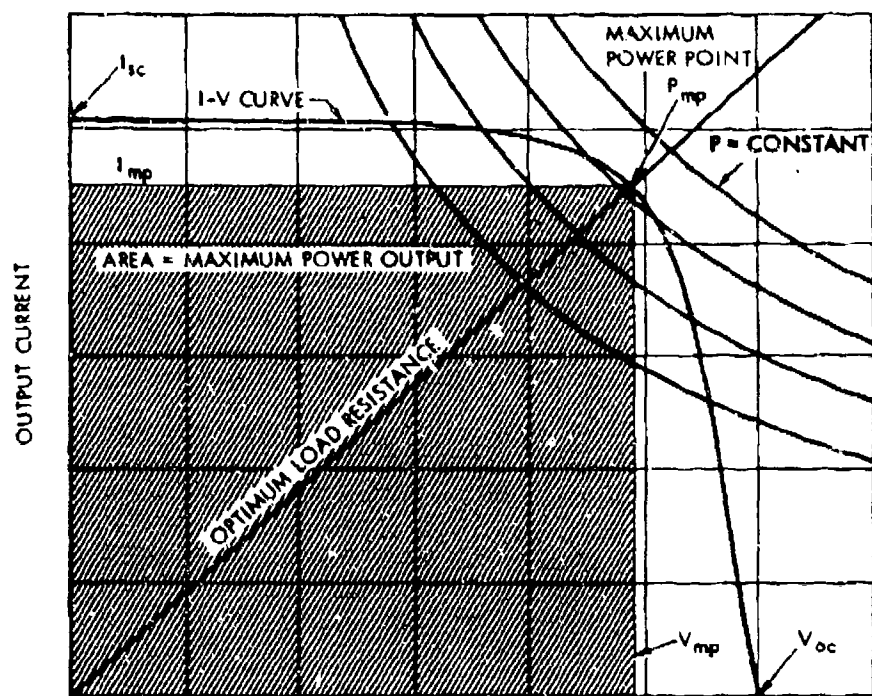


## B. ELECTRICAL CHARACTERISTICS

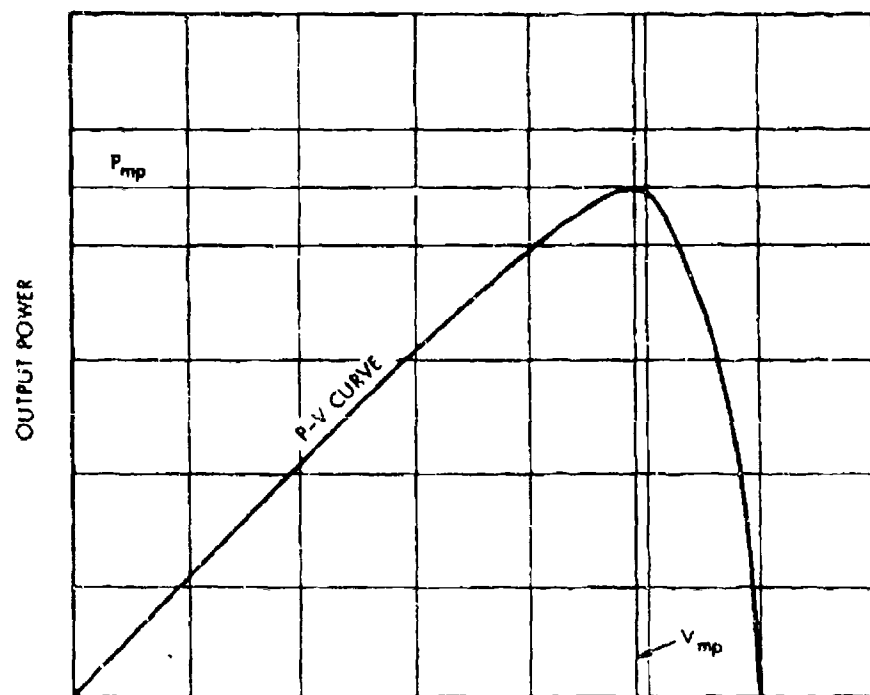
### 1. I-V Curve

The most complete description of electrical characteristics of a solar cell is given by its current-voltage characteristics. These current-voltage characteristics are commonly referred to and best illustrated by the I-V curve, shown in Figure 4 [Ref. 6:p. 3.2-1]. Any point on the curve has a corresponding current ( $I$ ) and voltage ( $V$ ) associated with it. A rectangle is created by projecting one vertical and one horizontal line from the selected point on the curve to the V-axis and I-axis, respectfully. The area of this rectangle equates to the power identified with this point. The rectangle with the largest possible area equates to the maximum (or optimum) power point,  $P_{mp}$ . In addition to  $P_{mp}$ , there are two other points of significance located on the I-V curve. They are the short-circuit current,  $I_{sc}$  (cell terminal voltage is zero), and the open-circuit voltage,  $V_{oc}$  (cell terminal current is zero). [Ref. 6:p. 3.2-1]

In conjunction with the  $P_{mp}$ , there exists a maximum power current,  $I_{mp}$ , and a maximum power voltage,  $V_{mp}$ . Typically, the values for  $P_{mp}$ ,  $I_{mp}$ , and  $V_{mp}$  are determined from experimentally obtained I-V curves. Upon inspection of Figure 4a, one can see the point of tangency of the I-V curve and a constant power curve is not sharply defined. It is helpful to construct a P-V curve, as shown in Figure 4b, to assist in defining the  $P_{mp}$  point more accurately.



(a)



(b)

**Figure 4.** Solar Cell Electrical Output Characteristics; (a) I-V Curve, and (b) P-V Curve [Ref. 6:p. 3.2-1]

The  $I$ - $V$  curve also extends into the third and fourth quadrants as shown in Figure 5. However, it is common practice to consider the  $I$ - $V$  curve in the first quadrant primarily; this contains the operating information of greatest interest.

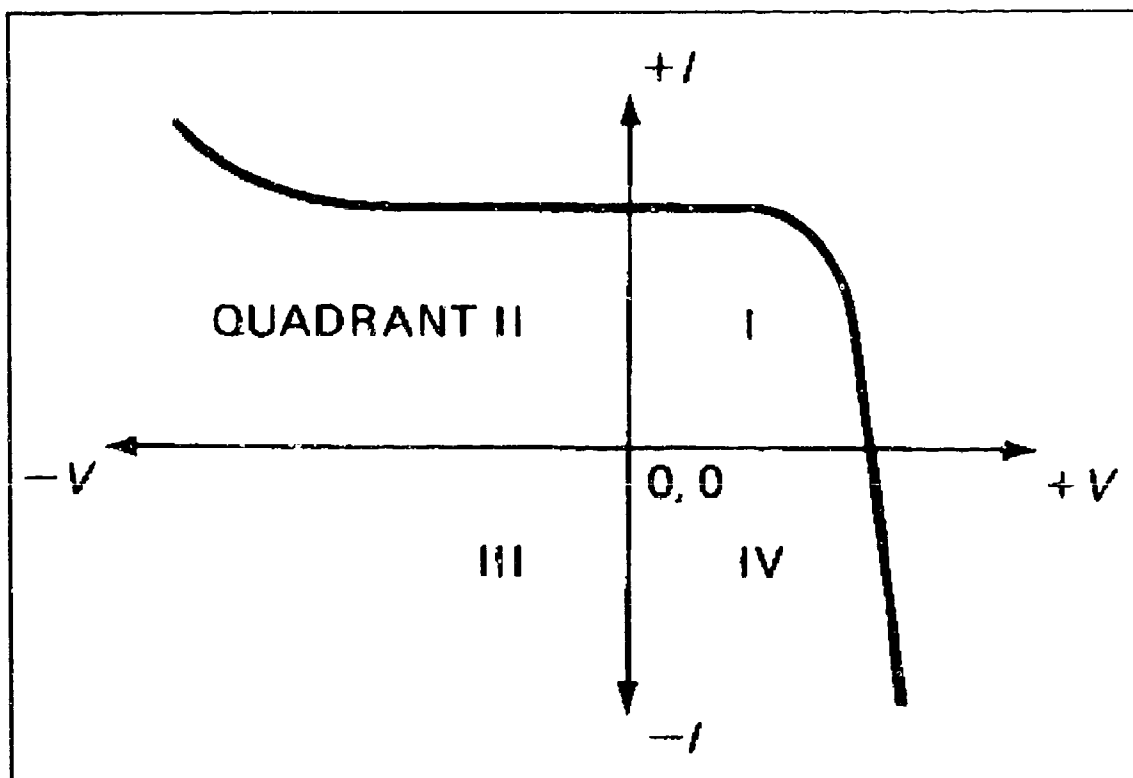


Figure 5.  $I$ - $V$  Curve in 3 Quadrants [Ref. 7:p. 168]

Quadrant II of Figure 5 represents the *reverse bias* region of the  $I$ - $V$  curve. It is evident that negative cell voltages occur in this quadrant, and that power is dissipated within the cell. [Ref. 7:p. 77] This can result in a non-illuminated or partially illuminated string of series connected solar cells draining current from the illuminated strings. A blocking, or isolation diode inserted between each solar cell string and the power bus prevents this from

occurring. The diode will conduct current from the illuminated solar cells to the bus, yet block current flow from the bus into the solar cells in the event that the string output voltage falls below the bus voltage. [Ref. 7:p. 297]

A typical I-V curve and P-V curve for the K6700 BFR product is shown in Figure 6. The values used to generate this curve were provided by the contractor. These values, and the equations used to generate the graph, are given in Appendix B. The I-V curve shown in Figure 6 is generated assuming constant temperature and illumination. Standard test conditions for generating I-V curves for solar cells to be used in a space application are typically:

- A 25°C or 28°C cell temperature
- Light intensity of one solar constant (135.3 mW/cm<sup>2</sup>)
- Light spectrum of air mass zero (AM0: the absence of any atmospheric attenuation of the light spectrum [Ref. 6:p. 2.4-6]).

[Ref. 7:p. 388]

The effects associated with changing the temperature and light intensity are discussed in the following sections.

## **2. Effects of Light Intensity**

The sunlight intensity is technically known as the *radiant solar energy flux density*, and is measured in units of watts per square meter (W/m<sup>2</sup>). With regard to PANSAT, the major concerns associated with sunlight intensity directly incident on the solar cells depend upon the following:

- Angle of incidence (i.e., the angle between the normal to the solar array and a light ray from the sun).
- Solar distance (i.e., the distance of the array from the sun)
- Light transmission losses in coverglasses, cover adhesive, and other optical elements.

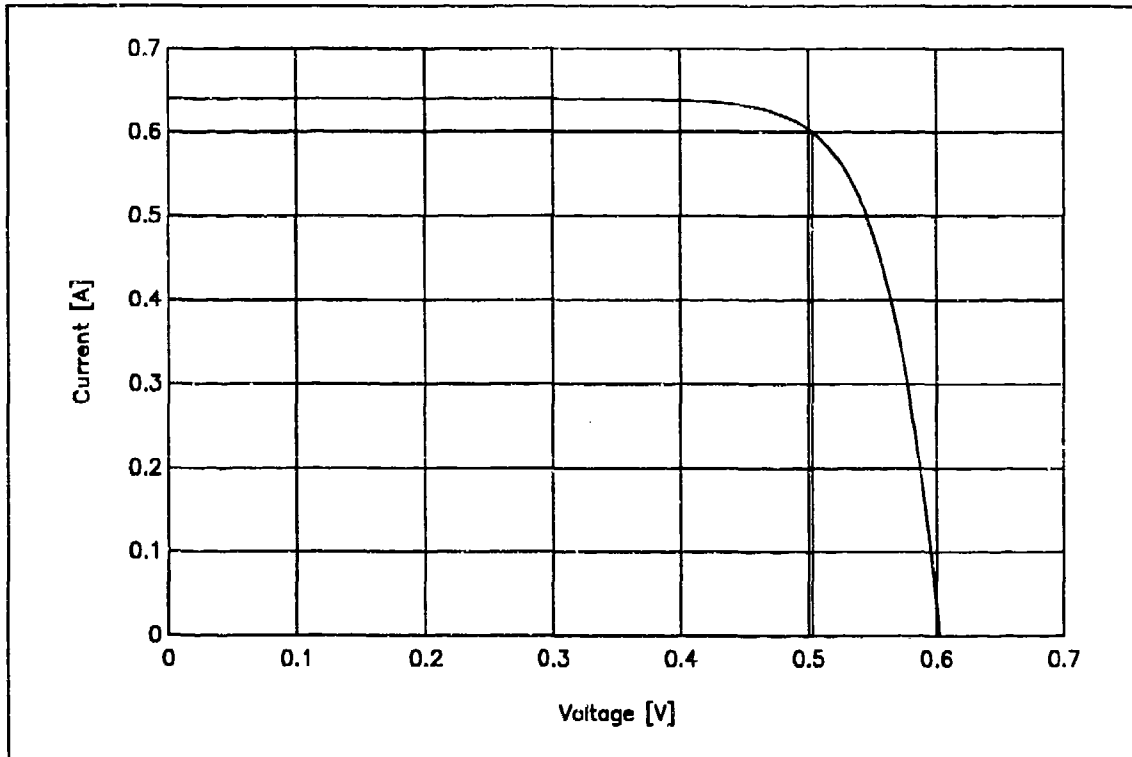


**Figure 6.** The I-V Curve of the K6700 Silicon Solar Cell Used for the Solar Panels of PANSAT. The Associated Equation and Parameters Used to Generate the Curve in are Appendix B.

The output characteristics of the solar cell changes with respect to change in the illumination intensity incident on the solar cell (assuming certain parameters, such as cell temperature and spectral distribution of the light, are held constant). This is evident in Figure 7 which indicates that

the  $I$ - $V$  curve shifts toward lower current and toward higher voltage values as the intensity decreases. [Ref. 7:p. 172]

The energy per unit area from the sun at the fringes of the earth's atmosphere is  $1353 \text{ W/m}^2$  and is defined as one solar constant,  $S$  [Ref. 6:p. 2.4-2]. For solar cells designed to operate at approximately one solar constant intensity, the shape of the  $I$ - $V$  curve is essentially invariant with intensity, over the range from approximately 0.5 to 2 solar constants [Ref. 7 :p. 172]. Therefore, the solar distance for a near-earth space array, such as PANSAT's, may be considered constant. As a result, the greatest change in sunlight intensity will occur because of change in the effective area of the solar array due to spacecraft orientation; and, while entering and exiting eclipse.

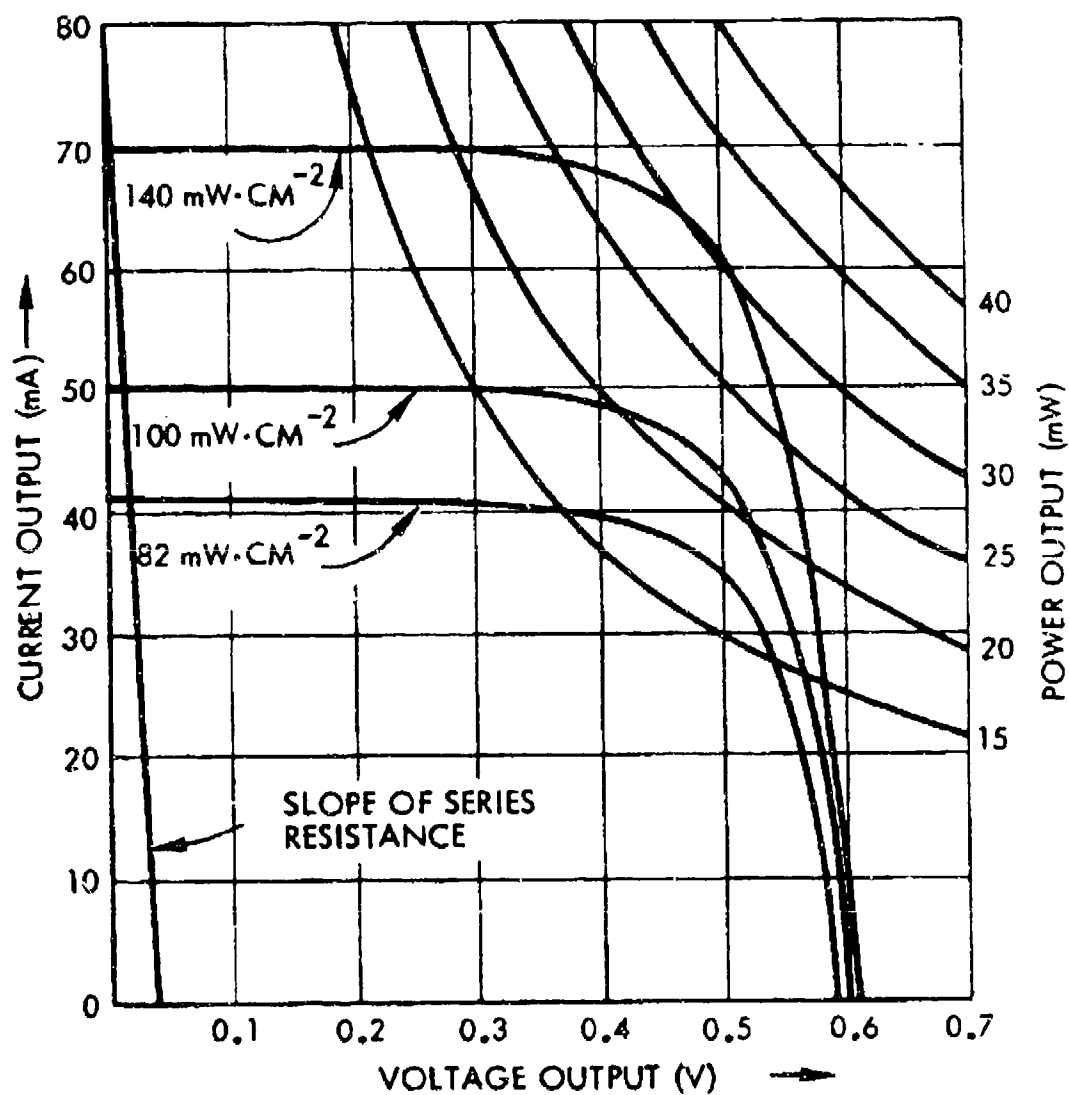


**Figure 7.** Typical I-V Curve at Three Different Illumination Levels (Constant Spectral Distribution and Temperature)  
[Ref. 6:p. 3.5-1]

### 3. Effects of Temperature

Varying the temperature of a solar cell causes three changes in the  $I$ - $V$  curve of the cell:

- Scaling of the  $I$ - $V$  curve along the current axis
- Translation (shifting) of the  $I$ - $V$  curve along the voltage axis
- Change in the shape of the  $I$ - $V$  curve which affects the "roundness" of the "knee" region of the  $I$ - $V$  curve.

[Ref. 7 :p. 173]

The first two changes listed above are evident in Figure 8. There is an increase in the solar cell operating temperature, producing a slight increase in the short-circuit current of the solar cell, and significantly decreasing the solar cell voltage. [Ref. 7 :p. 173] The temperature coefficient for the current is typically less than  $0.03\%/^{\circ}\text{C}$ , and is dependent on the cell thickness, junction depth, antireflective coating, and state of radiation. The temperature coefficient for voltage is negative, and is typically  $2.2$  to  $2.3$   $\text{mV}/^{\circ}\text{C}$ . The voltage coefficient is essentially independent of radiation damage. [Ref. 8 :p. 339]

Precise analytical thermal cycles cannot be predicted because of the tumbling nature of PANSAT. However, the environmental requirements call for compliance with a thermal cycling within the range of  $-65^{\circ}\text{C}$  to  $140^{\circ}\text{C}$  over a six hour duration [Ref. 4 :p. 10].



#### 4. Effects of Radiation

During the mission life of a satellite, radiation found in the space environment degrades the performance of a solar array. Materials comprising a solar array are subject

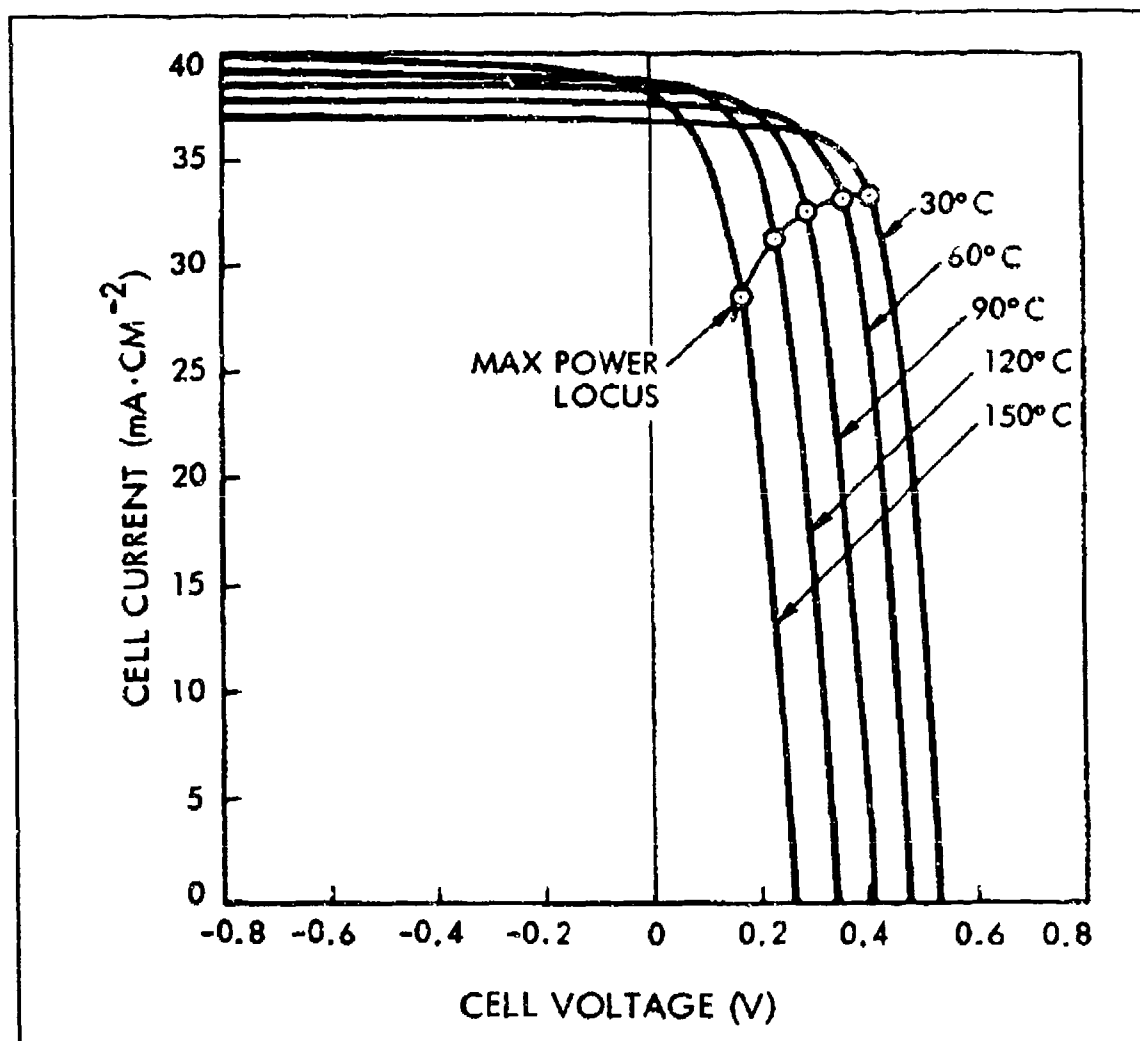


**Figure 8.** Current-Voltage Characteristics for Varying Temperature at One Solar Constant Intensity [Ref. 6 :p. 3.5-2]

to permanent mechanical damage at the atomic level because of irradiation by energetic or fast massive particles such as: electrons, protons, neutrons, or ions. These particles can

interact with the materials in several ways. The most dominant interactions are (1) elastic and inelastic collisions with atomic nuclei and (2) inelastic collisions with atomic electrons. [Ref. 9 :p. 3-1] Degradation is found in the short-circuit current output, the open-circuit voltage output, the maximum power output, the energy conversion efficiency, and the spectral response. Changes in other parameters are found to affect the temperature coefficients and the shape of the  $I$ - $V$  curve. Figure 9 illustrates the effect of exposure of a typical solar cell  $I$ - $V$  curve to a heavy dose (approximately  $10^{15}$  e/cm<sup>2</sup>) of 1-MeV electrons. Additionally, Figure 9 shows increases in temperature coefficients for  $I_{sc}$  and no change in the temperature coefficients for  $V_{oc}$  and  $V_{mp}$ . [Ref. 6 :p. 3.3-1]

Irradiation by electrons and protons is the primary contributor to the reduction in the energy conversion efficiency of the solar cells. In LEO both geomagnetically trapped electrons and protons are responsible [Ref. 6 :p. 2.5-5]. Due to the variety of proton and electron energies present in the space environment, a method was devised to convert the various types of radiation into a standard measure. To realize this standard, the concept of normally incident damage equivalent 1-MeV fluence (fluence is the integrated flux, or total number of particles per area in a given time period) was developed. Equivalent damage

coefficients are used to make the conversion. The unit of

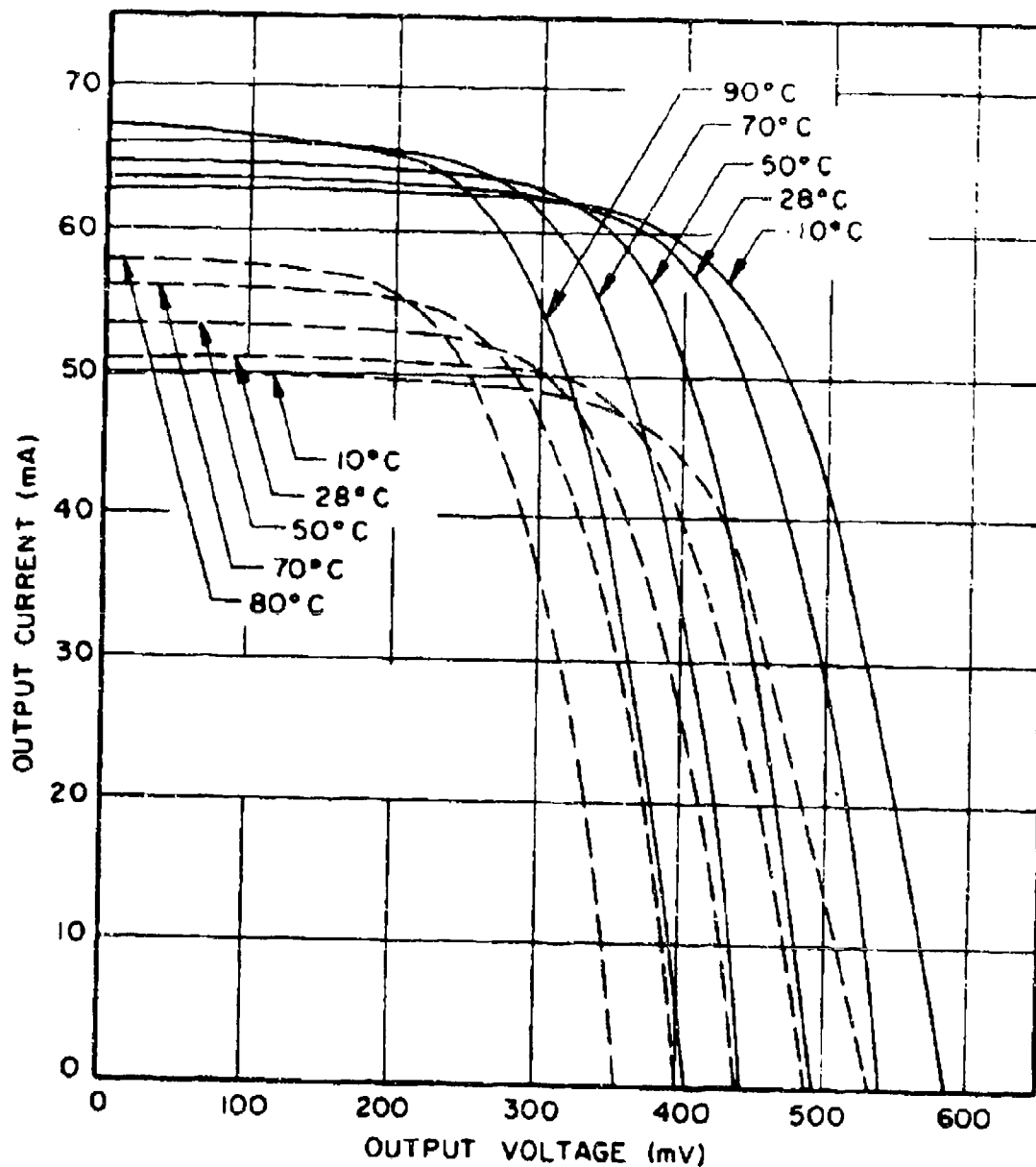


**Figure 9.** Variations of Solar Cell I-V Curves with Temperature Before (Solid Lines) & After (Dashed Lines) Irradiation [Ref. 6 :p. 3.3-2]

equivalent fluence is 1-MeV electrons per  $\text{cm}^2$  ( $\text{e}/\text{cm}^2$ ) for a specified period of time, usually one year or EOL. [Ref. 6:p. 2.5-2]

### **C. GENERAL CONSTRUCTION**

The solar array design is complete and Spectrolab, Inc. has been selected as the contractor. Therefore, the following describes the construction and parameters of the solar array.

#### **1. Solar Array Cells/Panels**

##### **a. Power Analysis**

A dynamic analysis program, provided by the NPS SSAG, was used to determine the average effective surface area of PANSAT as  $1259 \text{ cm}^2$ . The average effective area of  $1259 \text{ cm}^2$  for the solar array of PANSAT was based on the assumption that the cell dimensions would be  $2.0 \text{ cm} \times 4.0 \text{ cm}$ . [Ref. 4:p. 2] However, to meet the size requirements of the panels, the contractor was compelled to trim the width of the cells from  $2.0 \text{ cm}$  to  $1.92 \text{ cm}$ . The 4% reduction in cell size was extrapolated to support the assumption of a 4% reduction in the average effective area of PANSAT. Therefore, the average available area for power output was reduced to  $1209 \text{ cm}^2$ . [Ref. 10:p. 2] The contractor provided the values in Table I below as a summary of the power analysis for the proposed cells [Ref. 10:p. 2]. Finally, the power analysis of the contractor affirms that the array performance is  $23.4 \text{ W}$  at  $15.82 \text{ V}$  at BOL, and  $21.67 \text{ W}$  at  $15.27 \text{ V}$  at EOL; thus meeting the NPS requirements of  $21.6 \text{ W}$  at  $15.2 \text{ V}$  [Ref. 5:p. 10].

### b. General Characteristics

The solar cells shall be n/p, single crystal, K6700, silicon solar cells. Each solar cell shall have the dimensions of 1.92 cm in width, 4.0 cm in length, and 0.020 cm in thickness. They shall have a nominal base resistivity of 10 ohm-cm. The back surface reflector (BSR) of the solar cells shall consist of a highly reflective metal surface between the solar cell wafer back and the back side contact.

**Table I. POWER ANALYSIS FOR THE K6700 SOLAR CELL WITH THE DIMENSIONS OF 1.92 CM X 4.00 CM**

Description	Loss Factors		Output	
	V	I	V <sub>mp</sub> [mV]	I <sub>mp</sub> [mA]
Bare Cell	-	-	500.00	307.00
Assembly	-5 mV	x 0.99	495.00	303.93
Filtering	-	x 0.99	495.00	300.89
UV & MM	-	x 0.98	495.00	294.87
Radiation	x 0.965	x 0.978	477.68	288.38

This metal surface shall be titanium-palladium-silver (Ti-Pd-Ag) overlaid on aluminum. A back surface field (BSF) will be produced by doping the underside of the back of the cell to create a p+ field. A shallow diffused junction with a nominal junction depth of 0.12  $\mu\text{m}$  shall be place within the cell. The collector grids for the cell shall be optimized. The grids shall be constructed of Ti-Pd-Ag; and shall be vacuum metallized and sintered. [Ref. 4:p. 4]

Solar cell contacts are metallizations on the solar cell p- and n-type semiconductor surfaces which allow the making of low-resistance electrical connections to the cell [Ref. 7:p. 187]. The contacts on the n-type surface shall be along the length dimension of the solar cell. The "n" contact shall be sintered (sintering or annealing is a method for increasing solar efficiency in polycrystalline thin-film cells [Ref. 11:pp. 334 & 357]), Ti-Pd-Ag metallized, and optimized for current collection and weight.

The contact on the p-type side of the cell shall cover at least 90% of the inactive solar cell surface. The "p" contact shall be sintered and Ti-Pd-Ag metallized [Ref. 4:pp. 4-5].

The contact strength is the ability of metallizations to adhere to the solar cell semiconductor material [Ref. 7:p.189]. To determine the contact bond integrity, the contractor shall perform a peel strength test for the "n" and "p" contacts of the solar cell [Ref. 4:p. 5].

Bare Si has a reflection coefficient that ranges between approximately 33% and 54% over the desired spectral range of 0.35  $\mu\text{m}$  to 1.1  $\mu\text{m}$ . Therefore, to increase the efficiency of the cell, an antireflection coating (ARC) is applied [Ref. 11:pp. 271-272]. The active surface of the solar cells for PANSAT shall be treated with an  $\text{Al}_2\text{O}_3$ -Ti<sub>2</sub> dual ARC [Ref. 4:p. 5].

## **2. Substrate**

Solar cells are held mechanically in place on a typically flat plate-like support known as the substrate [Ref. 7:p. 3]. Back shielding is also provided by the substrate. The substrate will be furnished to the contractor by NPS as Government Furnished Material (GFM). NPS shall design the substrate to withstand thermal and dynamic environments of the specifications. The substrates will be aluminum 6061-T6 plates of nominal dimensions 18.098 cm x 18.098 cm square with thickness of 1.27 cm, 0.635 cm, and 0.159 cm.

Electrical isolation of the substrate will be provided by 0.0508 mm thick Kapton which will be adhered to the substrate with RTV 566 adhesive [Ref. 4:pp. 2-3]. The substrate will be al dined.

## **3. Coverglass**

Coverglass acts as a front shield for the solar cells. They are coated, transparent plates of inorganic material with approximately the same dimensions as the solar cells [Ref. 6:p. 4.4-1]. Covers provide temperature control, and protection against degradation from charged particle radiation and micrometeoroid erosion [Ref. 7:p. 243].

The coverglass selected for PANSAT shall be produced from Corning Glass 7940 fused silica. Its dimensions shall be flush with or extend past the edges of the cells with a nominal thickness of 0.030 inches. The exposed surface of the coverglass shall be treated with an ARC of magnesium fluoride

(MgF<sub>2</sub>). The ultra-violet rejection shall be greater than 80% at 0.300  $\mu\text{m}$   $\pm$  0.020  $\mu\text{m}$ . [Ref. 4:p. 6]

#### **4. Adhesives**

##### **a. Coverglass to Solar Cell**

The coverglass shall be bonded to the cell with Dow Corning 93-500; a resilient, transparent adhesive. Voids and/or air pockets with diameters in excess of 0.050 inches (1.27 mm) within the adhesive, will not be tolerated. Voids less than 0.005 inches (0.127 mm) in diameter are acceptable. There shall be no more than five voids per assembly with a diameter between 0.005 (0.127 mm) and 0.050 inches (1.27 mm). [Ref. 4:p. 6]

##### **b. Solar Cell to Substrate**

The solar cells shall be bonded to the insulated substrate with Dow Corning 93-500. The adhesive shall be of minimum thickness to obtain a good bond for the array application, and shall show no flow out into the cell interconnect stress relief loops. [Ref. 4:p. 7]



### III. EPS SOLAR ARRAY: PERFORMANCE ANALYSIS

#### A. INTRODUCTION

To ensure the EPS has the ability to provide adequate power to the PANSAT subsystems, the electrical characteristics of the solar array must be understood. The EPS must be capable of coping with any fluctuations in the solar array power output, so these possibilities must be investigated. Excessive power on the bus could cause damage to the EPS. In contrast, insufficient power on the bus could place constraints on the proposed normal operation of PANSAT. As a result, an attempt must be made to predict the maximum and minimum power output of the solar array to safeguard against unexpected contingencies.

The solar cell array electrical performance is described as the electrical power output capability of the array under specified operating conditions, and following some specified environmental exposure [Ref. 6:p. 9.4-1]. A variety of factors must be considered when modeling the power output of a solar array. These factors include the number of cells illuminated, which depends directly upon:

- The orientation of the satellite with respect to the sun
- The operating temperature of the solar array
- Degradation of the cells performance due to assembly and exposure to the space environment

- The resulting shifts in the  $I$ - $V$  curve of the solar cells.

The factors which influence the solar array output will be investigated separately, and then combined at the end to create PANSAM (PANSAT Solar Array Model), a computer model which simulates the solar array electrical performance.

## **B. EFFECTIVE AREA OF PANSAT WITH RESPECT TO THE SUN**

The surface area of each solar panel can be represented by a surface area vector. The direction of each surface area vector is normal to the corresponding panel and pointing outward. Each panel has 32,  $4.0 \times 1.92 \text{ cm}^2$  cells resulting in a magnitude of  $245.76 \text{ cm}^2$  for each surface area vector. Panels illuminated by the sun will have a component of their surface area vector pointing towards the sun. The sum of the sun-pointing components of the illuminated panels is the effective area, and is dependent on the orientation of the satellite relative to the sun. The change in effective area during the sunlight portion of the orbit is examined in the following discussion.

### **1. Frames of Reference**

As a means of describing the orientation of each panel with respect to the sun, three frames of reference must be defined. The first frame of reference considered describes spatial position relative to the orbit, and is denoted as **A**. The coordinate system defining the **A** frame is a dextral basis comprised of three orthonormal vectors, denoted as **i**, **j**, and

**k.** To facilitate defining the **A** frame, assume that the orbital twilight can be ignored and a plane perpendicular to the orbital plane separates orbit night from orbit day (eclipse from sunlight). This plane shall be referred to as the *shadow plane*. The orientation of **A** is defined as it exits the orbit night and passes through the shadow plane as follows:

- **i** lies in the orbital plane pointing in the direction tangential to the orbit and perpendicular to the shadow plane
- **j** points to earth along the line of intersection between the orbital plane and the shadow plane
- **k** is perpendicular to the orbital plane and lies within the shadow plane

The initial orientation of the **A** frame is illustrated in Figure 10.

In Figure 10, the inclination,  $i$ , is the angle measured from the earth's equatorial plane to the orbital plane. The solar declination,  $\delta$ , is the angle between the earth's equatorial plane and the ecliptic plane. The angle  $\gamma$  is the difference between the inclination and declination, that is

$$\gamma = i - \delta \quad (1)$$

Furthermore, the solar declination,  $\delta$ , varies periodically on an annual basis from a maximum of  $+23.44^\circ$  at summer solstice (June 21), to  $-23.45^\circ$  at winter solstice (December 22), and  $0^\circ$  during vernal equinox (March 21) and autumnal equinox (September 21) [Ref. 8:p. 347]. Figure 11

shows the coordinate system with respect to the orbital plane. Note that the coordinate system defining the A frame of

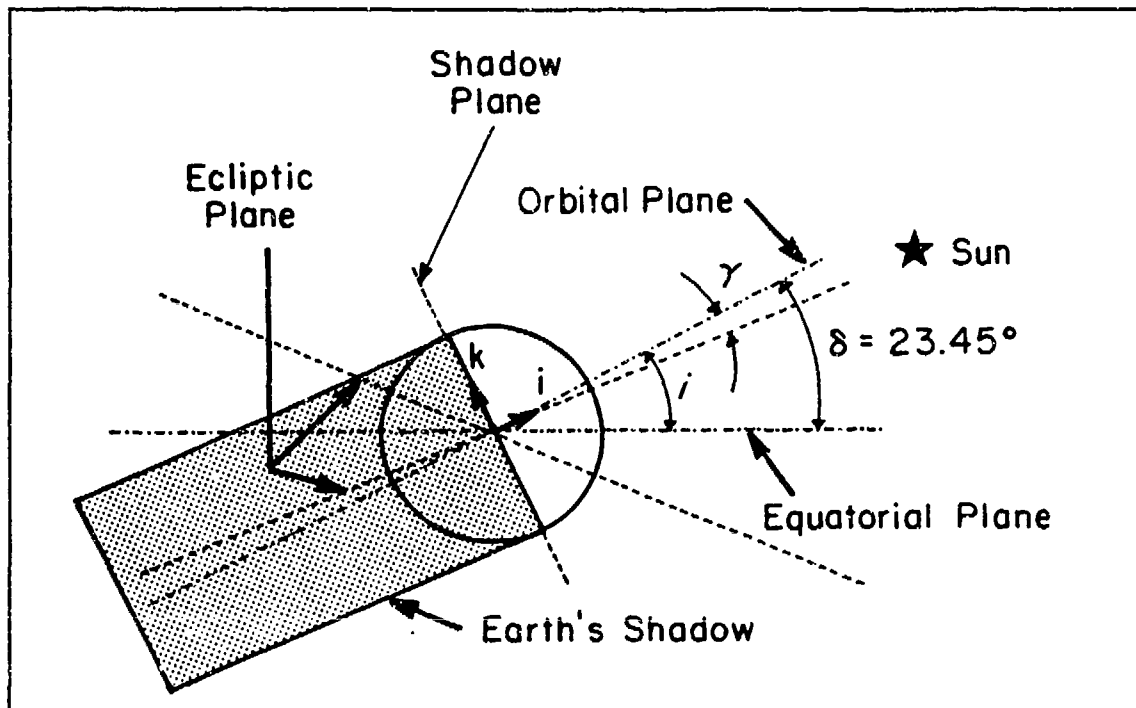
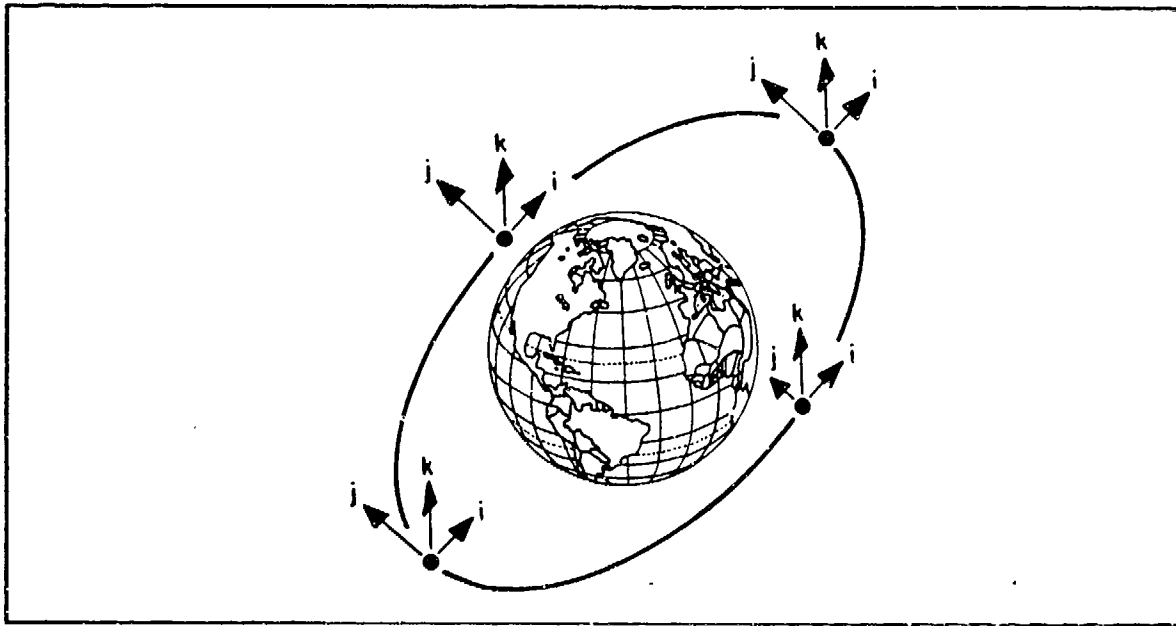


Figure 10. Illustration of the A Frame of Reference Describing the Orbit of PANSAT Relative to the Sun

reference maintains a constant orientation as it moves along the orbital path.

The next frame of reference described is the body frame of reference affixed to the spacecraft, denoted as B. As with A, the B frame is a coordinate system determined by a dextral basis comprised of three orthonormal vectors, denoted as  $\mathbf{o}$ ,  $\mathbf{p}$ , and  $\mathbf{q}$ . The B frame is attached to the satellite so that each of the vectors,  $\mathbf{o}$ ,  $\mathbf{p}$ , and  $\mathbf{q}$ , is associated with one of three panels offset from one another by  $90^\circ$ . The coordinate system is oriented so that each orthonormal vector is centered on, perpendicular to, and pointing outward from

its respective panel, as shown in Figure 12. Although the **B** frame and the spacecraft are stationary relative to one



**Figure 11.** Illustration of the **A** frame looking down upon the orbital plane

another, they are free to rotate with respect to the **A** frame in the directions indicated in Figure 12. Positive rotation is specified by the *right-hand-rule*. The measure of rotation, relative to the **A** frame, is indicated by the angles  $\phi$ ,  $\theta$ , and  $\psi$ . When the angles  $\phi$ ,  $\theta$ , and  $\psi$  are simultaneously equal to zero, the **B** frame coincides with the **A** frame. Furthermore, the surface area vector for each panel is defined in the **B** frame of reference.

The final frame of reference is used to describe direction relative to the sun vector. Again, the definition uses a dextral coordinate system with a basis formed by three orthogonal unit vectors **I**, **J**, and **K**. The solar frame of

reference is denoted as  $S$ . The unit vectors  $I$  and  $J$  lie in the ecliptic plane (the equatorial plane of the sun) and  $K$  is perpendicular to the ecliptic plane.

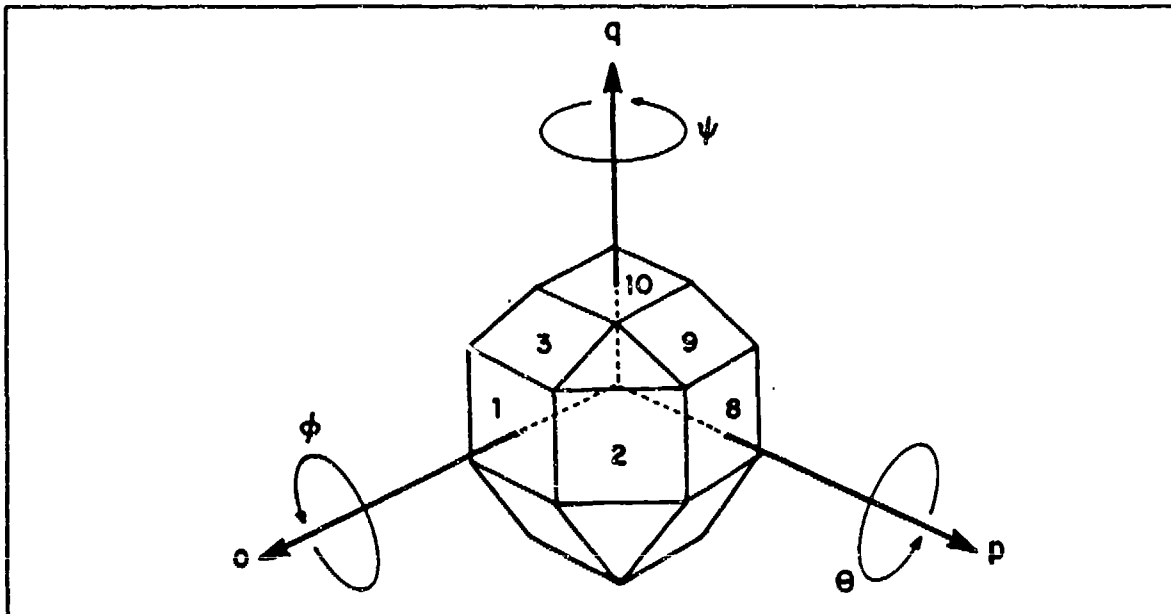


**Figure 12.** Depiction of the Body Frame of Reference,  $B$ , Affixed to PANSAT in the Above Orientation

## 2. Orientation with Respect to the Sun

The objective is to determine the portion of the solar array illuminated by the sun as PANSAT freely tumbles through the sunlit portion of its orbit. This is equivalent to determining the sun-pointing component of each surface area vector corresponding to each panel, and summing them together. The problem is described in three different frames of reference. As PANSAT, and thus the  $B$  frame, rotates with respect to the  $A$  frame, a method must be used that will permit a surface area vector defined in the  $B$  frame to be defined in the  $A$  frame. Once the vector is defined in the  $A$  frame, it

must then be translated into the **S** frame in order to find the sun-pointing component. Changing a vector from one basis to another is accomplished using a *coordinate transformation*. Following a coordinate transformation, a vector still has the same length and direction, it is merely expressed with respect to a different basis. [Ref. 12:p. 74]. Changing from one basis to another can be streamlined using matrix methods [Ref. 12:p. 75]. Given that **A** and **B** frames are coincident when the angles  $\phi$ ,  $\theta$ , and  $\psi$  are simultaneously equal to zero, the basis vectors of **A** (**i**, **j**, and **k**) will coincide with the basis vectors of **B** (**o**, **p**, and **q**) respectively. Figure 13 illustrates the result of rotating frame **B** through a positive rotation of angle  $\psi$  about the **k**-axis.

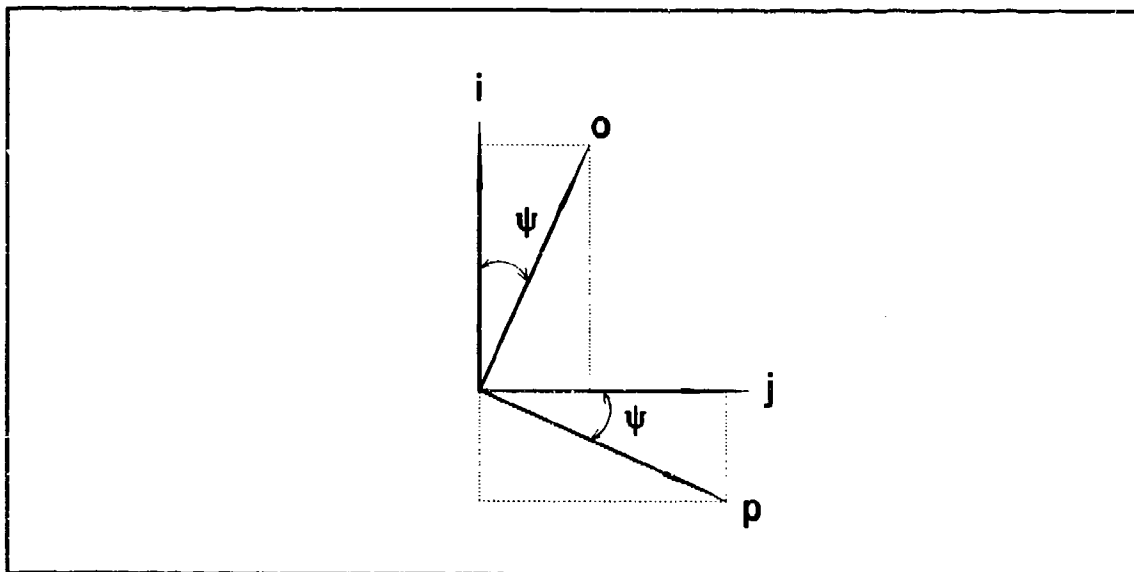


**Figure 13.** Rotation of the **B** Frame, About the **k**-axis of the **A** frame, by Angle  $\psi$

Now consider a vector **a** which may be expressed in terms of the **A** frame as

$$a_A = a_i i + a_j j + a_k k \quad (2)$$

or in terms of the B frame as

$$a_B = a_o o + a_p p + a_q q. \quad (3)$$

From Figure 13, it can be seen that the unit vectors  $i$ ,  $j$ , and  $k$  are related to the unit vectors  $o$ ,  $p$ , and  $q$  by the following equations:

$$\begin{aligned} i &= \cos(\psi) o - \sin(\psi) p + (0) q \\ j &= \sin(\psi) o + \cos(\psi) p + (0) q \\ k &= (0) o + (0) p + (1) q \end{aligned} \quad (4)$$

Substituting these equations into Equation 3 and equating it with Equation 2 yields

$$\begin{aligned} a_i &= a_o \cos(\psi) - a_p \sin(\psi) + a_q (0) \\ a_j &= a_o \sin(\psi) + a_p \cos(\psi) + a_q (0) \\ a_k &= a_o (0) + a_p (0) + a_q (1) \end{aligned} \quad (5)$$

By denoting  $\cos(\psi)$  and  $\sin(\psi)$  as  $c\psi$  and  $s\psi$  respectively, Equation 5 can then be represented by matrix notation in the form

$$\begin{bmatrix} a_i \\ a_j \\ a_k \end{bmatrix} = \begin{bmatrix} c\psi & -s\psi & 0 \\ s\psi & c\psi & 0 \\ 0 & 0 & 1 \end{bmatrix} \times \begin{bmatrix} a_o \\ a_p \\ a_q \end{bmatrix} \quad (6)$$



By denoting the *direction cosine matrix* obtained by rotating frame **B** about the **k**-axis as  $\mathbf{M}_k$ , Equation 6 can be written more compactly as

$$\mathbf{a}_{ijk}^T = \mathbf{M}_k \times \mathbf{a}_{opq}^T \quad (7)$$

where  $\mathbf{a}_{ijk}$  and  $\mathbf{a}_{opq}$  are vectors comprised by the coefficients of  $\mathbf{a}_A$  and  $\mathbf{a}_B$ , respectfully. The superscript  $T$  denotes the transpose of the vector. Similarly, with a positive rotation of angle  $\phi$  about the **i**-axis, the direction cosine matrix  $\mathbf{M}_i$  can be derived:

$$\mathbf{M}_i = \begin{bmatrix} 1 & 0 & 0 \\ 0 & c\phi & -s\phi \\ 0 & s\phi & c\phi \end{bmatrix} \quad (8)$$

Finally, a positive rotation about the **j**-axis of angle  $\theta$  yields

$$\mathbf{M}_j = \begin{bmatrix} c\theta & 0 & s\theta \\ 0 & 1 & 0 \\ -s\theta & 0 & c\theta \end{bmatrix} \quad (9)$$

To account for rotations about all three axes, the vector  $\mathbf{a}_B$  must be multiplied by each matrix in the same sequence in which each associated rotation occurs. Since PANSAT will be freely tumbling in orbit, the order in which the rotations take place is considered to be entirely arbitrary. For this discussion, the chosen sequence of

rotation is about the  $i$ -,  $j$ -, and then  $k$ -axis, yielding

$$\mathbf{a}_A^T = \mathbf{M}_i \times \mathbf{M}_j \times \mathbf{M}_k \times \mathbf{a}_B^T \quad (10)$$

Performing the matrix multiplication as indicated in Equation 10 leads to the direction cosine matrix

$$\mathbf{M} = \begin{bmatrix} c\psi c\theta & -c\phi s\psi + c\psi s\phi s\theta & s\phi s\psi + c\phi c\psi s\theta \\ c\theta s\psi & c\psi c\phi + s\phi s\theta s\psi & -c\psi s\phi + c\phi s\theta s\psi \\ -s\theta & c\theta s\phi & c\phi c\theta \end{bmatrix} \quad (11)$$

Therefore, any vector in the body frame of reference,  $\mathbf{a}_B$ , can be transformed into a vector in the orbit frame of reference,  $\mathbf{a}_A$ , by multiplying by the direction cosine matrix  $\mathbf{M}$ , such that

$$\mathbf{a}_{ijk}^T = \mathbf{M} \times \mathbf{a}_{opq}^T \quad (12)$$

Since the diameter of the sun is 109.2 times the diameter of the earth [Ref. 6:p. 2.3-1], and the distance between the sun and earth is so great compared to their diameters (the distance is approximately  $1.37 \times 10^6$  times the sun's diameter [Ref. 6:p. 2.3-1]), the solar rays reaching the earth are essentially parallel. With this assumption, the  $i$  and  $k$  unit vectors of the  $\mathbf{A}$  frame are considered coplanar with the  $\mathbf{I}$  and  $\mathbf{K}$  unit vectors of the  $\mathbf{S}$  frame. As a result, the translation of a vector from the  $\mathbf{A}$  frame to the  $\mathbf{S}$  frame reduces to a two dimensional problem as shown in Figure 14. The relationship between the two sets of unit vectors in

Figure 14 is very similar to that in Figure 13. Therefore, using an approach similar to the one for determining the direction cosine matrix for a rotation about one axis, the direction cosine matrix enabling the translation of a vector from frame **A** to frame **S**, is established. First, a vector in the **A** frame,  $\mathbf{a}_A$ , can be represented in the **S** frame as

$$\begin{aligned} a_I &= -a_i \cos(\gamma) + a_j(0) + a_k \sin(\gamma) \\ a_J &= a_i(0) - a_j(1) + a_k(0) \\ a_K &= a_i \sin(\gamma) + a_j(0) + a_k \cos(\gamma) \end{aligned} \quad (13)$$

As before, by denoting  $\cos(\gamma)$  and  $\sin(\gamma)$  as  $c\gamma$  and  $s\gamma$  respectfully, Equation 13 above can then be represented in matrix notation form as:

$$\begin{bmatrix} a_I \\ a_J \\ a_K \end{bmatrix} = \begin{bmatrix} -c\gamma & 0 & s\gamma \\ 0 & -1 & 0 \\ s\gamma & 0 & c\gamma \end{bmatrix} \times \begin{bmatrix} a_i \\ a_j \\ a_k \end{bmatrix} \quad (14)$$

Using the transformation matrix in Equation 14, the surface area vector of each panel can be described in the **S** frame. Since only the component of each surface area vector in the **I** direction is of interest, the matrix can be reduced to a transformation vector which determines this component in the **S** frame:

$$\begin{bmatrix} a_I \\ a_J \\ a_K \end{bmatrix} = [-c\gamma \ 0 \ s\gamma] \times \begin{bmatrix} a_i \\ a_j \\ a_k \end{bmatrix} \quad (15)$$

### 3. Computation of the Effective Area

An algorithm must be developed which can determine the effective area of PANSAT during a typical orbit. As PANSAT tumbles through orbit, its orientation relative to the **A** frame can be described as the angles  $\Phi$ ,  $\theta$ , and  $\Psi$  revolved about the

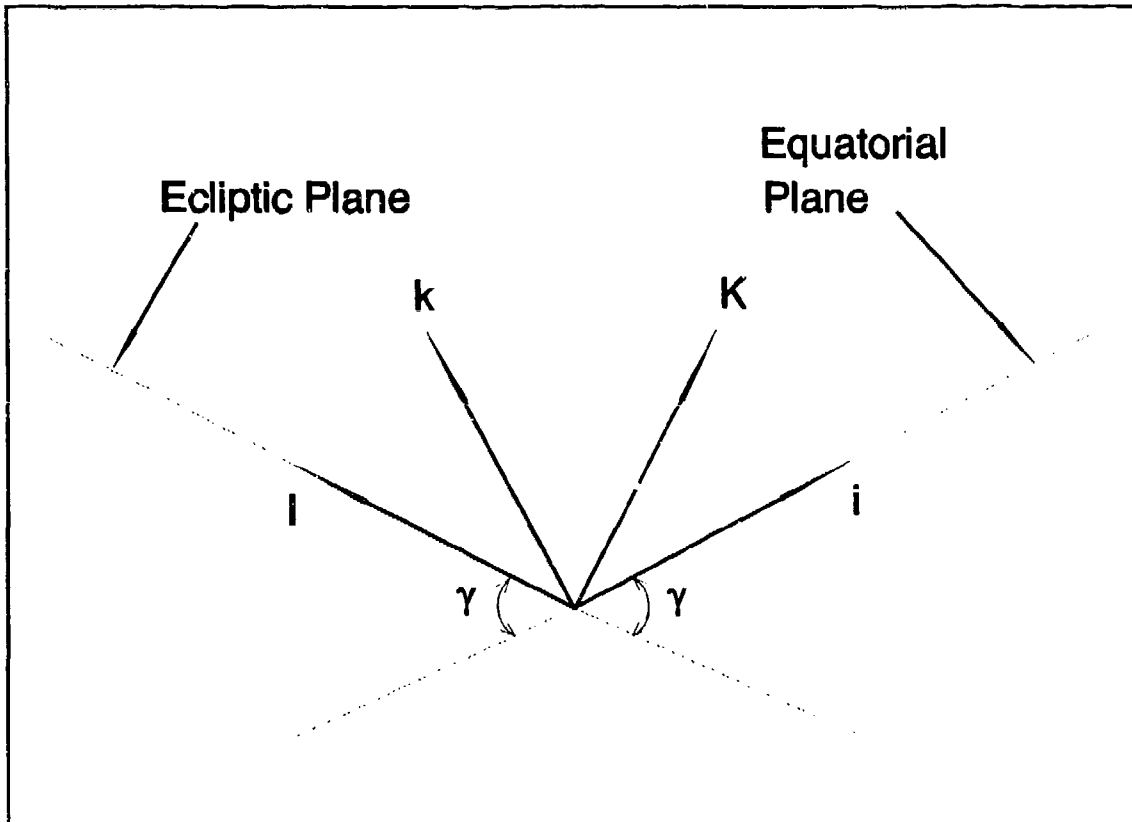


**Figure 14.** Relationship Between the Orthonormal Vectors  $i$  and  $k$ , and the Orthonormal Vectors  $I$  and  $K$

$i$ -,  $j$ -, and  $k$ -axes, respectfully. The amount of rotation about the  $i$ -,  $j$ -, and  $k$ -axes with respect to time are denoted as  $\dot{\Phi}$ ,  $\dot{\theta}$ , and  $\dot{\Psi}$ , respectfully. As the **B** frame, and hence, the satellite, rotates about the  $i$ -,  $j$ -, and  $k$ -axes at rates of  $\dot{\Phi}$ ,  $\dot{\theta}$ , and  $\dot{\Psi}$ , the new position of the surface area vector for each

panel is translated into the **A** frame using the direction cosine matrix in Equation 11. Once the surface area vector of each panel is translated into the **A** frame, the sun-pointing component for each surface area vector is determined using Equation 15. Thus, the sun-pointing components are summed to provide the effective area of PANSAT corresponding to the orientation associated with the time in sunlight.

To accomplish this, the orientation of the surface area vectors for each panel must be defined with respect to the body frame of reference, **B**. The panels are numbered as illustrated in Figure 15. Panels one, eight, and ten are perpendicular to the **o**-, **p**-, and **q**-axis, respectfully. This means the direction of the surface area vectors of panels one, eight, and ten are pointing in the direction of the **o**, **p**, and **q** unit vectors, respectfully. Panel six is the base plate and makes no contribution to the solar array effective area regardless of the orientation of the satellite. As a result, only 17 of the panels need to be considered when determining the accumulative effective area.

Only the panels with a surface area vector component pointing in the direction of the sun (**-I**) contribute to the effective area. So, a panel with a surface area vector component pointing in the **+I** direction is in the shadow of the satellite, and is not contributing to the effective area. Therefore, the effective area of such a panel is set to zero by the algorithm.

Initially, the algorithm will be used to investigate the maximum, minimum, and average effective areas of PANSAT. Appendix C describes how the PANSAT model is rotated in small increments of 0.1 radian/sec about each axis. The increment of 0.1 radian/sec was selected to provide manageable run times without sacrificing accuracy. Although the algorithm will not

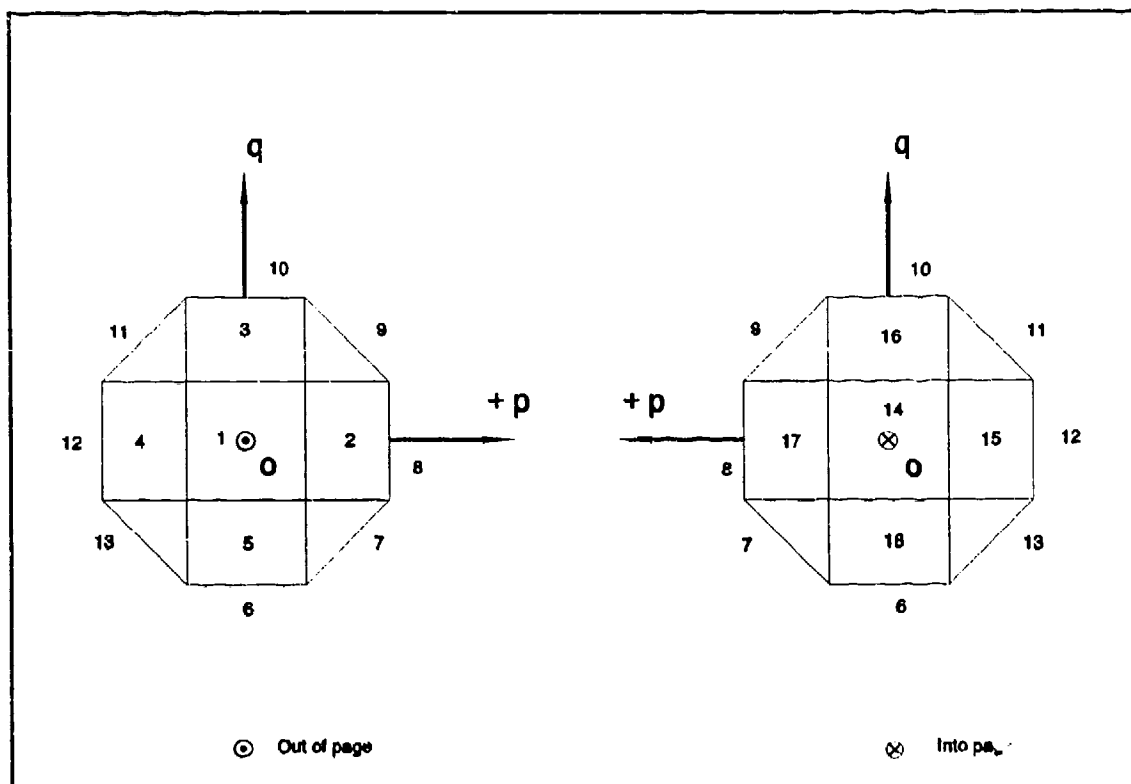


**Figure 15.** Diagram Illustrating the Numbering of the Panels and Their Relation to One Another

exhaust all possible orientations, it will provide numbers adequate for the desired analysis. The algorithm described above is implemented using the MATLAB® program in Appendix C. Each of the surface area vectors are given in the code; note that the baseplate, panel six, is set equal to zero. The

resulting values for the effective area are a minimum of 696.37 cm<sup>2</sup>, a maximum of 1139.2 cm<sup>2</sup>, and an average of 1036.9 cm<sup>2</sup>. This average effective area is 17.6% less than that determined by the SSAG (1259 cm<sup>2</sup>), and 14.2% less than that used by the contractor (1209 cm<sup>2</sup>).

Next, the algorithm is used to develop a program that allows the user to establish the initial orientation of PANSAT upon entering sunlight and to assign the rotation rate about each axis [Appendix C]. For the purpose of illustration, the program was run with an initial orientation such that the B frame was coincident with the A frame, a 480 Km altitude, during summer solstice, with the expected rotation rate of 0.02 °/s [Ref. 13]. The resulting plot is shown in Figure 16. The maximum, minimum, and average effective area was 1139.1, 941.3, and 1095.2 cm<sup>2</sup>, respectively.

### C. THERMAL ANALYSIS OF PANSAT

The transient thermal analysis of PANSAT was conducted utilizing the *Transient Thermal Analysis* software package [Ref. 14]. An extensive transient thermal analysis of PANSAT must still be performed, yet it is beyond the scope of this thesis. However, with the transient thermal analysis software package, reasonable approximations of the equilibrium transient temperatures of PANSAT were obtained for a typical orbit.

## 1. Software Program Objective and Overview

The transient thermal analysis software package is able to predict the transient temperature in a physical configuration by performing a finite-difference analysis of a model of the configuration. It does so by calculating the transient temperatures in a user-defined nodalized model of the geometry to be analyzed. The model can consist of up to

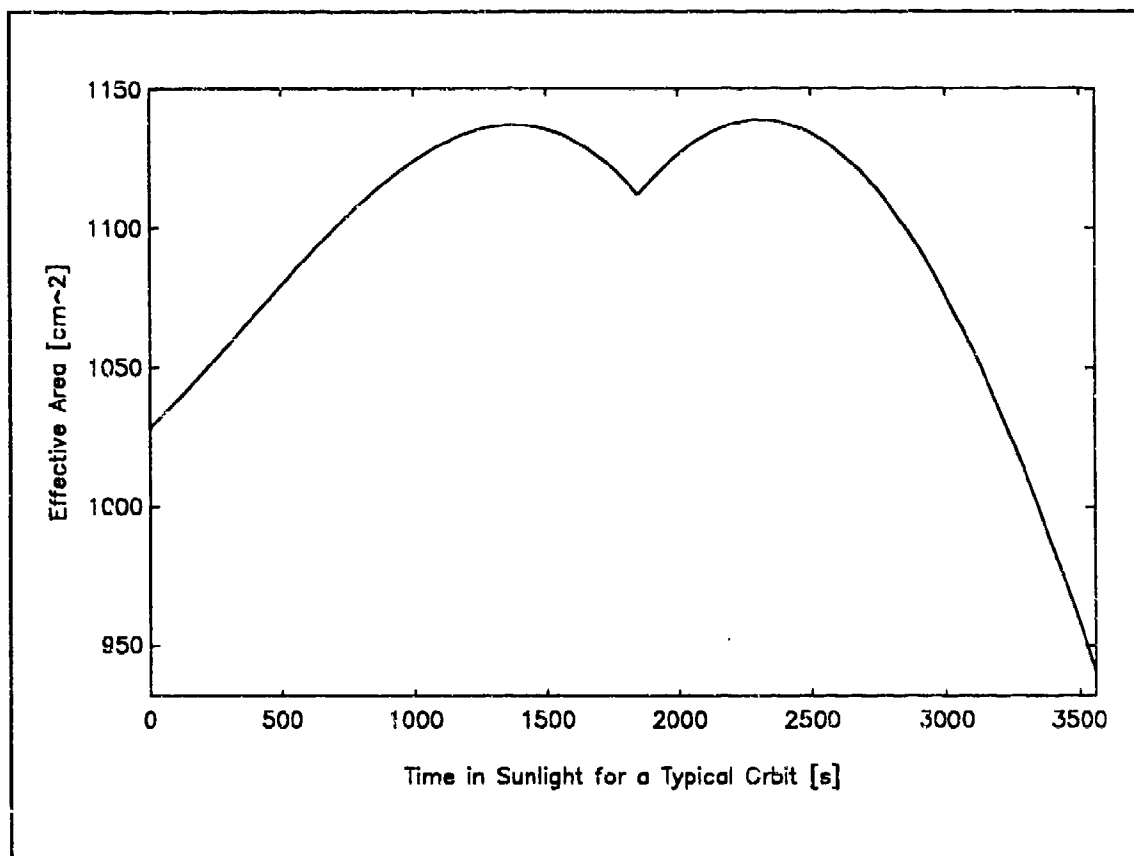


**Figure 16.** Effective Area for a Typical Orbit

300 nodes connected through a network of user-defined conductance paths. Each node may be connected to constant or time dependent temperature sinks through conduction, radiation, or a variety of convective boundary conditions.



Furthermore, each node may have heat inputs which are functions of time or node temperature. Certain user-defined conductance paths may also have path conductances that vary with time or temperatures. The program can also analyze models having fluid flow through the nodes. Finally, the model may include certain nodes whose specific heat may vary with time, temperature or undergo a phase change [Ref. 14:p. 1].

The thermal analyzer software consists of two programs, one for the transient thermal analyzer and one for a model builder. The model builder program writes an input file which is used by the analyzer program to calculate temperatures. Once the transient calculation is complete, the final node temperatures are written to a summary output file which may be observed by the user or used as initial temperatures for a subsequent run when an iterative process is required to determine equilibrium transient temperatures [Ref. 14:pp. 1-2].

## **2. Transient Thermal Analysis for PANSAT**

The transient thermal analysis for PANSAT used the same 248-node model developed for the static thermal analysis of PANSAT. Two models were developed:

- The first model is for the sunlight portion of the orbit in which there is an external heat input due to radiation from the sun
- The second model is for the eclipse phase, in which there is no external heat input due to radiation from the sun

The heat generated internally by the electrical components

was set to zero based on the assumption that a method of passive thermal control will be employed to dissipate all internal heat. The 68 Kg mass of PANSAT was assumed to be divided equally among the 248 nodes; that is, the weight of each node is

$$\frac{68 \text{ Kg}}{248 \text{ Nodes}} \approx 274.2 \frac{\text{grams}}{\text{node}}.$$

The models were further simplified by assuming all nodes had the specific heat of aluminum (896 [W·s/°K]).

Assuming an orbit altitude of 480 Km at summer solstice, the sunlight model was run for 3497 [s] and the eclipse model for 2145 [s], equating to the sunlight period and the eclipse period, respectfully [Appendix D]. Since the symmetry of PANSAT and the uniformity of its exterior surface, it is assumed that conduction will allow the exterior to be considered approximately isothermal. Therefore, the worst case will occur when PANSAT is stationary, with regard to its tumble rate. That is, while in sunlight, the same side is facing the sun with a panel perpendicular to satellite-sun ray vector, and the opposite side is in shadow. Additional assumptions include:

- No time dependent temperatures
- No fluid flow through the nodes
- No time or temperature dependent conductances
- No time or temperature dependent heat inputs
- No time or temperature dependent node heat capacities

- No change of phase

The thermal analyzer program was run initially with the sunlight model and all nodes set equal to  $15^{\circ}\text{C}$ . The ensuing output file contained the node temperatures that would result from PANSAT being exposed to the sun for the sunlit portion of the orbit (approximately 3500 s). Next, the thermal analyzer program was run with the eclipse model. The output file containing the node temperatures from the sunlight run was used as an input file to assign the initial node temperatures for the eclipse portion of the orbit (approximately 2150 s). Subsequently, the thermal analyzer program was run again with the sunlight model. This iteration used the node temperatures in the output file from the eclipse run as the initial nodes temperatures for the second sunlight run. This alternating procedure was continued for 10 iterations until the temperature difference for a given node for two subsequent runs remained at less than 0.6%. The output files containing the node temperatures for the final sunlight and eclipse runs were placed in a data file. A MATLAB<sup>®</sup> program was then used to read the data file and plot the results, as shown in Figure 17. Figure 17 indicates that for the side of PANSAT facing the sun, the minimum temperature which occurs upon exiting eclipse is  $16.6^{\circ}\text{C}$ . Furthermore, the maximum temperature which occurs upon entering eclipse is  $32.7^{\circ}\text{C}$ . For the side opposite the sun, the minimum temperature is  $17.5^{\circ}\text{C}$  and the maximum is  $28.9^{\circ}\text{C}$ . The

temperature difference between the two sides is small, and Figure 17 demonstrates that the assumption of an isothermic

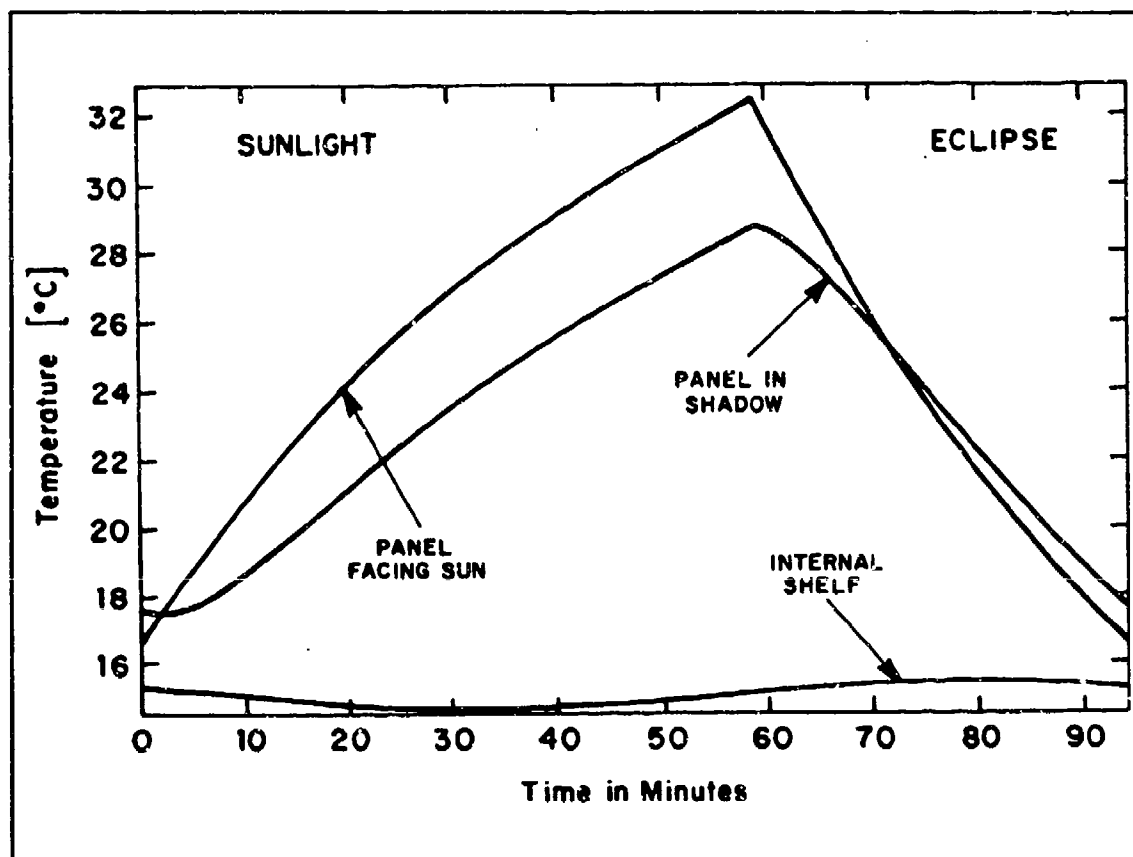


Figure 17. The Surface Temperature of PANSAT Plotted Against Time for a Typical Orbit. The Plot Includes: the Panels Facing and Opposite the Sun, and an Internal Shelf

exterior is acceptable. However, for power output performance, the hot case is of greatest concern, and therefore will be used as the worst case for analysis [Ref. 6:p. 3.5-2].

#### D. DETERMINATION OF THE SOLAR CELL AND ARRAY I-V CURVES

The preferred method for predicting solar cell and array performance is shifting the cell or array I-V characteristics

along their current and voltage coordinates and adjusting the curve shape when required. The proper sequence for generating such a curve is:

- Begin with the initial, bare cell characteristics obtained under standard test conditions (28°C cell temperature, one solar constant intensity, and an air-mass-zero spectrum).
- Using the parameters associated with the bare cell under standard test conditions, determine  $I_{sc}$ ,  $V_{oc}$ ,  $I_{mp}$ , and  $V_{mp}$  corresponding with the radiation damage equivalent 1 MeV fluence for prescribed mission.
- Adjust the I-V curve for the operating solar intensity actually incident on the solar cell through degraded optical elements and at off-point angles. Include any cover installation loss or gain.
- Adjust the I-V curve for the operating temperature .
- Scale up the cell characteristics to the array levels and include isolation diode and wiring losses, and external series resistance effects. [Ref. 7:pp. 80-81]

### 1. Bare Cell Characteristics

The bare cell parameters for the Series 6700 solar cells used for PANSAT were provided by the contractor. The following parameters are for bare cells at BOL under standard test conditions:

$$\begin{aligned}V_{oc} &= 605 \text{ mV} \\V_{mp} &= 500 \text{ mV} \\I_{mp} &= 307 \text{ mA} \\I_{sc} &= 319 \text{ mA}\end{aligned}$$

[Ref. 5:p. 2]. The corresponding I-V curve is shown in Figure 6.

### 2. Radiation Damage

PANSAT is expected to be in a radiation-benign orbit during its two year mission. The preliminary 1 MeV equivalent

electron fluence provided to the contractor by the SSAG is  $1.80 \times 10^{13}$  electrons/cm<sup>2</sup> at an altitude of 833 Km and a 0° inclination [Ref. 4:p. 9].

Radiation damage tests were performed on K6700 solar cells by Hughes Space and Communications Group at the Dynamitron 1 MeV electron facility at JPL in September 1983. From the results of these tests and the mission criteria provided by SSAG, the contractor was able to provide the radiation loss factors for a 30 mil coverslide thickness. The radiation loss factor for  $I_{sc}$  and  $I_{mp}$  is 0.978; the radiation loss factor for  $V_{oc}$  and  $V_{mp}$  is 0.965. [Ref. 5:p.5]

The bare cell parameters at BOL can be multiplied by their associated loss factors to provide the radiation-damaged cell parameters after two years:

$$\begin{aligned} I_{scu} &= I_{sc} \times 0.978 \\ I_{mpu} &= I_{mp} \times 0.978 \\ V_{ocu} &= V_{oc} \times 0.965 \\ V_{mpu} &= V_{mp} \times 0.965 \end{aligned} \tag{16}$$

The additional "u" subscript indicates the unglassed condition.

### 3. Glasped Solar Cell I-V Curve

The I-V curves for the unglassed cells are shifted parallel to the current axis until the solar cell short-

circuit current after glassing is

$$I_{scg} = I_{scu} \times F_c \quad (17)$$

where  $F_c$  is the cover glass installation factor. The other cell parameters after glassing are

$$\begin{aligned} I_{mpg} &= I_{mpu} + (I_{scg} - I_{scu}) \\ V_{ocg} &= V_{ocu} \\ V_{mpg} &= V_{mpu} \end{aligned} \quad (18)$$

where the additional subscript "g" denotes cell parameters in the glassed condition. [Ref. 6:p. 9.4-5] The contractor provided a cover installation loss or filtering factor,  $F_c$ , of 0.99 [Ref. 10:p. 2].

#### 4. Effects of Intensity Change on Solar Cell I-V Curve

For the glassed solar cells damaged because of exposure to radiation, the I-V curve can be shifted along the current and voltage axes by the amounts  $\Delta I_1$  and  $\Delta V_1$  given by

$$\begin{aligned} \Delta I_1 &= (S' - S) \times I_{scg} \\ \Delta V_1 &= -\Delta I_1 \times R_s \end{aligned} \quad (19)$$

where  $S'$  is the effective solar intensity and  $S$  is one solar constant (the solar intensity at which the cells were originally tested) [Ref. 7:p. 83].

The effective solar intensity,  $S'$ , is defined as the actual, "effective" light level which is incident upon the

active surface of the solar cell and is given by

$$S' = (S_i/D^2) \times F_t \times \cos(\Gamma) \quad (20)$$

where the terms are defined as

- $S_i$  = sunlight intensity (in units of solar constants)
- $D$  = array-sun distance (in units of AU)
- $F_t$  = solar cell cover transmission factor
- $\Gamma$  = angle of incidence

[Ref. 6:p. 9.4-5]

The solar intensity,  $S_i$ , varies throughout the year, as does the solar declination angle, and is given in Table II

**TABLE II.** VARIATION OF SOLAR INTENSITY WITH EARTH-SUN DISTANCE [REF. 8:p. 348].

Date	Solar Intensity, $S_i$ (mW/cm <sup>2</sup> )	Relative	Declination Angle, $\delta$
March 21 (vernal equinox)	136.2	1.0066	0°
June 21 (summer solstice)	131.1	0.96896	+23.44°
Sept. 23 (autumnal equinox)	134.5	0.99408	0°
Dec. 22 (winter solstice)	139.7	1.0325	-23.44°

for four selected times of year. Table II shows that the minimum solar intensity occurs at summer solstice. As a



result, a design requirement for a solar array is to produce the demanded current and voltage output at the EOL summer solstice condition [Ref. 8:p. 347]. Therefore, the performance analysis will investigate the solar array output of PANSAT during summer solstice.

Referring to Equation 19, for reduced intensity where  $S'$  is less than  $S$ ,  $\Delta I_1$  is negative and  $\Delta V_1$  is positive. This leads to a reduced short-circuit current,  $I_{scs}$ , and a slight shift toward higher voltages; however, the actual cell open-circuit voltage will decrease by

$$V_{S'} = k \log\left(\frac{S'}{S}\right) \quad (21)$$

where  $k$  depends on the cell type. The change in the four solar cell parameters due to a change in solar intensity (indicated by the additional subscript "s") is given by

$$\begin{aligned} I_{scs} &= I_{scg} + \Delta I_1 \\ &= I_{scg} \times (1 + S' - S) \\ I_{mps} &= I_{mpg} + \Delta I_1 \\ V_{ocs} &= V_{ocg} + \Delta V_1 + \Delta V_{S'} \\ V_{mps} &= V_{mpg} + \Delta V_1 + \Delta V_{S'} \end{aligned} \quad (22)$$

[Ref. 7:p. 83]

## 5. Solar Cell I-V Curve at Operating Temperature

The difference between the actual solar cell operating temperature,  $T_{op}$ , and the reference temperature,  $T_o$ , also

necessitates an adjustment to the I-V Curve. The I-V curve can be shifted along the current and voltage axes by the amounts  $\Delta I_2$  and  $\Delta V_2$  given by

$$\begin{aligned}\Delta I_2 &= \beta_I \times I_{sc} \times (T_{op} - T_0) \\ \Delta V_2 &= \beta_V \times (T_{op} - T_0)\end{aligned}\tag{23}$$

In the thermal analysis section, the operating temperature for a typical orbit was determined to vary from a minimum of 16.6°C at the end of eclipse to a maximum of 32.7°C prior to entering eclipse. In this temperature range, the temperature coefficient for current,  $\beta_I$ , and the temperature coefficient for voltage,  $\beta_V$ , as provided by the contractor, is approximately  $2.188 \times 10^{-2}$  mA/(°Ccm<sup>2</sup>) and -2.1 mV/°C, respectively [Ref. 15:p. 3]. The values of  $\beta_I$  and  $\beta_V$  are positive and negative, respectively. As a result, for an operating temperature greater than  $T_0$ ,  $I_{sc}$  will increase and  $V_{oc}$  will decrease. The four cell parameters resulting from an operating temperature other than  $T_0$  (denoted by the additional subscript "T") are

$$\begin{aligned}I_{sc_T} &= I_{scs} + \Delta I_2 \\ I_{mp_T} &= I_{mps} + \Delta I_2 \\ V_{oc_T} &= V_{ocs} + \Delta V_2 \\ V_{mp_T} &= V_{mps} + \Delta V_2\end{aligned}\tag{24}$$

[Ref. 7:p. 83]

## 6. Degraded Solar Cell I-V Curve

Further adjustment of the solar cell I-V curve is necessary to account for degradation from panel assembly and temperature cycling losses, denoted as  $F_A$  and  $F_{TC}$ , respectively. Also, because of exposure to ultraviolet (UV) light and micrometeorites (MM), additional losses exist.

### a. Assembly Factors

Assembly factors account for the reduction in solar cell output due to assembly and installation processes. These assembly factors may be represented as (1) dimensionless ratios applied to output power, current, or voltage (2) an incremental series resistance or (3) as voltage differences. Typically, both ratios and voltage drops are used. [Ref. 7:p. 80] An additional series resistance in the solar cell is associated with soldering, welding, etc. Losses resulting from the total series resistance are accounted for by a voltage reduction per cell denoted as  $\Delta V_3$ . The introduction of additional series resistance tends to depress the maximum power point voltage without affecting the open-circuit voltage. The resulting voltage parameters are represented by the equations

$$\begin{aligned} V_{mpd} &= V_{mpT} - \Delta V_3 \\ V_{ocd} &= V_{ocT} \end{aligned} \tag{25}$$

[Ref. 7:p. 84]. The contractor assumed a voltage loss of 5 mV per cell to account for the increase in series resistance in

the cell caused by the soldered contact points and interconnect material [Ref. 5:p. 4].

Due to mismatches in the indices of refraction between the coverglass, the adhesive, and the solar cell, there is a reduction in current referred to as *glassing losses* [Ref. 7:p. 245], denoted as  $F_g$ . The contractor estimates that the mismatch due to the differing indices of refraction will result in a further 1% loss in current [Ref. 5:p. 4]. This will lead to a *glassing loss factor* of

$$F_g = 0.99$$

**b. Ultraviolet and Micrometeorite Losses**

The optical transmission factor,  $F_t$ , is a combination of all factors which effect the amount of light reaching the solar cell active surface. These factors include darkening of the solar cell coverslide and adhesive, and darkening of deposits on the coverslide, due to exposure to ultraviolet light. The contractor determined degradation due to UV exposure to be approximately 1%. [Ref. 5:p. 4] As a result, the optical transmission factor is

$$F_t = 0.99$$

On short duration missions, it is assumed that micrometeorites cause little or no power loss. On longer missions it is common practice to assume a 0.5% loss of power/annum due to the combined effects of ultraviolet

radiation and micrometeorites. For missions spanning one to four years, the standard loss factors used to account for the degradation due to the exposure to UV and MM is 0.98. [Ref. 5:p. 5] The loss factor caused by UV exposure,  $F_u$ , is assumed to be 0.99; therefore, dividing combined loss factor of 0.98 by  $F_u$ , will yield the loss factor associated with exposure to micrometeorites

$$F_{MM} = 0.99$$

The optical transmission factor,  $F_g$ , is accounted for in Equation 20. Therefore, the current parameters resulting from degradation due to cell mismatch, and micrometeorite exposure at EOL are given by

$$\begin{aligned} I_{mpd} &= I_{mpT} \times F_g \times F_{MM} \\ I_{scd} &= I_{scT} \times F_g \times F_{MM} \end{aligned} \tag{26}$$

## 7. Total Change of the Solar Cell I-V Curve

By combining the above computations, I-V curves can be generated for a solar cell of PANSAT at a given operating temperature and under the conditions described previously. Figure 18 shows the I-V curve of a bare cell at BOL under standard test conditions contrasted with the I-V curves of the same cell at EOL during summer solstice with operating temperatures of 16.6°C, 28.0°C, and 32.7°C. The operating temperatures correspond to exiting eclipse, standard test conditions, and entering eclipse, respectfully. The main

program and subroutines used to generate Figure 18 are given in Appendix B.

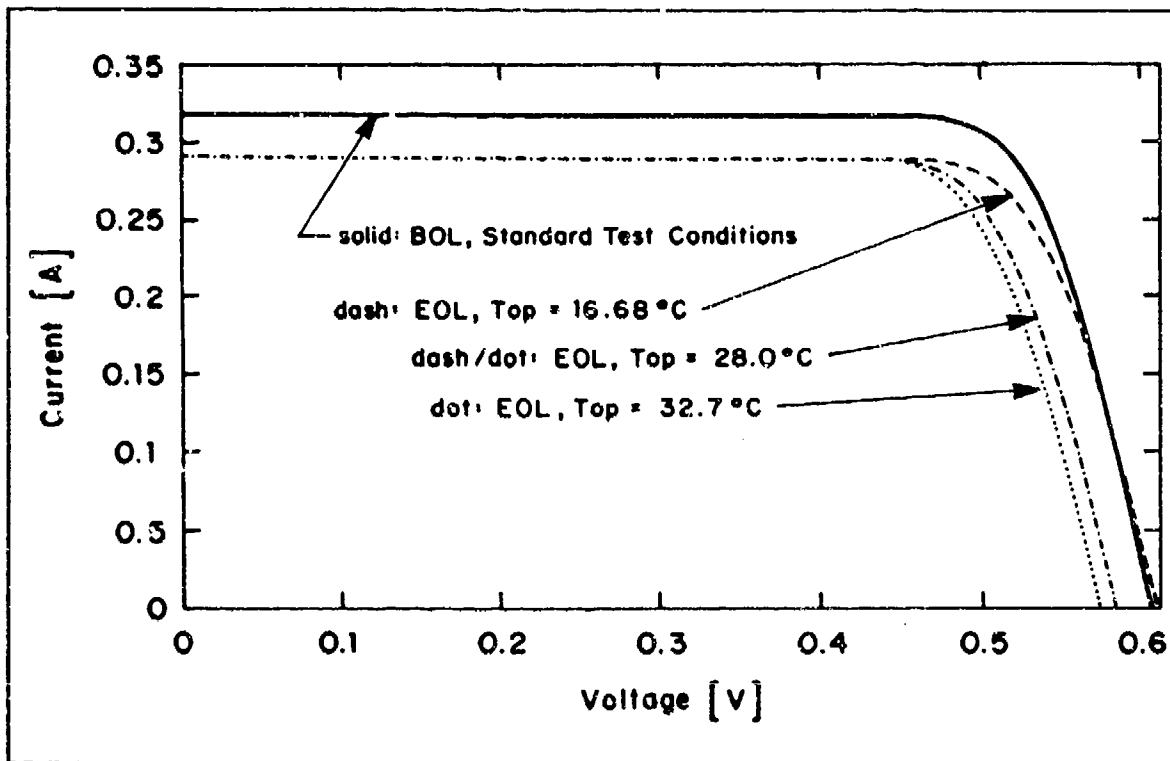


Figure 18. I-V Curves at: BOL Under Standard Test Conditions (solid); EOL at  $T_{op} = 16.68^{\circ}\text{C}$  (dash); EOL at  $T_{op} = 28.0^{\circ}\text{C}$  (dash\dot); EOL at  $T_{op} = 32.7^{\circ}\text{C}$  (dot)

#### E. DETERMINATION OF THE SOLAR ARRAY OUTPUT POWER

To determine the output performance of PANSAT's solar array, all previously mentioned factors must be considered. The design of the EPS must allow it to accommodate the worst case scenario in addition to a typical orbit. Therefore, it is advantageous to investigate the performance of the solar array during the worst case in addition to its performance during normal operation.

## 1. The Solar Cell Array Model

The solar cell model previously discussed must be electrically connected into series-parallel matrices to form an entire array for the solar cell array analysis. Typically, an additional series resistance is used to represent the solar cell interconnectors and the array wiring, and a voltage drop to account for blocking diodes are considered [Ref. 7:p. 65]. The additional series resistance for cell interconnectors is accounted for in the voltage drop  $\Delta V_i$  (equal to 5 mV). The blocking diode voltage drop,  $V_D$ , is typically 0.38 V. The panel wiring loss,  $V_W$ , accounts for the resistance of the 22 gauge wire used as circuit leads to the terminal board. The resistance,  $R_W$  is a linear function of temperature, and is given by the contractor as

$$R_W = 50 + 180 \times 10^{-3} \times T \text{ [m}\Omega\text{/m]}$$

where  $T$  is the temperature of the wire (assumed to be  $T_{op}$ ). The longest circuit leads are 40 in (approximately one meter); therefore, this is considered the worst case, and will be used in all cases [Ref. 5:pp. 8-9]. This results in a wiring loss for each panel of

$$V_W = I_S \times R_W \quad (27)$$

where  $I_S$  is the total current from the string (panel) under consideration.

The number of cells connected in parallel form a submodule, and the number of submodules in series which provide power directly to the bus is called a string [Ref. 7:p. 66]. In the case of PANSAT, each panel consists of a submodule of one cell which results in strings of 32 cells connected in series.

The array consists of all the strings feeding a particular bus system. By summing all the string currents at constant voltage values and accounting for the isolation diode and wire loss drops, an equation may be obtained for the array. If the array voltage  $V_A$  is determined by a load, such as a power regulator, a charging energy storage battery, or by a number of other power-producing strings, then because of the dependence of the string voltage,  $V_s$ , on  $V_A$ ,  $V_s$  is given by

$$V_s = V_A + V_D + V_W \text{ and } I_s = I_D \quad (28)$$

where  $I_s$  and  $I_D$  are the string and diode currents, respectfully. [Ref. 7:p. 66]

For an array of  $m$  strings, with each string being illuminated at a different intensity, the array current, a function of the array voltage, is described by

$$\begin{aligned} I_A(V_A) &= \sum_{j=1}^m I_{sj}(V_A) \\ &= \sum_{j=1}^m I_j(V_s - V_D - V_W) \times k_j \end{aligned} \quad (29)$$



where the constant  $k_j$  indicates the intensity modifier applied to the current from panel  $j$  [Ref. 7:pp. 66-67].

## 2. Development of the PANSAT Solar Array Model (PANSAM)

Thus far, the different factors that contribute to the output of the solar array have been examined with an effort to divide the analysis into a logical progression. In each circumstance, an algorithm was described and implemented with code. Now these algorithms must be coupled together to provide the user with an interactive program which allows the user to define selected initial values - such as, PANSAT's orientation, the bus voltage, the orbit inclination, and the sun's declination - and gather a performance analysis of the solar array for these selected values. This collection of algorithms will be referred to as PANSAM (PANSAT Solar Array Model).

Initially, the study will consider the situation in which the bus voltage is not determined by the battery or regulator, such that

$$\begin{aligned} V_A &= V_S - V_D - V_W \\ &= N_S \times V - V_D - V_W \end{aligned} \tag{30}$$

where  $N_S$  is the number of cells in series and  $V$  in this case is the maximum power point voltage,  $V_{mp}$ , of an individual cell. The case in which the bus voltage is forced by the battery voltage can be examined in future work once the battery design and selection is complete and voltage characteristics are

known. Two examples of battery voltage characteristics are change with temperature and charging.

The output current, voltage, and power for sequential increments of time throughout the sunlit portion of the orbit are determined by PANSAM. It begins by defining the fixed values such as:

- The electrical parameters of the bus and solar cells
- The loss factors associated with the solar array construction and exposure to the space environment
- The values used to calculate the orbital parameters for a satellite in low earth orbit.

Assuming PANSAT is launched from a space shuttle, the inclination is fixed at a typical  $28^\circ$ . Additionally, because the thermal analysis data was for an orbit altitude of 480 Km, this will be used as the fixed altitude of the analysis. However, to accommodate thermal analysis data of a different altitude, PANSAM could be easily changed to make altitude a user input variable. Next, PANSAM allows the user to select the angular rate of change about the *i*-, *j*-, and *k*-axes of the **A** frame, and the initial values of  $\phi$ ,  $\psi$ , and  $\theta$  which describe the initial orientation of PANSAT with respect to the **A** frame. The operating temperature data from the thermal analysis is then loaded as a vector to be used for calculating the temperature effects on the current and voltage.

Next, the algorithm and code described earlier to determine the total surface area illuminated by the sun is incorporated to find which panels are illuminated and the

angle of incidence corresponding to each panel for each increment of time. The cosine of the angle of incidence, denoted as  $\cos(\Gamma)$ , is needed to find the effective solar intensity,  $S'$ , given in Equation 20. In turn, the effective solar intensity is required to determine the effects of intensity change on current and voltage as given in Equation 19. The surface area vector in the **A** frame is given in Equation 2 as

$$\mathbf{a}_A = a_i \mathbf{i} + a_j \mathbf{j} + a_k \mathbf{k} \quad (2)$$

Once transferred into the **S** frame, it is denoted as

$$\mathbf{a}_S = a_I \mathbf{I} + a_J \mathbf{J} + a_K \mathbf{K} \quad (31)$$

where  $a_i$ ,  $a_j$ , and  $a_k$  are given by Equation 13 as

$$\begin{aligned} a_I &= -a_i \cos(\gamma) + a_j(0) + a_k \sin(\gamma) \\ a_J &= a_i(0) - a_j(1) + a_k(0) \\ a_K &= a_i \sin(\gamma) + a_j(0) + a_k \cos(\gamma) \end{aligned} \quad (13)$$

By defining the sun vector,  $\mathbf{S}$ , as pointing parallel to, and in the opposite direction of  $\mathbf{I}$ , it is defined in the **S** frame as

$$\mathbf{S} = -\mathbf{I} + (0) \mathbf{J} + (0) \mathbf{K} \quad (32)$$

Using the definition of the dot product of two vectors [Ref. 16:p. 21] yields

$$\begin{aligned} \mathbf{a}_S \cdot \mathbf{S} &= a_I \cdot (-1) + a_J \cdot (0) + a_K \cdot (0) \\ &= -a_I \end{aligned} \quad (33)$$

By definition, the cosine of the angle between the two vectors is given by

$$\cos(\Gamma) = \frac{\mathbf{a}_s \cdot \mathbf{S}}{\|\mathbf{a}_s\| \|\mathbf{S}\|} \quad (34)$$

[Ref. 16:p. 58]. The terms in the denominator of Equation 34 represent the magnitude of the vectors  $\mathbf{a}_s$  and  $\mathbf{S}$ . Since  $\mathbf{S}$  is equal to  $-\mathbf{I}$ , and  $\mathbf{I}$  is a unit vector with a magnitude of one,  $\mathbf{S}$  has a magnitude of one. Furthermore, the magnitude of  $\mathbf{a}_s$  is given by

$$\|\mathbf{a}_s\| = \sqrt{a_I^2 + a_J^2 + a_K^2} \quad (35)$$

which is simply the length of the surface area vector [Ref. 16:p. 22]. Using one as the length of  $\mathbf{S}$ , and Equations 13, 33, and 35, Equation 34 yields

$$\cos(\Gamma) = \frac{a_I \cos(\gamma) - a_K \sin(\gamma)}{\sqrt{a_I^2 + a_J^2 + a_K^2}} \quad (36)$$

Equation 36 is the sun-pointing component of the surface area vector calculated by the effective area program divided by the magnitude of the entire surface area vector.

Once the cosine of the angle of incidence is determined and the effective solar intensity calculated, the respective subroutines can be summoned to find  $I_{scd}$ ,  $I_{mpd}$ ,  $V_{ocd}$ ,  $V_{mpd}$ ,  $K_2$ , and  $I$  associated with each illuminated panel. For each increment of time, the current for the illuminated panels

is summed and multiplied by the corresponding voltage to find the output power.

Note that when very small angles of incidence occur, the values for the currents  $I_{scd}$  and  $I_{mpd}$  are either negative or unrealistically small. This causes the subroutine for determining  $K_2$  to diverge and a result is never obtained. Therefore, an 'if' statement was introduced to divert the program for these circumstances.

The code for the program is given in Appendix B. For demonstration, the program was run using the initial orientation corresponding to the **B** frame coincident with the **A** frame ( $\theta$ ,  $\Psi$ , and  $\phi$  equal to zero), the solar declination for the summer solstice ( $23.44^\circ$ ), and an angular rate of change equal to  $0.02^\circ/\text{s}$  [Ref. 13] for each axis. The calculations were made in five second increments to facilitate timeliness. The values for the operating temperature, the effective area, the output voltage, and the power were divided by their respective maximums to normalize the parameters, and then plotted together over the sunlit portion of the orbit for comparison. This is shown in Figure 19.

The contractor predicts the power output of the array will be 21.67 W at summer solstice after two years. This is based on an average effective area of  $1209 \text{ cm}^2$ , which would equate to a power output of approximately  $17.9 \text{ mW/cm}^2$ . This value is multiplied by the effective area computed by PANSAM

and plotted in conjunction with the power output found by FANSAM for comparison, as shown in Figure 20.

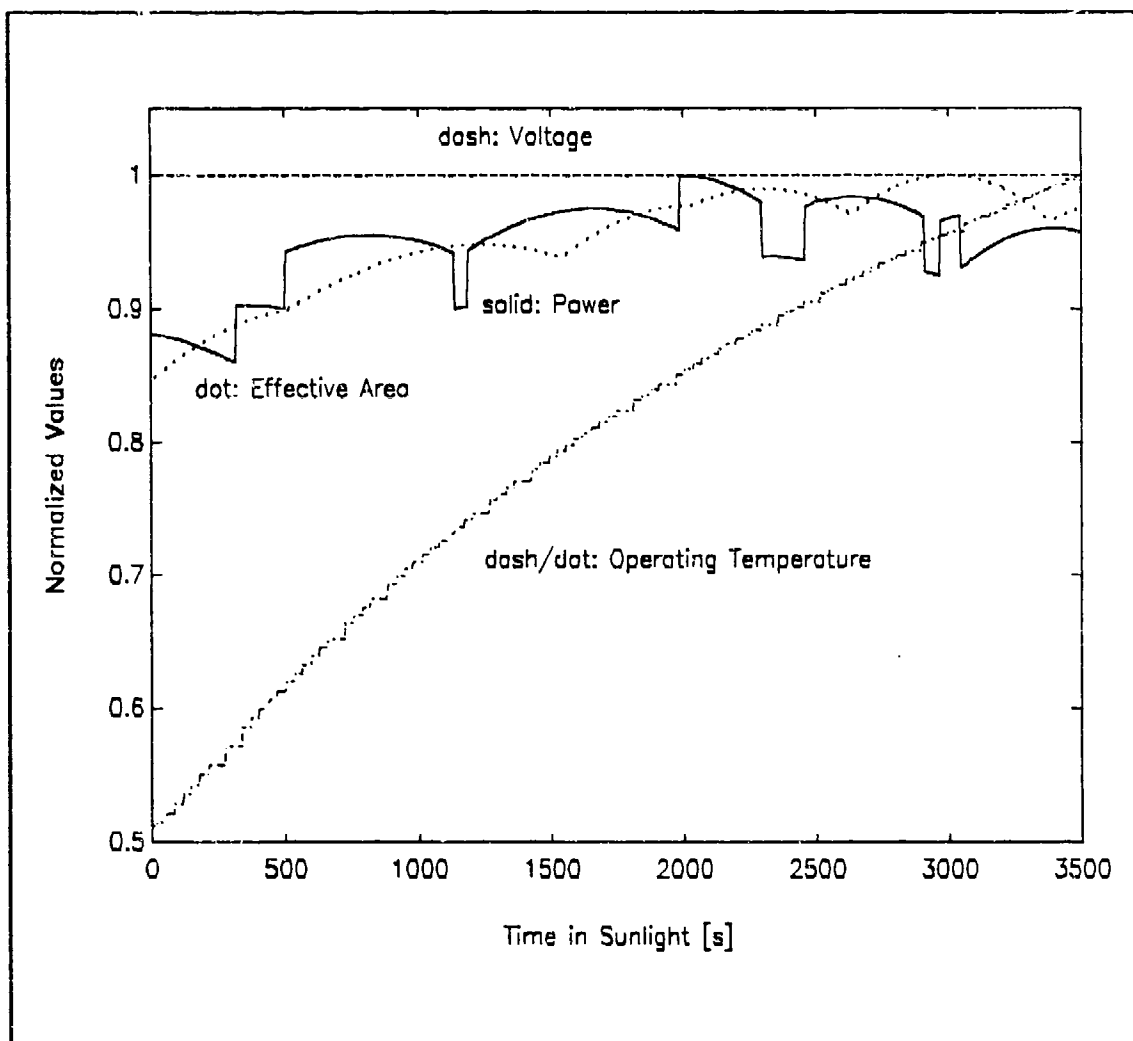


**Figure 19.** The Normalized Values of  $T_{op}$ ,  $V$ ,  $P$ , and  $A_{eff}$  Plotted for the Sunlit Portion of the Orbit

The plots of the power curve determined by PANSAM in Figures 19 and 20 indicate several discontinuities. Graphically, these discontinuities can be interpreted as a sudden increase or decrease in the amount of power generated by the solar array. Close inspection of Figure 20 indicates

the magnitude of the discontinuities are approximately 0.75 W. This equates to roughly a 4% deviation in power and is

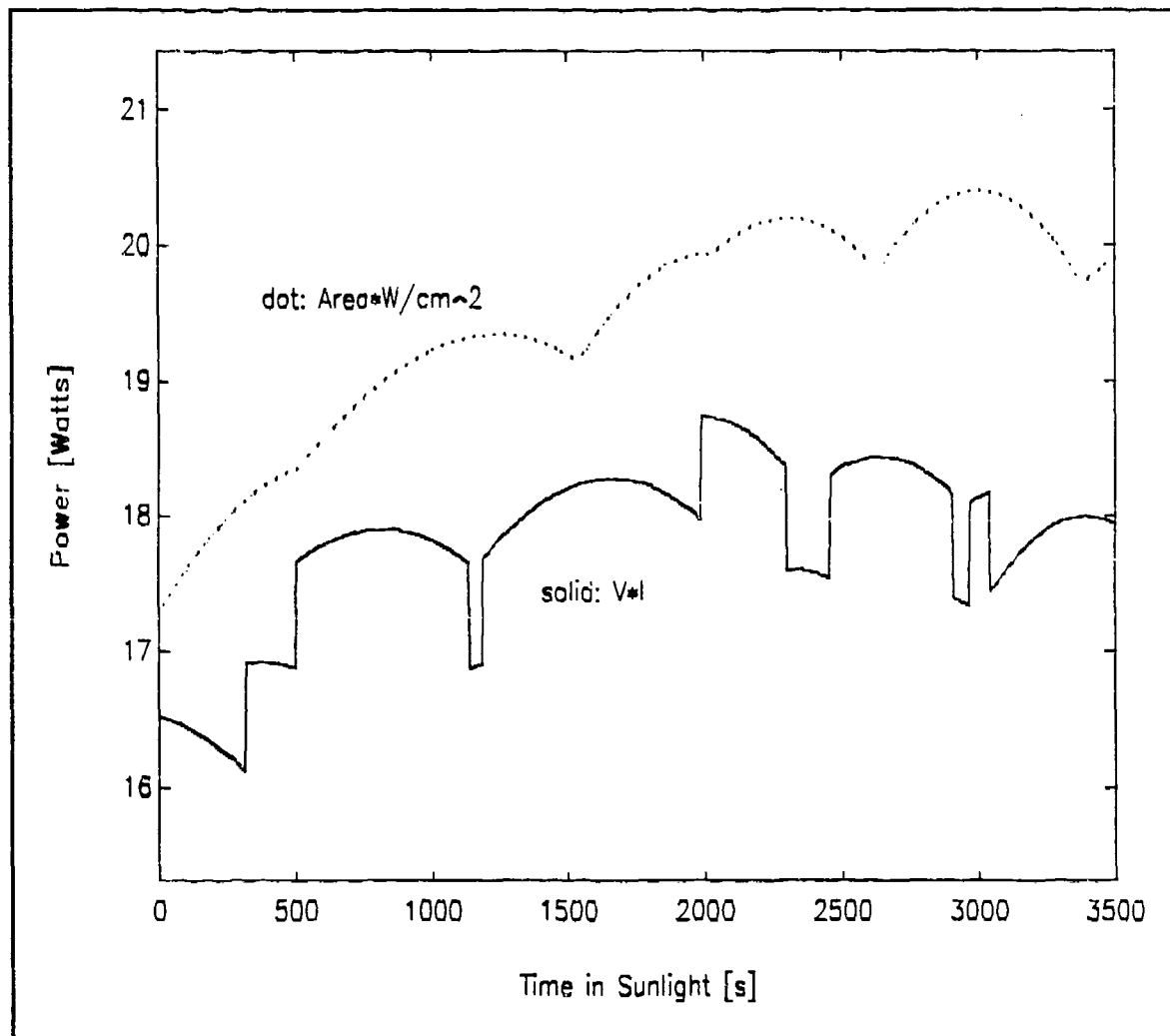


**Figure 20.** Power Output Found Using Effective Area Compared to Power Output Found by Program

considered insignificant. Note that the discontinuities occur just prior to, or just after the effective area reaches local maximum. This may result from one or more panels having enough of a sun-pointing surface area vector component to contribute to the total area. However, the corresponding

angle of incidence is large enough so that the solar array's refraction index precludes the panel(s) from contributing to the total current. That is, the size of the angle of incidence crosses a threshold causing the current of a particular panel (or panels) to either 'cut on' or 'cut off'.

Table III contains the maximum, minimum, and average values of the power computed by PANSAM, and the power obtained by the product of the effective area and  $17.9 \text{ mW/cm}^2$ , denoted as  $P_{IV}$  and  $P_A$ , respectfully. Also, the percent difference between the respective values is shown for comparison. The percent difference, between the average power of  $17.8 \text{ W}$  determined by PANSAM and the  $21.67 \text{ W}$  provided by the contractor, is  $17.7\%$ .

**Table III.** COMPARISON OF POWER OBTAINED FROM PANSAM,  $P_{IV}$ , WITH POWER CALCULATED USING EFFECTIVE AREA,  $P_A$

	$P_{IV} \text{ [W]}$	$P_A \text{ [W]}$	% Diff
Maximum	18.7	20.4	8.3
Minimum	16.1	17.3	6.9
Average	17.8	19.4	8.3

### 3. Investigation of the Worst Case

With respect to the surface temperature, the worst case for the power output will occur when the solar array



temperature is the hottest. For any orbit, this occurs just prior to entering eclipse.

When considering solar intensity, the worst case will occur during summer solstice when the solar intensity is near its lowest point, approximately 96.9% of the solar constant [Ref. 8:p. 348].

With regard to the effective area, the worst case occurs when it is minimum. This occurs when the base plate is perpendicular to the solar rays. In order to determine the orientation of PANSAT in this situation, the angles  $\Phi$  and  $\theta$  must be determined in the **A** frame. In the previously described orientation, the **q**-axis will be parallel to the **I**-axis, therefore the amount of rotation about the **q**-axis,  $\Psi$ , is arbitrary. To determine this orientation, assume the **o**-, **p**-, and **q**-axes of the **B** frame coincide with the **i**-, **j**-, and **k**-axes of the **A** frame. Referring once again to Figure 12, one can see that by rotating the **B** frame about the **p**-axis by an angle  $\theta$  equal to  $90^\circ - \gamma$ , the **q**-axis will be aligned with the **I**-axis. Therefore, the appropriate orientation will be accomplished when

$$\Psi = \Phi = 2n\pi \quad (\text{for } n = 0, 1, 2, \dots)$$

where

$$\theta = \gamma.$$

Assuming an inclination of  $28^\circ$  and a declination at summer solstice of  $23.44^\circ$ , then

$$\gamma = 28^\circ - 23.44^\circ = 4.56^\circ$$

Also, recall that the rate of rotation about each axis is  $0.02^\circ/\text{s}$  [Ref. 13] and that the altitude of the orbit is 480 Km, which means a sunlight period of approximately 3560 seconds [Appendix A]. The desired orientation at the end of the orbit's sunlight portion is

$$\psi = \Phi = 2n\pi$$

where

$$\gamma = 4.56^\circ \times \frac{\pi}{180^\circ} = 0.0253\pi \text{ [rad]}$$

By working backwards, the orientation of PANSAT upon exiting eclipse can be determined.

The entire amount of rotation about the o-axis necessary to obtain the desired orientation is determined by multiplying the rate of change by the duration of the sunlight period,  $\tau_{\text{sun}}$ . The resulting product is subtracted from the final position,  $\Phi_f$ , to obtain the initial orientation,  $\Phi_i$ .

That is

$$\begin{aligned}\Phi_i &= \Phi_f - \dot{\Phi} \times \tau_{sun} \\ &= 3600 - 0.020/s \times 3560s \\ &\approx 1.6\pi\end{aligned}$$

Because  $\Psi_f = \Phi_f = 2\pi$  then  $\Psi_i = \Phi_i = 1.6\pi$ .

Using the same approach to find  $\theta_i$  results in

$$\begin{aligned}\theta_i &= \theta_f - \dot{\theta} \times \tau_{sun} \\ &= 900 - \gamma - \dot{\theta} \times \tau_{sun} \\ &= 900 - 0.020/s \times 3560s \\ &\approx 0.079\pi\end{aligned}$$

Using  $\Psi_i$ ,  $\Phi_i$ , and  $\theta_i$  defined above to obtain the initial orientation for the worst case scenario, PANSAM was run for summer solstice after two years. The parameters  $T_{op}$ ,  $V$ ,  $P$ , and  $A_{eff}$  were normalized and plotted together as shown in Figure 21.

As with the case for a typical orbit, the effective area is multiplied by  $17.9 \text{ mW/cm}^2$  and plotted with the power output found by PANSAM as shown in Figure 22. Table IV contains the maximum, minimum, and average values of the power computed by the program, and the power obtained by the product of the effective area and  $17.9 \text{ mW/cm}^2$ , denoted as  $P_{IV}$  and  $P_A$ , respectfully. Percent differences are shown for comparison.

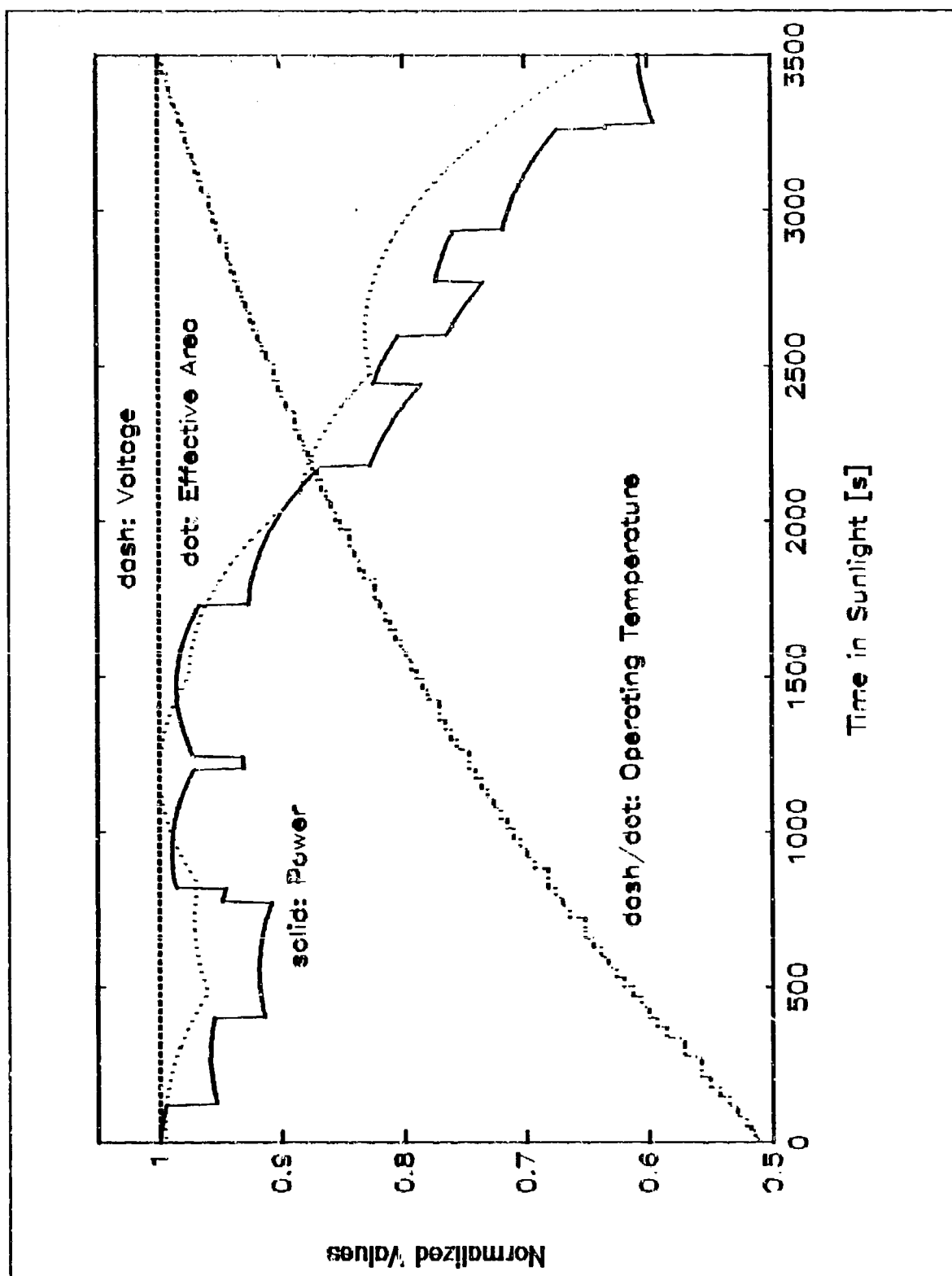
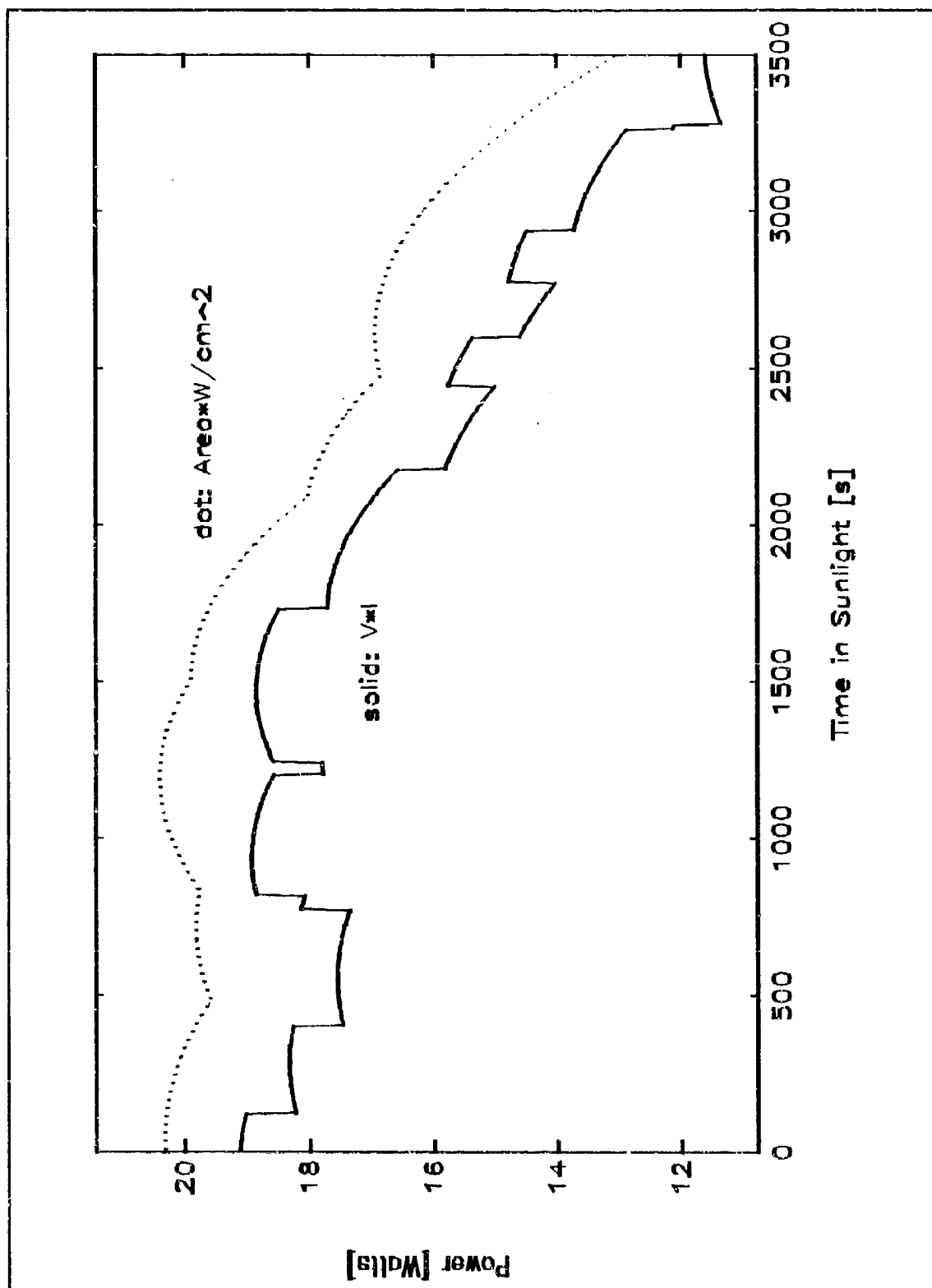


Figure 21. The Normalized Values of  $T_{op}$ ,  $V$ ,  $P$ , and  $A_{eff}$  Plotted for the Sunlit Portion of the Orbit.



**Figure 22.** Power Output Found Using Effective Area Compared to Power Output Found by PANSAM.

**Table IV.** COMPARISON OF POWER OBTAINED FROM PROGRAM,  $P_{IV}$ ,  
WITH POWER CALCULATE USING EFFECTIVE AREA,  $P_A$

	$P_{IV}$ [W]	$P_A$ [W]	% Diff
Maximum	19.1	20.4	6.3
Minimum	11.4	12.5	8.9
Average	16.5	18.3	9.8

#### IV. POWER CONDITIONING and CONTROL SUBSYSTEM (PCCS)

##### A. INTRODUCTION

Power for PANSAT is furnished by the solar array as the primary power source in conjunction with two Ni-Cd batteries acting as the secondary power source. The power is utilized by EPS regulatory circuitry to (1) charge and discharge the batteries, and (2) condition the power in order to meet the necessary power requirements for housekeeping, communication, and control. This regulatory circuitry comprises the power conditioning and control subsystem (PCCS).

The EPS will employ the centralized, hybrid regulation scheme shown in Figure 23 to supply power to the individual subsystems of PANSAT. The PCCS design stressed simplicity in order to increase reliability.

Since the maximum power supplied by the solar array is within acceptable levels, there is no regulation scheme provided to shunt excess power and regulate the main bus. The main bus voltage will be determined by the load which include the DC/DC converters and the battery charge circuits. Both the battery charge regulator (BCR) and the battery conditioning circuitry (BCC) will employ transistors to act as on/off switches. The transistors will be controlled by the C&DH (control and data handling) microprocessor to either

activate or deactivate each regulator depending on its operation mode.

The subsequent sections discuss the various alternatives investigated while considering designs for implementing the

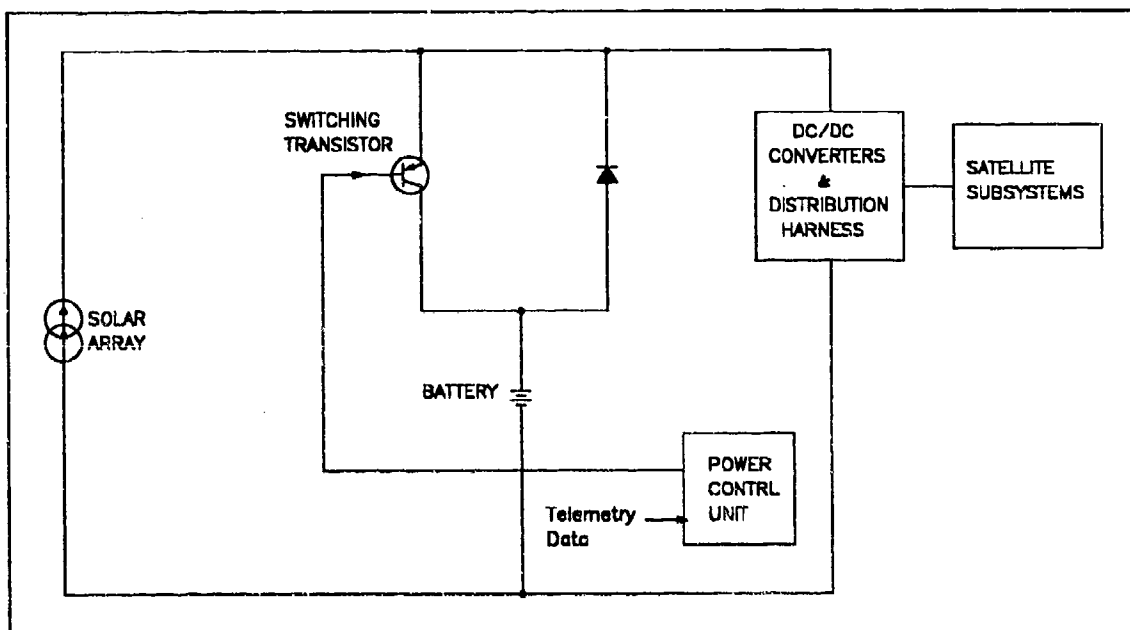


**Figure 23.** Block Diagram of the Hybrid Regulation Scheme Used for PANSAT

PCCS. These sections are followed by an explanation for the method selected to implement the PANSAT PCCS. Finally, a description of the operation of the PCCS is provided.

## **B. POWER BUS**

### **1. Regulation Topologies**

Three basic bus regulation topologies were considered for PANSAT: (1) regulated, (2) partially regulated, and (3) unregulated.



**a. Regulated Bus**

Figure 24 depicts the concept of a fully regulated bus with a simple block diagram. In the regulated configuration, the distribution bus is isolated from the energy source by regulators which regulate the voltage during both sunlight and eclipse periods. While the satellite is in

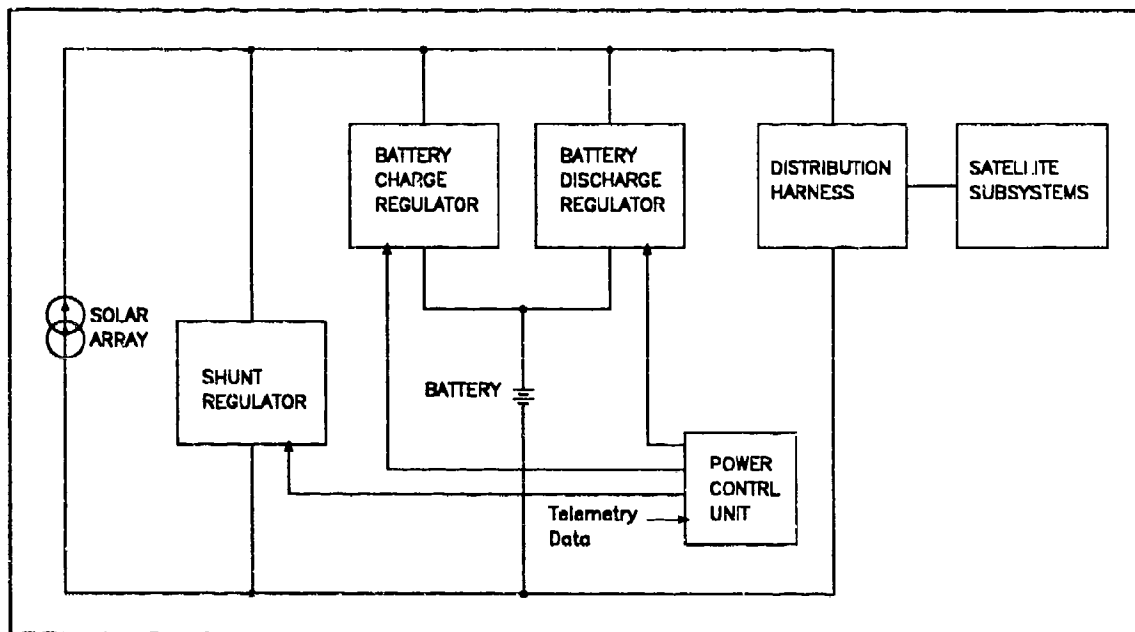


**Figure 24.** Block Diagram of Fully Regulated Configuration

sunlight, the solar array voltage is regulated by a shunt regulator. During eclipse, the discharge voltage of the battery is regulated by a discharge voltage regulator. The discharge voltage regulator results in a decrease in the discharge efficiency because of the increase in power control electronics. Furthermore, there is an increase in thermal dissipation. [Ref. 8:p. 368]

### *b. Partially Regulated Bus*

A partially regulated bus (Figure 25) is similar to a fully regulated bus. During the sunlight portion of the orbit, the solar array voltage is regulated by a shunt regulator and a battery charge regulator is incorporated to charge the battery during the orbit day. However, the discharge voltage regulator is replaced with a diode so that, during eclipse, the bus voltage is unregulated.

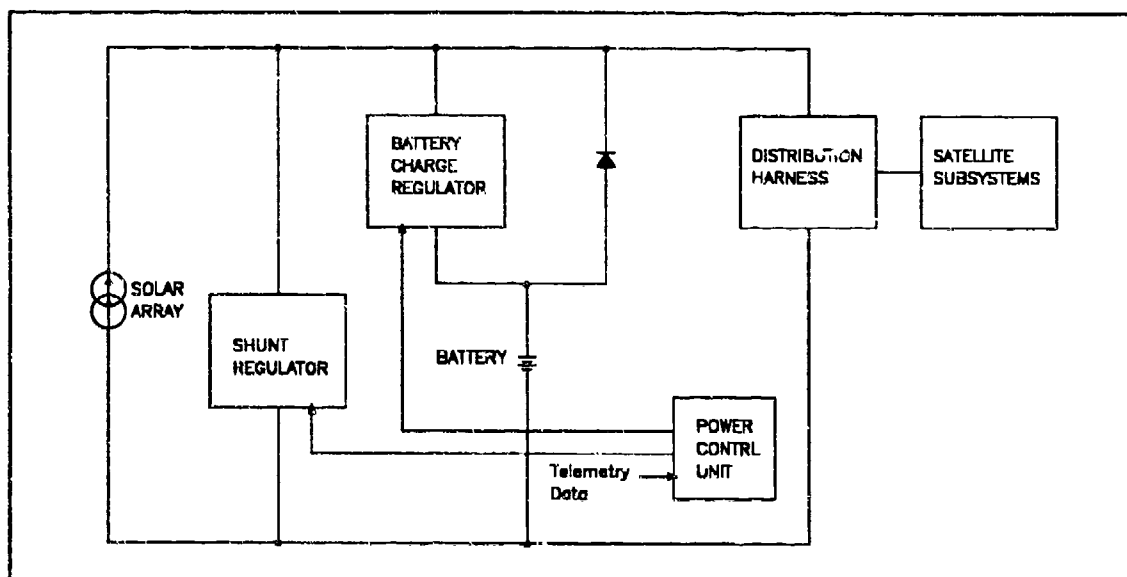
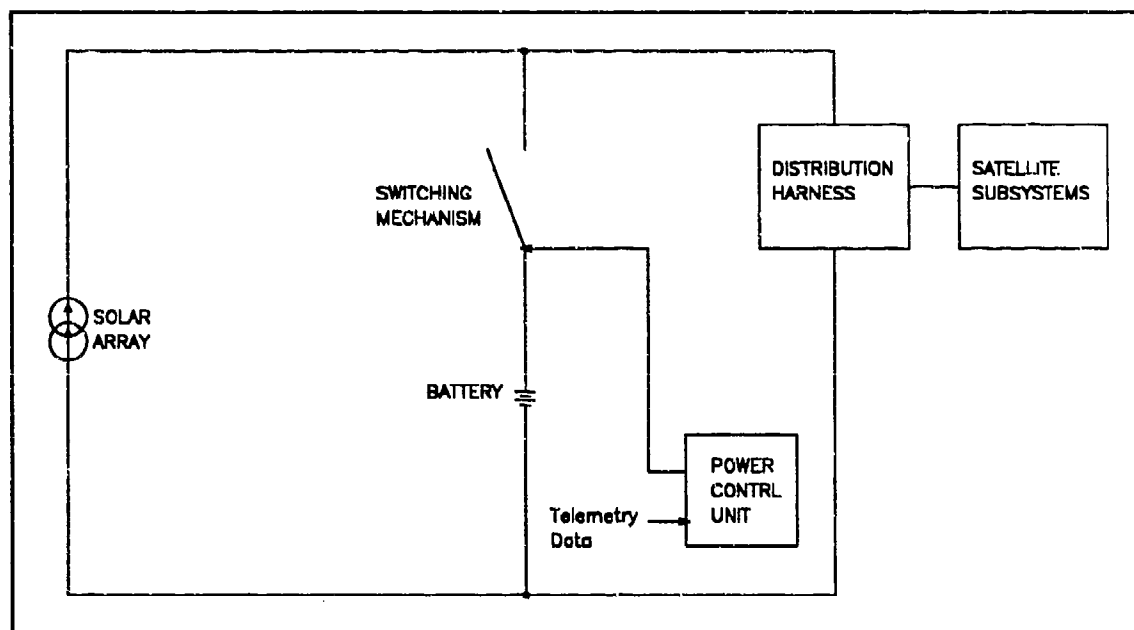


Figure 25. Block Diagram of the Partially Regulated Bus.

### *c. Unregulated Bus*

The basic configuration of an unregulated bus is depicted in the block diagram in Figure 26. In this configuration, the solar array and batteries are connected directly to the distribution bus. As a result, if the satellite is in the sunlight phase, and the batteries are not being charged, the distribution bus voltage assumes the value

of the solar array voltage. If in eclipse or the battery is being charged, the distribution bus voltage assumes the value of the battery. Figure 26 illustrates that the control unit turns the switch on if the battery is being charged or discharged. The primary advantage to the unregulated bus is



**Figure 26.** Block Diagram of an Unregulated Bus.

the simplicity in the hardware to implement it. The main disadvantage is that the distribution bus can fluctuate a great deal. For example, prior to exiting eclipse, the bus voltage is set by the voltage of the batteries after discharge; upon entering sunlight the bus voltage is determined by the cool solar array, which is producing its maximum power. This results in a large step voltage increase on the bus. Additionally, the solar array voltage is

dependent on its temperature and its aspect to the sun; therefore, the bus voltage will vary with the solar array voltage.

## **2. Centralized Versus Decentralized**

Regardless of whether the spacecraft power bus is regulated or unregulated, the individual subsystems of the spacecraft may require a variety of input-voltage needs. For example, each subsystem may require an input voltage which is higher, lower, or the inverse of the bus voltage. This alteration of the bus voltage is achieved by the appropriate use of DC/DC converters. If the power conditioning takes place at the individual loads, the system is decentralized. However, if the power system is conditioned prior to reaching the power distribution harness, it is centralized.

PANSAT has only three major subsystems, and their combined voltage input needs include +15, -15, and +5 Vdc. Additionally, PANSAT's small size allows the loads to be in close proximity of the EPS. Therefore, because each subsystem has the same voltage requirements and the distribution bus is relatively small, the centralized scheme was chosen for PANSAT.

## **C. DESIGN CONSIDERATIONS FOR THE PANSAT PCCS**

### **1. Overview**

The PANSAT EPS will employ a centralized bus which combines the partially regulated and unregulated bus concepts into a hybrid regulation scheme. The contribution from the

unregulated concept is that there is no shunt regulator and the battery is charged via a C&DH microprocessor controlled switching transistor instead of a regulator. The portion borrowed from the partially regulated concept is that the battery discharges onto the bus via a diode vice a regulator or switching mechanism. A simplified block diagram for the PANSAT hybrid regulation concept appears in Figure 23.

## **2. Dissipative and Nondissipative PCCSs**

The PCCS can be divided into two major categories based on their working principle: (1) dissipative; and (2) nondissipative systems. The dissipative system does not extract maximum power from the solar array; the unused power is dissipated. In contrast, the nondissipative system extracts maximum power from the solar array, and thus dissipates less power. [Ref. 17:p. 114]

### **a. Dissipative PCCS**

The dissipative system can be further sub-categorized depending on whether it employs a regulated or partially regulated bus, as previously discussed. A simplified schematic of a dissipative system used in conjunction with a regulated bus is shown in Figure 24. During sunlight, the power from the solar array is used by the satellite subsystems, and for charging the battery. While the battery is charging, the BCR is primarily responsible for regulating the bus voltage. When the satellite is in eclipse, or the power demand exceeds the solar array output, the

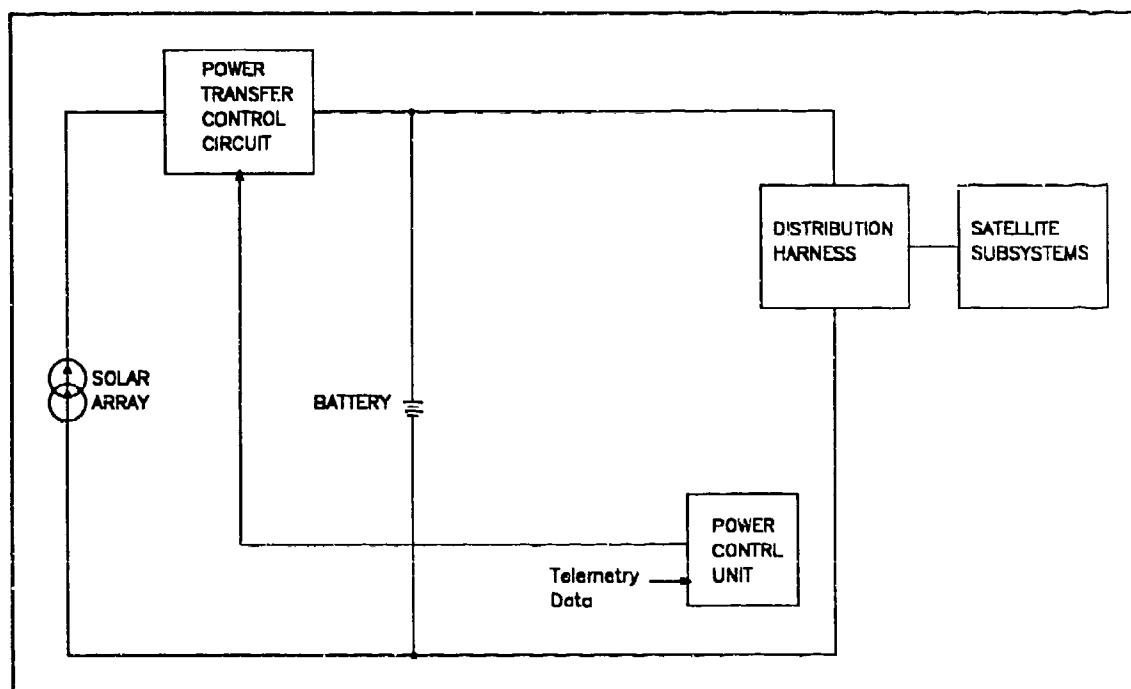
battery discharge regulator (BDR) provides power from the battery to the bus and regulates the bus voltage. The power to the load comes directly from the solar array. Therefore, this arrangement is also referred to as a *direct energy transfer* (DET) power system. [Ref. 17:p. 115]

Figure 25 shows a simplified block diagram of a dissipative system used with a partially regulated bus. As in the case with regulated bus dissipative power system, the BCR regulates the bus while the battery is charging and the SR sheds excess power once the battery is charged. However, during discharge, the battery is connected directly to the bus via the diode.

***b. Nondissipative PCCS***

The nondissipative system can also be further subclassified depending on whether it employs a regulated or unregulated bus, as previously discussed. A simplified schematic of a nondissipative unregulated bus power system is shown in Figure 27. For this configuration, a maximum power transfer control circuit is used to load the solar array at or near the maximum power point (MPP) of the solar array's *I-V* curve. [Ref. 17:p. 115] The output of the circuitry is used to charge the battery as well as supply power to the satellite subsystems. Once the battery is fully charged, the circuitry electronically moves the operation of the solar array off the MPP and toward the open circuit voltage. The bus voltage varies as the battery is charged or discharged. For the case

of the nondissipative regulated bus power system, an additional regulator is added to regulate the bus, as shown in Figure 28. [Ref. 17:p. 129]



**Figure 27.** A Simplified Schematic of a Nondissipative Unregulated Bus Power System.

The discussion above indicates that regulators are important components in a PCCS, regardless of the configuration used. Therefore, the most commonly used regulators will be investigated in the next section.

### 3. Types of Regulators

One of the major components of the PCCSs examined thus far is the regulator. Regulators can also be classified as either dissipative (linear) or nondissipative (switch-mode).

### a. Dissipative Regulators

Dissipative regulators can be separated into series or shunt type regulators. The shunt regulator (SR) shunts any current from the solar array that is in excess of

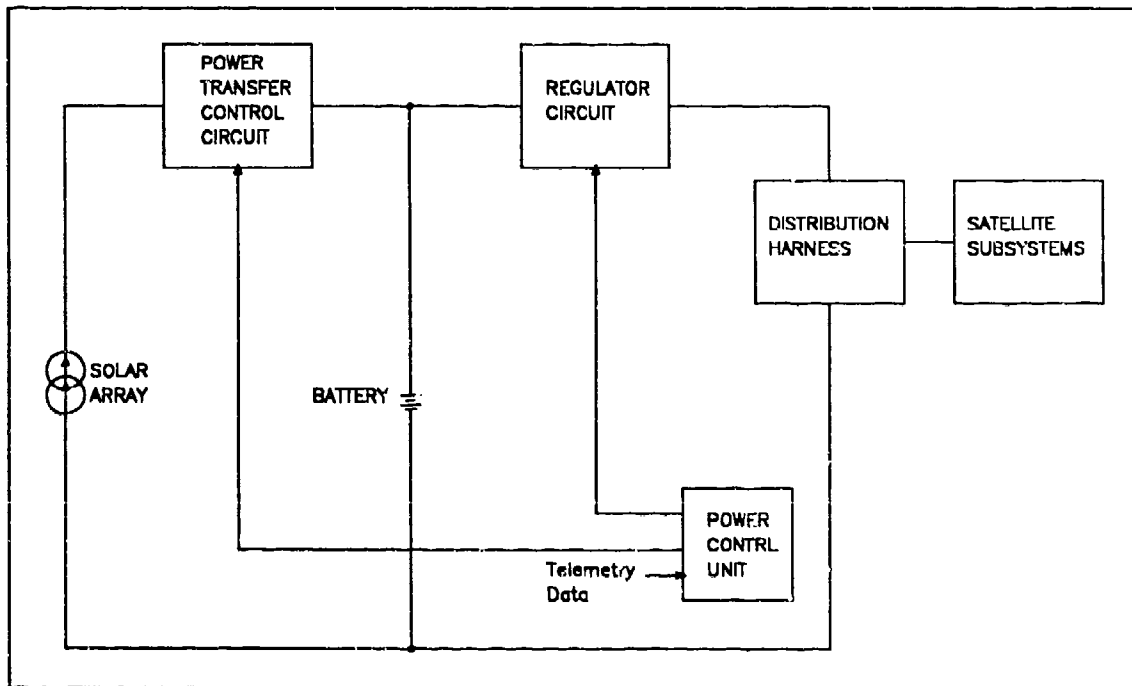


**Figure 28.** A Simplified Schematic of a Nondissipative Regulated Bus Power System

the current required by the satellite subsystems and for charging the battery. The SR is intended to maintain the bus voltage at a predetermined value regardless of changes in the current demand. There is a variety of ways to implement the shunt regulator, however, they are all fundamentally the same in functionality, and can be represented by the schematic in Figure 29. Basically, the bus voltage is compared to a reference voltage,  $V_{REF}$ , and if the bus voltage exceeds the



predetermined value, the amplified difference switches the transistor on and the excess current is shunted through the transistor. [Ref. 17:p. 118]

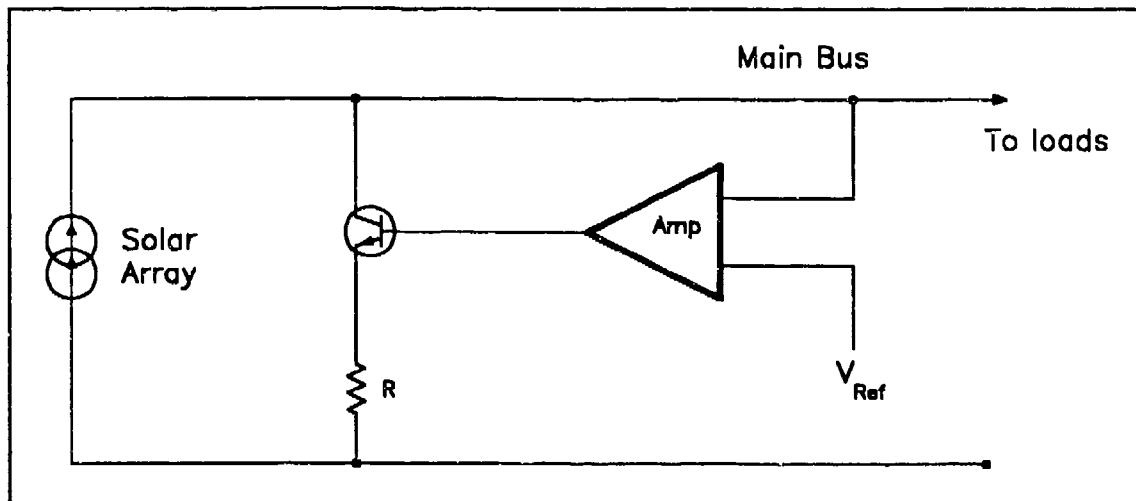


**Figure 29.** Simple Schematic of a Shunt Regulator

Figure 30 is a schematic diagram for the series regulator. As with the shunt regulator, the bus voltage is

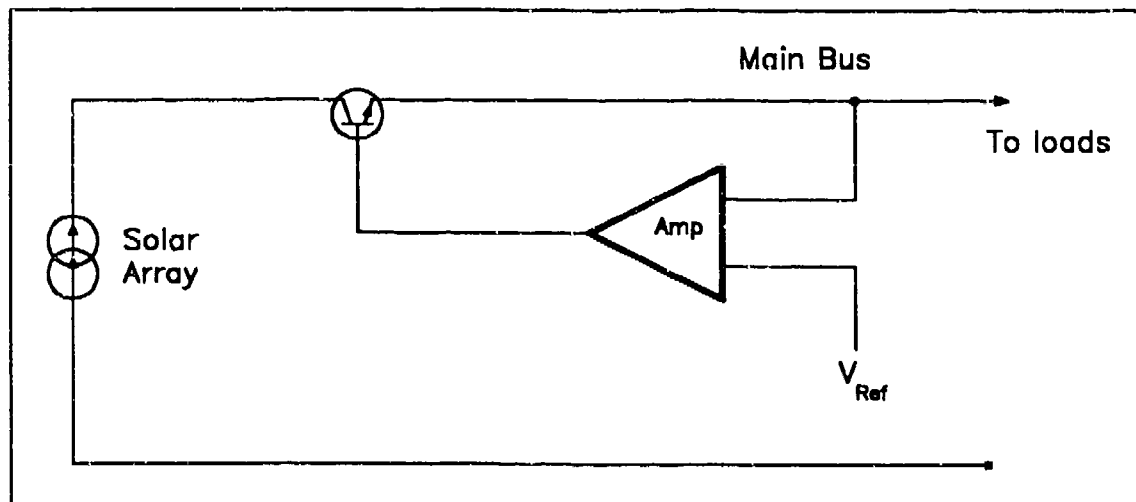


**Figure 30.** Simple Schematic of a Series Regulator

compared with a predetermined reference voltage and the voltage difference is amplified, and used to bias a pass

transistor. The pass transistor in series with the solar array and the load in contrast to the shunt which places the transistor in parallel with the solar array and the load. [Ref. 8:p. 360]

#### ***b. Nondissipative Regulators***

Nondissipative type regulators operate in a switching mode and their output voltage can be less than, equal to, or greater than the input voltage. In each case, the output voltage is compared to a reference voltage, and in many cases the difference is used to generate a pulse width modulated (PWM) signal. [Ref. 17:p. 116].

The PWM signal is normally at a fixed frequency and the switching device is usually a power BJT or MOSFET. The duty cycle,  $D$ , is the ratio of the time the switch is on,  $t_{ON}$ , to the total period,  $T$ , that is

$$D = \frac{t_{ON}}{T}$$

The duty cycle can be increased or decreased to regulate the length of time the switch is off and on, hence the phrase: *pulse width modulated*. The three types of switch-mode regulators considered were the buck, boost, and buck-boost.

The circuit diagram for a buck regulator is given in Figure 31. Circuit analysis yields the average output

voltage,  $V_{OUT}$ , of

$$V_{OUT} = DV_{IN}$$

where  $0 < D < 1.0$  and  $V_{IN}$  the input voltage. Therefore, the output voltage is **always less** than the input voltage. [Ref. 18:pp. 190-192]

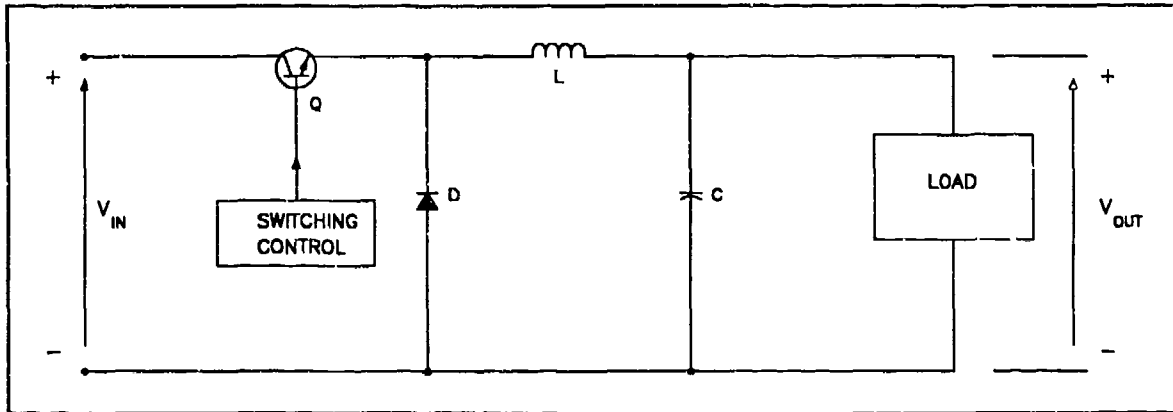


Figure 31. The circuit diagram for a buck regulator

The circuit diagram for a boost regulator is given in Figure 32. An analysis of the circuit yields the average output voltage,  $V_{OUT}$ , of

$$V_{OUT} = \frac{V_{IN}}{1 - D}$$

where  $0 < D < 1.0$  and  $V_{IN}$  is the input voltage. Therefore, the output voltage is **always greater** than the input voltage. [Ref. 18:pp. 193-195].

The circuit diagram for a buck-boost regulator is given in Figure 33. An analysis of the circuit yields the average output voltage,  $V_{OUT}$ , of

$$V_{OUT} = -\frac{D}{1-D} V_{IN}$$

where  $0 < D < 1.0$  and  $V_{IN}$  is the input voltage. A buck-boost

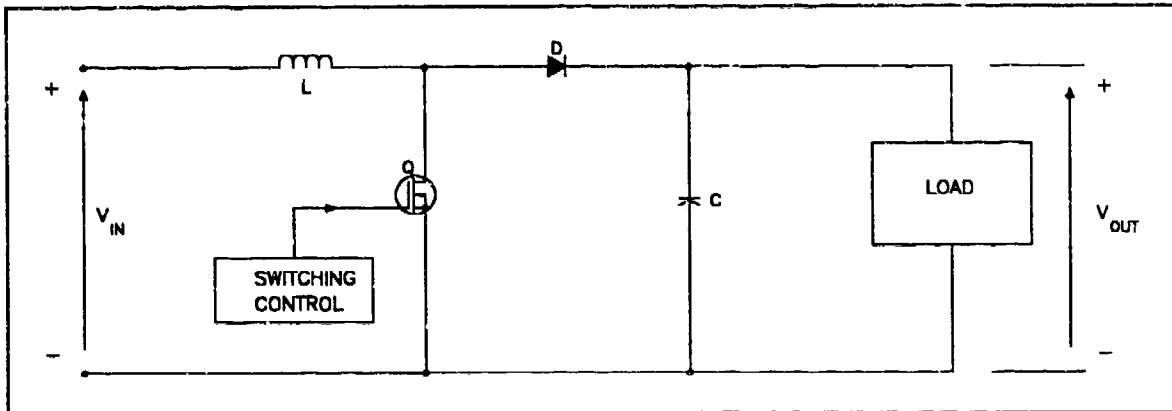


**Figure 32.** The circuit diagram for a boost regulator regulator can provide an output voltage which can be less than, greater than, or equal to, the input voltage. The

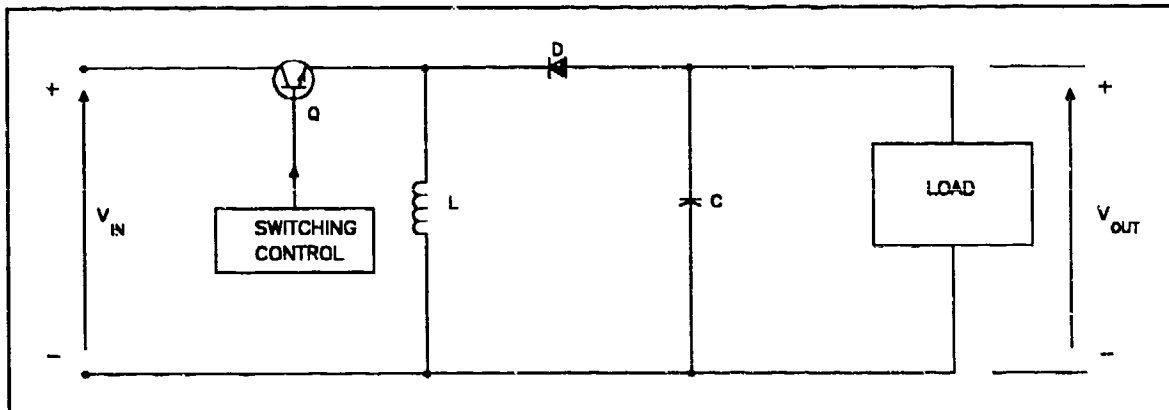


**Figure 33.** The circuit diagram for a buck-boost regulator polarity of the output voltage is opposite to that of the input voltage. [Ref. 18:pp. 196-198]

#### 4. PCCS Topology Selection for PANSAT

The voltage requirements for the PANSAT subsystems are +15, -15, and +5 Vdc. The Datel TWR 5/1000-15/200-D12 is a triple output DC/DC converter presently being considered to furnish these requirements for the PANSAT subsystems. The input specifications for the Datel DC/DC converter include a voltage range of 9 V to 18 V and a full load output current of 1.12 A. Since the solar array of PANSAT cannot exceed these specifications even under the best of conditions at BOL, a shunt regulator is unnecessary.

The battery charge regulator (BCR) can be implemented with any of the regulators discussed in the previous section. Because the C&DH microprocessor can provide a PWM signal, the nondissipative switch-mode regulators were initially considered because of their high efficiencies and low heat dissipation. The buck-boost regulator was the first choice because of its ability to step-up or step-down the voltage. However, it was eliminated because its output would have to be inverted. This would lead to additional power loss and complexity (decreasing reliability). The need to step down the voltage from the solar array is unlikely. This led to the dismissal of the buck regulator. With regard to the boost regulator, its transistor would be in shunt with the battery making it difficult to protect against a short circuit. To increase the reliability of the BCR, the decision was made to decrease the complexity by not using a PWM driven regulator.

Instead, a single power transistor would be used as an on/off switch controlled by the C&DH microprocessor.

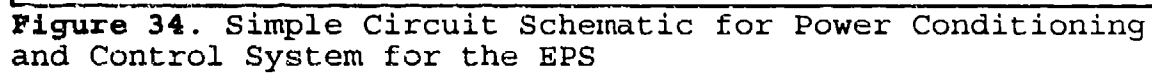
The BDR is usually implemented with a boost-type switching regulator, which boosts the battery voltage to the bus voltage level and maintains it [Ref. 19:p. 155]. For PANSAT, it will not be necessary to boost the battery voltage. Therefore, the battery is connected directly to the bus via a diode.

The result of the discussion above is a scheme which combines the partially regulated and unregulated bus concepts into a hybrid regulation topology used in conjunction with a centralized bus as shown in Figure 23. In the next section, the simplified circuit diagram of the proposed PCCS for PANSAT is given along with a brief description of the circuit.

#### **D. DESCRIPTION OF OPERATION**

A simple schematic of the circuit used to implement the PCCS described in the previous section is shown in Figure 34. An isolation diode connects each solar panel to the power bus. Denoted as components D1 through D17, these diodes are used to prevent current from flowing into shadowed or partially illuminated solar panels. The resistor R1 is a precision resistor of about 0.01 to 0.05 Ohms. The voltage drop across R1 is amplified to provide the C&DH microprocessor with the charge current entering the battery being charged.

The components Q1\_BC1, Q2\_BC1, R2, R3, C1, L1, and D18 comprise the BCR for battery, B1. Component Q1\_BC1 is the power transistor used as an on/off switch to provide current



flow for charging battery B1. The transistor, Q2\_BC1, is controlled by the C&DH microprocessor to switch Q1\_BC1 on and off. The resistors R2 and R3 are used for biasing the transistors. When PANSAT passes from eclipse into sunlight, the bus voltage can jump from 9 V to nearly 16 V as the energy source changes from the discharged batteries to the cool solar array. The inductor, L1, and the capacitor, C1, constitute an LC filter to smooth this voltage jump from a step to a ramp function, in order to guard against instability in the DC/DC converter input. As Q1\_BC1 is switched from on to off, a rapid change in the current through L1 could result in a circuit damaging voltage spike across the inductor due to the relationship

$$V_L = L \frac{di}{dt}$$

To prevent this, a *free-wheeling* diode, D18, was included in the circuit to allow the energy stored in the magnetic field of the inductor to dissipate at an acceptable rate.

The battery is connected directly to the bus via diode D19 so the battery can furnish power for the EPS during eclipse. Except for a small voltage drop across the diode, D19 permits uninhibited power flow unto the bus while preventing current flow from the bus to the battery. Additionally, the diode prevents the battery, B2, from discharging into B1.

The resistor R4 and transistor Q\_BCC1 are used to discharge B1. This is to allow periodic battery conditioning



to guard against memory effects associated with Ni-Cd batteries [Ref. 8:p. 353].

The battery B2 offers redundancy to PANSAT EPS. The components Q1\_BC2, Q2\_BC2, R5, R6, C2, L2, and D20 serve the same function with regard to B2 as Q1\_BC1, Q2\_BC1, R2, R3, C1, L1, and D18 do for B1, respectively. Similarly, D21 is analogous to D19, and R7 and Q\_BCC2 are analogous to R4 and Q\_BCC1.

## V. BATTERIES

### A. INTRODUCTION

The battery is intended to supply power to the satellite during launch and for each eclipse. In addition, if necessary, the batteries will supplement the solar array during peak power usage. Nickel-cadmium (Ni-Cd) is the type battery selected for use by PANSAT. A second Ni-Cd battery will be used to provide redundancy for the system. Each battery will be constructed from nine-1.25 V, 5.0 Ah, series connected cells. Therefore, each battery will be rated at 11.25 V and 5.0 Ah at BOL.

The design was conducted for the worst case scenario of one battery failure. Under these circumstances, the remaining battery must be capable of providing power to spacecraft subsystems during the each eclipse phase for the entire mission life.

As discussed in the previous chapter, the batteries are connected to bus via diodes instead of regulators or transistors. This is to ensure reliability. Therefore, the battery with the lowest voltage will establish the bus voltage. The solar array of PANSAT can provide approximately 15 Vdc. The batteries will consist of nine cells each to ensure recharge voltage requirements can be met. The minimum battery voltage at EOL is predicted to be 10.3 Vdc at the end of eclipse (for single battery operation). Limiting the

number of cells in each battery to nine ensures the bus voltage remains adequate for recharging the batteries during the sunlight portion of the orbit. If this were not the case, the solar array would be unable to maintain the bus voltage above the battery voltage. Therefore, whichever battery was not being charged (assuming it is fully charged) would discharge onto the bus and into the battery being charged.

#### **B. SELECTION OF THE NICKEL-CADMIUM (Ni-Cd) BATTERY**

There are many varieties of secondary batteries available for commercial use. The four primary candidates for PANSAT are: lead acid (Pb-Acid), nickel-cadmium (Ni-Cd), nickel-hydrogen (Ni-H<sub>2</sub>), and nickel-metalhydride (Ni-MH).

The Ni-MH battery was eliminated from consideration because, as of this writing, it has not been flight tested in a satellite. Therefore, its reliability is questionable. The sealed Pb-Acid battery was initially considered the primary choice for PANSAT [Ref. 8:p. 64]. NASA requires terrestrial batteries, such as the sealed Pb-Acid battery, to be in a sealed battery box designed and built with very stringent safety criteria. A box similar to the one designed by the SSAG for the space thermoacoustic refrigerator (STAR) experiment was initially proposed for use. [Ref. 8:p. 76]. However, the box built for STAR was quite massive and extremely expensive [Ref. 20]. Considering the desired redundancy for the batteries in PANSAT, two boxes would be

prohibitive in mass, volume, and cost. As a result, the sealed Pb-Acid battery has been eliminated from consideration.

Although Ni-H<sub>2</sub> are proven aerospace batteries, they were eliminated because of their high cost in comparison to the other candidates. Additionally, they have not been used on-board a LEO spacecraft [Ref. 17:p. 112].

Although the four candidate batteries were narrowed to the Ni-Cd battery by the process of elimination, the Ni-Cd battery is an excellent choice by its own merit. Some of the advantages of the Ni-Cd battery include [Ref. 21:pp. 35-37]:

- high energy density
- fast charge capability (recharge in less than an hour)
- capable of a high number of charge/discharge cycles
- capable of operating over a wide range of temperatures
- continuous overcharge capability.

Additionally, Ni-Cd batteries constructed of Ni-Cd aerospace cells have proven reliable on several space missions.

### **C. BATTERY CONCEPTS AND CONSTRUCTION**

A storage cell is an electrochemical device that stores energy in the chemical form and this chemical energy is converted into electrical energy during discharge [Ref. 17:p. 104]. A battery is constructed from individual storage cells. Manufacturers usually produce storage cells with standard ampere-hour (Ah) ratings and cell voltages. A specified number of cells with the selected Ah rating can be placed in

series to produce a battery with the desired voltage. Similarly, a specified number of cells can be placed in parallel to provide the desired ampere-hour rating.

### **1. Primary vs Secondary**

If the chemical changes within the storage cell have exhausted one or both of the electrodes, and if the active materials cannot be regenerated by passing an electric current through the cell in the reverse direction, the storage device is considered a *primary cell*. Primary cells are not rechargeable. The reaction is reversible if the chemical reaction can be reversed by causing current to flow into the cell and the capacity can be completely restored. Therefore, a storage cell that is reversible is a *secondary cell*. [Ref. 22:pp. 4-5]

### **2. Nickel-Cadmium Battery Fundamentals**

Storage cells generally consist of three major components; a positive electrode or cathode, a negative electrode or anode, and a chemical bath or electrolyte. Also, a casing to contain the electrodes and electrolyte is associated with the battery cell. A potential difference is established when the electrodes are immersed in the electrolyte. When a load is externally connected between the electrodes, the potential difference causes current to flow from the cathode to the anode. The cathode is reduced by the absorption of electrons, which are released by the oxidation of the anode. [Ref. 22:pp. 1-2]

Cathodes are typically metallic oxides. Anodes are, without exception, metals, which are corrodible in varying degrees in the electrolyte [Ref. 22:p. 5]. Many different batteries, with a variety of characteristics, have been produced by using various materials for the anode, cathode, and electrolyte.

The nickel-cadmium (Ni-Cd) battery cell is comprised of four basic components: a cathode made of nickel; an anode made of cadmium; an aqueous electrolyte, which is a solution of 35% potassium hydroxide (KOH); and a separator made of nylon or perhaps of polypropylene, which holds the electrolyte in place and isolates the electrodes. [Ref. 8:p. 350]

### 3. Capacity

A battery is rated according to its capacity,  $C$ , given in units of ampere-hours (Ah). Multiples of  $C$  represent the ability of a battery to provide a certain value of current over the corresponding period of time. Battery charge and discharge rates are expressed by these multiples of the " $C$ " rate. A battery discharging at a multiple of one ( $1C$ ) will expend its nominal capacity in one hour. For example, a 10-Ah-capacity battery will provide 10 A for one hour if the rate is  $C$ . Furthermore, at the  $0.25C$  rate, the rated capacity will be delivered in about 4 hours and at the  $4C$  rate in about 0.25 hour [Ref.8:p. 351].

#### **4. Depth of Discharge (DOD)**

Depth of discharge (DOD) is defined as the capacity removed from the battery divided by its actual capacity, expressed as a percentage [Ref. 21:p. 274] For satellites in LEO averaging approximately 5500 orbits per year, the maximum recommended DOD is 25%. However, the manufacturers suggest using a DOD as low as 10%. [Ref. 25] A more shallow DOD allows a greater number of charge/discharge cycles and prolonged battery life. However, given a desired discharge current, a shallower DOD requires a higher capacity,  $C$ , in to supply the desired current. This results in an increase in the weight and volume of the battery.

Assuming a DOD between 10 and 25%, the battery required for PANSAT would be between 8.0 and 3.2 Ah, respectively (Appendix D). In an attempt to minimize battery costs, a standard capacity of 5.0 Ah is recommended for use.

#### **5. Performance Characteristics**

The properties of importance for all secondary batteries, are:

- energy density
- discharge properties
- charge characteristics
- charge retention
- life
- mechanical stability.

#### ***a. Energy Density***

The energy density of a battery is defined as the amount of energy available per unit of battery weight or volume. The energy density is dependent on the theoretical electrochemistry of the system, the utilization of the active materials involved, the internal cell design and the cell arrangement in the battery. [Ref. 22:p. 339] Energy density is generally expressed as watt-hours per kilogram [Wh/Kg] at any specified rate of discharge [Ref. 22:p. 5]. Typical energy density values for Ni-Cd batteries range from 22 to 26 W-h/Kg [Ref. 8:p. 350].

#### ***b. Discharge Properties***

The discharge parameters of primary concern are cell (or battery) voltage and capacity. The voltage of a Ni-Cd cell remains relatively constant until most of its capacity is discharged, at which point the voltage drops off sharply [Ref. 21:p. 39].

Discharge rate and temperature greatly influence the discharge characteristics of electrochemical cells. Increased rate and low temperature result in lower cell voltage and decreased capacity during discharge. However, Ni-Cd cells are far less influenced by these parameters than others systems, such as Pb-Acid cells. Ni-Cd cells can be effectively discharged at high rates without losing very much of the rated capacity and they can be operated at both high and low temperatures. [Ref. 22:pp. 339-340]



### c. Charge Characteristics

In a typical orbit, PANSAT will be in sunlight for approximately one hour. Therefore, the EPS must be able to charge both batteries in roughly one hour. Typically, this is achieved using the *fast-charge* method of charging. The term *fast-charge* applies to charging techniques which permit the battery to be charged at the 1C rate or greater resulting in a full charge in one hour or less [Ref. 21:p. 78]. Ni-Cd cells are unable to sustain indefinite overcharge at fast-charge rates. Therefore, fast-charging schemes require terminating the high-rate charge prior to the battery receiving excessive overcharge.

In the case of PANSAT which requires 3 Ah to 8 Ah batteries, a 1C rate would demand a solar array output current of 3 A or 8 A, respectively. Assuming the best conditions, PANSAT's solar array current output will average roughly 1.34 A. This is far less than the current required for a fast-charge. Therefore, *float-charge* is the recommended method for charging the batteries.

Although the selection of the battery charge control method will not be addressed in this thesis, a voltage and temperature sensing control method of *float-charge* is recommended. This recommendation is based on the availability of the voltage and temperature of each battery as telemetry data furnished to the CD&H microprocessor; a mission requirement specification.

#### d. Charge Retention

The charge of a Ni-Cd battery diminishes over time whether it is used or not. This loss of charge is caused by internal effects and is known as *self-discharge*. The self-discharge rate is a function of internal electrochemical reactions and the temperature at which the battery is stored. [Ref. 21:p. 105]

The rate of self-discharge is a function of the amount of capacity (charge) remaining in the cell and therefore behaves exponentially. As a result, the charge in the cell and the self discharge rate approach zero, the rate of decay in the cell voltage also approaches zero and the voltage tends to remain in the 1.0 to 1.1 volt region for an extended period of time.

The equation for the normal capacity retention function is

$$C_R = C_A \times e^{-t/\tau}$$

where  $C_R$  = retained capacity

$C_A$  = actual or initial capacity

$\tau$  = time constant in days (to 36.8% of  $C_A$ )

$t$  = open circuit rest time in days

This equation results in typical exponential decay. The time constant for the loss of capacity is dependent on both storage temperature and cell construction. Typical time constants for Ni-Cd cells at room temperature

range from 100 to 200 days. [Ref. 21:p. 106] At temperatures below  $-20^{\circ}\text{C}$  there is virtually no self-discharge, whereas at  $45^{\circ}\text{C}$  the rate of capacity loss is about three times higher than at  $25^{\circ}\text{C}$  [Ref. 22:p. 345].

#### *e. Life*

The useful life of a Ni-Cd battery are most greatly affected by battery temperature, depth of discharge, and excessive overcharge [Ref. 8:p. 353].

(1) Temperature Effects. Temperature is the most important environmental factor affecting normal cell wear-out. Elevated temperatures cause accelerated deterioration in the separator and seal materials. This rate of degradation is a direct function of the cell temperature. Therefore, exposing the batteries to high ambient or overcharge temperatures will produce a reduction in life from that expected at  $23^{\circ}\text{C}$ . Generally, the cell life is reduced by one half for every  $10^{\circ}\text{C}$  increase in temperature. [Ref. 21:p. 113] Consequently, every attempt must be made to keep the PANSAT batteries at approximately room temperature.

The sources of heat in a spacecraft is from absorption of solar energy by external surfaces and heat generated internally by spacecraft components. The space environment acts as a heat sink. Heat is transferred throughout the spacecraft by conduction and away from the spacecraft by radiation. The objective of thermal control is to provide adequate heat transfer. Heat radiates from the

external surfaces of the spacecraft into space so that temperature sensitive components, such as the batteries, remain within their specified temperature limits during all mission phases.

PANSAT must incorporate a passive thermal control system. In contrast to an active thermal control system, a passive thermal control system does not have moving parts, moving fluid, or electric power input other than the power dissipation of spacecraft functional equipment. Passive thermal control techniques include thermal coatings, thermal insulation, heat sinks, and phase-change materials. [Ref. 8:p. 295]

If PANSAT were permitted to remain in the shadow of the earth indefinitely, it would eventually reach a static equilibrium temperature of nearly  $-70^{\circ}\text{C}$ . In contrast, if PANSAT were to remain in sunlight, it would eventually stabilize to an equilibrium temperature of approximately  $+60^{\circ}\text{C}$  [Ref. 23]. However for each orbit, PANSAT is in the shadow of the earth for about 36 minutes and in sunlight for roughly one hour. Therefore, it never obtains either of these static temperatures, and the actual range will fall somewhere inside these extremes. At the time of this writing, a formal transient thermal analysis for PANSAT had not been conducted, therefore the proposed temperature range of the satellite is based on the preliminary analysis presented in Chapter III. It is assumed the appropriate passive thermal control

techniques will be employed to maintain the internal temperature of PANSAT within an acceptable temperature range for efficient operation of the Ni-Cad batteries. The recommended range is between 20°F (-7°C) and 80°F (+27°C) [Ref. 24].

(2) Depth of Discharge Effects. Ni-Cd batteries have inherently deep discharge protection. However, an increase in the depth of discharge reduces the cycle life. The greater the depth of discharge in every cycle, the greater the work load on the active materials in the electrodes. This causes slight degradation to occur earlier than it would with shallow discharges. [Ref. 21:p. 114] PANSAT will require approximately 11,000 charge/discharge cycles during its 2 year mission life. The depth of discharge recommended by manufacturers for this number of cycles is between 10% and 25% [Ref. 24].

(3) Effect of overcharge. Overcharge is defined as continued charging of a cell after it has become fully charged. The electrical energy of the charge current is converted into chemical energy in the cell by the charging reactions, until the cell is fully charged. Once the active material has been converted into the charged state, the energy supplied by the charging current is used by the electrolyte in the cell to generate gases. [Ref. 21:p. 183] This gas production yields thermal energy which can cause a significant increase in the battery temperature [Ref. 21:p. 113].

Therefore, the recurrence of elevated temperatures associated with frequent overcharging can greatly contribute to the reduction in battery life, as described above.

*f. Mechanical Stability*

The sealed Ni-Cd battery is a very rugged device, both physically and electrochemically. The cells possess good resistance to shock and vibration. Some cells have been subjected to long-term exposure to 10g excitation in the axial and transverse directions over a frequency range of 100 to 500 Hz, with no loss in performance. [Ref. 21:p. 114]

## VI. RECOMMENDATIONS AND CONCLUSIONS

### A. SOLAR ARRAY

Analysis of the solar array determined that power available to the PANSAT EPS will be, on the average, 17.7% less than originally predicted by the SSAG staff. This reduction in available power is a result of less maximum (and average) effective area than originally thought. Also, the refraction index of the solar cell coverglass causes a power loss due to the solar panel's high angle of incidence with respect to the sun.

Recommendations include:

- Rewrite the code for PANSAM in a high level language, such as C, for greater efficiency. If the run times could be reduced, the user could investigate different scenarios in a more timely manner. This would increase the effectiveness of being able to investigate different cases with a change in one or more factors.
- Once a more thorough investigation of PANSAT's transient thermal analysis has been completed, the program should be run with the new operating temperature data. This would provide a far more accurate prediction of the solar array output.
- Expand the model to include a time variant voltage. The current model investigated only a constant bus voltage. In actuality, the voltage will vary with time throughout the sunlight portion of the orbit. The main contributor will be the change in the battery voltage as the batteries charge throughout the orbit day. Therefore, the present model must be coupled with a program that determines the change in battery voltage based on: (1) the initial battery voltage upon entering sunlight (the amount of discharge during eclipse); (2) the change in temperature and its effects on the batteries charge rate; and (3) a change in available charge current due

changing effective area and/or changing power demands by the PANSAT subsystems.

## **B. PCCS**

The design for PCCS was determined on a conceptual level. Simplicity was emphasized to increase reliability. However, a working, flight-ready prototype must still be built and tested. Recommendations include:

- Determine circuitry necessary to interface PCCS with EPS subsystems and EPS with GAS can.
- Model operation of circuit on simulation software. Establishing the smoothing effectiveness of the LC circuit on a large (3 to 7 V) voltage step, is of particular interest.
- Breadboard the prototype with selected MILSPEC components.
- Establish potential points of failures in the PCCS and devise contingencies that can be implemented autonomously by the C&DH microprocessor, or manually by the groundstation.
- Thoroughly describe all modes of operation to include: telemetry data required by the C&DH microprocessor to determine proper action and, all C&DH microprocessor generated control signals needed to execute proper action.

## **C. BATTERY**

The battery design indicated that for a DOD between 10 and 25%, the battery capacity would need to be between approximately 8 Ah and 3 Ah, respectfully. Selecting a standard size already provided by the manufacturer would assist in keeping the cost of the batteries at a minimum. Therefore, it is recommended that the 5 Ah cells be selected for use. Additional recommendations include:



- A cost analysis must be conducted to determine if terrestrial cells enclosed in a rugged, sealed battery container is more cost effective than aerospace cells. Additionally, if the battery container is found to be more cost effective, Pb-Acid batteries should be reconsidered as a candidate for the secondary power source.
- The manned *Space Vehicle Battery Safety Handbook*, JSC-20793, should be consulted again prior to final battery selection. The JSC-20793 is available through the Johnson Space Center (JSC).
- Thoroughly describe all modes of charging and discharging to include: telemetry data required by the C&DH microprocessor to determine proper charging, discharging, or possible failure; and, all C&DH microprocessor generated control signals needed to execute proper action.
- The heat generated by the batteries due to charging and discharging should be incorporated in a more thorough investigation of the transient thermal analysis of PANSAT.

#### D. CLOSING

The initial proposal for this thesis was to continue the design of the FANSAT EPS and provide a working prototype upon completion. However, once the extent of the design of an EPS was understood (considering an EPS for a satellite is usually designed by a team of engineers), the author had to concede to the fact that the undertaking was overly ambitious for one person and one thesis. The emphasis of the thesis was then directed more toward the analysis of the solar array. The work that had already been completed on the battery and the PCCS were also included.

The recommendation that the author considers paramount, is to divide the task of completing a working EPS prototype amongst more than one person. The EPS design could easily be

divided into four categories:

- Completion, prototyping and testing of the PCCS.
- Selection and testing of the battery.
- Interfacing of the PANSAT EPS with the GAS can.
- Interfacing of the PANSAT EPS with the other subsystems of PANSAT. This includes receiving control from, and providing telemetry data to the C&DH microprocessor.

Once all the subsystems of PANSAT have reached an adequate level of design so that a reliable power budget can be resolved, the PANSAT team can determine if the solar array can satisfy this power budget with regard to the present mission description. If not, the mission description must be altered to accommodate the power constraints resulting from the solar array design.

## APPENDIX A - ORBIT PARAMETER CALCULATIONS

### A. ORBIT PERIOD CALCULATIONS

Discussion of the terms, constants, and equations given below can be found in Chapter 2 of Reference 8, or in any text addressing fundamental orbital mechanics. First, a list defining the variables used in the calculations:

$R_0$  = Mean radius of earth  
= 6371.2 Km

$\mu_0$  = Gravitational constant for earth  
= 398,601.2 Km<sup>3</sup>/s<sup>2</sup>

$h$  = Altitude of satellite

$r$  = Magnitude of vector measured from the earth's center to the satellite (i.e.  $r = h + R_0$ )

$i$  = Inclination of satellite's orbit with respect to earth's equatorial plane

$\delta$  = Declination of the sun with respect to earth's equatorial plane  
= 28° for solstice and 0° for equinox

$T$  = Period of orbit

$T_e$  = Period of eclipse portion of orbit

The period of a satellite in orbit around the earth is given by the equation

$$T = 2\pi \sqrt{\frac{r^3}{\mu_0}} \quad (A-1)$$

The total eclipse period is given by the equation

$$T_e = \frac{T}{\pi} \arccos \left[ \frac{\sqrt{1 - \frac{R_E^2}{r^2}}}{\cos \delta} \right] \quad (\text{A-2})$$

The result of the equation for the period above is in seconds; therefore, the number of orbits for the life of the mission is given by

$$\frac{\text{Number of Orbits}}{\text{Mission Life}} = \frac{1 \text{ Orbit}}{T [s]} \times \frac{3600 [s]}{1 \text{ hour}} \times \frac{24 \text{ hours}}{1 \text{ day}} \times \frac{365.25 \text{ days}}{1 \text{ year}} \times \frac{\text{Number of Years}}{\text{Mission Life}}$$

Assuming the possible altitude of PANSAT may range from 160 Km to 800 Km, with an inclination of approximately 28°, and a mission life of two years, the appropriate parameters can be substituted into the above equations to generate the values in Table A-1.

## B. FOOTPRINT CALCULATION

### 1. Size of Footprint

A sketch illustrating the concept of a satellite's footprint, or swath (denoted as  $S$ ), is shown in Figure A.1. The swath is given by the equation

$$S = 2 \times \Theta (\text{deg}) \times \frac{60 \text{ nmi}}{\text{deg}} \quad (\text{A-3})$$

To determine the swath,  $\theta$  must be found from the equation

$$\theta = 90^\circ - \alpha - \arcsin\left(\frac{\cos\alpha}{1 + \frac{h}{R}}\right) \quad (\text{A-4})$$

To the determine the maximum, ideal footprint, assume the elevation angle is equal to zero degrees ( $\alpha = 0^\circ$ ), the

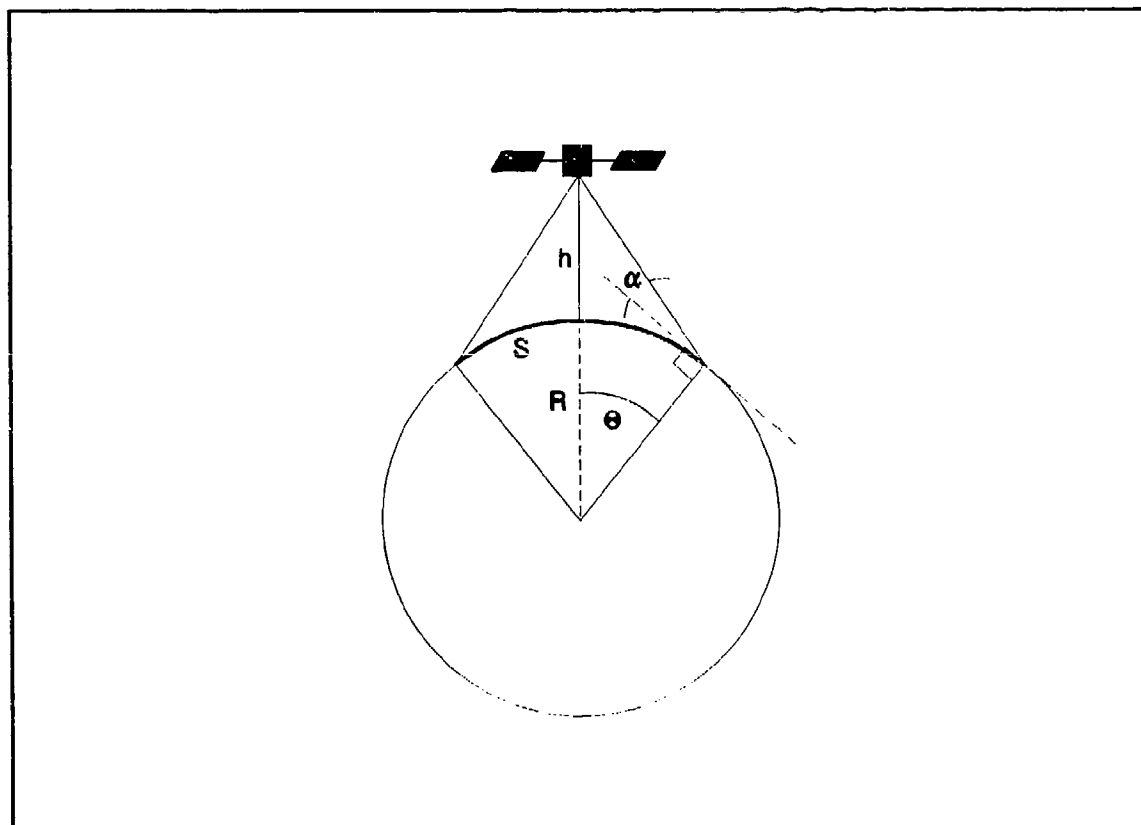


**Figure A.1.** Diagram Illustrating the Swath or Footprint of a Satellite

altitude is 480 Km ( $h = 480$  Km), and the radius of the earth is 6371.2 Km. Inserting these values in the appropriate equations yields

$$\theta = 21.57^\circ$$

which results in a footprint with the size of

$$S \approx 2590 nmi$$

**TABLE A-1. VARIOUS ORBITAL PARAMETERS FOR A TWO YEAR MISSION LIFE FOR ALTITUDES RANGING FROM 160 KM TO 800 KM; FOR BOTH SOLSTICE AND EQUINOX.**

h [Km]	T [min]	Number of Orbits	T <sub>e</sub> [min]		Percent of orbit in Eclipse	
			Solstice	Equinox	Solstice	Equinox
160	87.5	12021.9	37.0	37.6	42.3	43.0
200	88.4	11899.5	36.6	37.2	41.4	42.1
300	90.4	11636.3	35.8	36.5	39.6	40.4
400	92.4	11384.4	35.1	36.0	38.0	39.0
480	94.1	11178.7	34.7	35.8	36.9	38.0
600	96.5	10900.7	34.2	35.4	35.4	36.7
700	98.6	10668.6	33.9	35.2	34.4	35.7
800	100.7	10446.1	33.6	35.1	33.4	34.9

## 2. Time in Field of View of Satellite

By referring to Figure A.1, it can be seen that the length of time a ground station remains in the field of view (FOV) of a satellite,  $t_{FOV}$ , is equivalent to the amount of time it takes for the satellite to pass through an angle of  $2\theta$ . Realizing that one period,  $T$ , is the length of time required for a satellite to complete one orbit (one revolution),  $t_{FOV}$  can be found by establishing the ratio

$$\frac{t_{FOV}}{2\theta} = \frac{T}{2\pi} \quad (A-5)$$

As above, assuming the elevation angle is equal to zero degrees ( $\alpha = 0^\circ$ ) and applying some trigonometric identities,  $\theta$  can be determined from

$$\theta = \arccos\left(\frac{R_\oplus}{R_\oplus + h}\right) \quad (\text{A-6})$$

After solving Equation A-5 for  $t_{FOV}$  and inserting the appropriate parameters, Table A-2 can be generated with the values of  $t_{FOV}$ .

**TABLE A-2.** TIME IN FIELD OF VIEW ASSOCIATED WITH VARIOUS ALTITUDES

h [Km]	T [min]	$t_{FOV}$
160	87.5	6.18
200	88.4	6.96
300	90.4	8.66
400	92.4	10.16
480	94.1	11.28
600	96.5	12.84
700	98.6	14.08
800	100.7	15.28

## APPENDIX B - SOLAR ARRAY

### A. ANALYTICAL COMPUTER MODEL FOR I-V CURVE GENERATION

For the sake of brevity, the following includes only a minimal discussion and the actual equations used to generate the I-V curves in Figure 6. If a more indepth discussion of the material and/or the derivations of the equations are desired, the reader is referred to sections 9.2.1 and 9.2.3 of Reference 6.

The basic solar cell equation derived from solid-state physics theory does not represent the actual solar cell I-V curve with sufficient accuracy to be deemed useful. As a result of observations of the solar cell terminal characteristics under a variety of test conditions, three additional parameters - A,  $R_s$ , and  $R_{SH}$  - have been included into the equation to yield:

$$I = I_L - I_0 \left\{ \exp \left[ \frac{e(V + I R_s)}{A k T} \right] - 1 \right\} - \frac{V}{R_{SH}} \quad (B-1)$$

where the symbols are defined as follows:

- A = an arbitrary curve-fitting constant between 1 and 5
- $R_s$  = series resistance of the cell
- $R_{SH}$  = shunt resistance of the cell
- I = current output of the cell
- $I_L$  = light-generated current of the cell



$I_0$  = diode saturation current of the cell  
 $e$  = electronic charge  
 $V$  = terminal voltage of the cell  
 $k$  = Boltzmann's constant  
 $T$  = absolute temperature

Analytical expressions of the solar cell  $I$ - $V$  curve shape are derived from the equation above. The "Hughes" model was selected from Reference 7 because the necessary parameters for this model were available from the contractor. To simplify the mathematical development, the "Hughes" model neglected the  $V/R_{SH}$  term and redefined Equation B-1 through a change in variables. By letting  $K_1 V_{oc} = AkT/e$ ,  $K_2 I_{sc} = I_0$ , and  $I_L = I_{sc}$ , Equation B-1 becomes an implicit equation in terms of  $I$

$$I = I_{sc} - I_{sc} K_2 \left[ \exp \left( \frac{V + IR_s}{K_1 V_{oc}} \right) - 1 \right] \quad (B-2)$$

The equations for  $K_1$  and  $R_s$  are derived on pages 9.2-3 and 9.2-4 of Reference 6 and are as follows:

$$K_1 = \left[ \ln \left( \frac{1}{K_2} + 1 \right) \right]^{-1} \quad (B-3)$$

and

$$R_s = \frac{V_{oc} \left[ \frac{\ln \left[ 1 + \frac{1}{K_2} - \frac{I_{mp}}{K_2 I_{sc}} \right]}{\ln \left( \frac{1}{K_2} + 1 \right)} \right] - V_{mp}}{I_{mp}} \quad (B-4)$$

The variable  $K_2$  is given in an implicit equation as a function of  $I_{sc}$ ,  $I_{mp}$ ,  $V_{mp}$ , and  $V_{oc}$

$$\frac{I_{mp}}{I_{sc}} = \frac{\left( \frac{V_{mp}}{V_{oc}} \right) \ln \left( \frac{1}{K_2} + 1 \right)}{\left( \frac{1}{1 + K_2 - \frac{I_{mp}}{I_{sc}}} \right) - \frac{I_{mp}}{I_{sc}} \left[ \frac{V_{mp}}{V_{oc}} \ln \left( \frac{1}{K_2} + 1 \right) - \ln \left( \frac{1}{K_2} + 1 - \frac{I_{mp}}{K_2 I_{sc}} \right) \right]} \quad (B-5)$$

The final model is formed by substituting the numerical values of  $K_1$ ,  $K_2$ , and  $R_s$  from Equations B-3, B-5, and B-4 respectively, into an implicit equation obtained by solving Equation B-2 for  $I$

$$I = I_{sc} - I_{sc} K_2 \left[ \exp \left( \frac{(V + I R_s)}{K_1 V_{oc}} \right) - 1 \right] \quad (B-6)$$

which defines the cell  $I$ - $V$  curve. The parameters needed to fully define the model are  $I_{sc}$ ,  $I_{mp}$ ,  $V_{mp}$ , and  $V_{oc}$ . These were

provided by the contractor as:

$$I_{sc} = 319 \text{ mA}$$

$$I_{mp} = 307 \text{ mA}$$

$$V_{mp} = 500 \text{ mV}$$

$$V_{oc} = 605 \text{ mV}$$

These values are for the bare, 5700 series cells to be used for PANSAT. The parameters were determined at standard conditions (28°C and AMO). [Ref. 10:p. 2].

Using the parameters listed above as inputs, code was written in MATLAB® to implement the above equations. A subroutine is first used to determine  $K_2$  by iteration and then the calling program substitutes the value for  $K_2$  into the appropriate equations to calculate  $K_1$  and  $R_s$ . The program then utilizes a 'for loop' to implement Equation B-6, after which it plots the  $I$ - $V$  curve and the  $P$ - $V$  curve. The code is provided on the following pages. The results are:

$$K_2 = 1.9361e-15$$

$$K_1 = 0.02952$$

$$R_s = 0.15121$$

## B. SOFTWARE CODE FOR GENERATING I-V CURVES

%%%%%%%% THIS PROGRAM IS USED TO PLOT THE I-V AND P-V CURVES  
%%%%%%%% SHOWN IN FIGURE 6.

```
clg
clear
!del iv_fig6.met
```

%%%%%%%% DEFINE PARAMETERS OF BARE CELL PROVIDED BY  
CONTRACTOR

```
Isc = 0.319; % Short-circuit current
Voc = 0.605; % Open-circuit voltage
Vmp = 0.500; % Maximum power point voltage
Imp = 0.307; % Maximum power point current
```

%%%%%%%% CALL SUBROUTINE TO DETERMINE K2 & CALCULATE K1 & RS

```
K2 = get_K2b(Imp,Isc,Vmp,Voc);
K1 = 1/(log((1/K2) + 1));
RS = (Voc*((log((1 + K2 - Imp/Isc)/K2))/(log((1/K2) + 1))) -
Vmp)/Imp;
fprintf('iv_fig6.fil','K2 = %0.5g\nK1 = %0.5f\nRS =
%0.5f\n',K2,K1,RS)
```

```
V = [0:0.001:Voc];
```

%%%%%%%% CALL SUBROUTINE TO DETERMINE V ASSOCIATED WITH I

```
I = get_I(Isc,Imp,V,Voc,Vmp,K2);
P = I.*V;
axis([0,1.01*Voc,0,1.1*Isc])
x1 = [0 Vmp Vmp];
y1 = [Imp Imp 0];
plot(x1,y1,V,I,V,P),xlabel('Voltage [V]'),ylabel('Current
[A] & Power [W]'), grid
gtext('Isc')
gtext('Voc')
meta iv_fig6
pause
axis
```

---

```

function K2b = get_K2b(Imp,Isc,Vmp,Voc)

%      K2b = get_K2b(Imp,Isc,Vmp,Voc)
%
%      THIS SUBROUTINE IS USED TO DETERMINE K2 FROM
%      AN IMPLICIT FUNCTION FOR K2 GIVEN Imp, Isc,
%      Vmp, and Voc
n = 0;
tol = Imp/Isc;
diff = 1.0;
K2g = 1.0e-8;
diff = 1.0;
diff_b_4 = diff;
flag = 0;
while abs(diff) >= 1.0e-4
n = n + 1;
    Num = (Vmp/Voc)*log((1/K2g) + 1);
    Dem1 = 1/(1 + K2g - tol);
    Dem2 = tol*((Vmp/Voc)*log((1/K2g) + 1) - log((1/K2g)*(1
- tol)+ 1));
    Dem = Dem1 - Dem2;
    Im_ovrIs = Num/Dem;
    diff = tol - Im_ovrIs;
    fprintf('n = %0.0f\ndiff = %0.3g\nIm_ovrIs =
%0.3g\n\n',n,diff,Im_ovrIs)

        if abs(diff) > abs(diff_b_4)
            if flag == 0
                flag = 1;
            else
                flag = 0;
            end
        end
        if flag == 0;
            K2g = K2g*0.99;
        else
            K2g = K2g*1.01;
        end
        diff_b_4 = diff;

    end
K2b = K2g;
end

```

---

---

```

function v = getv(Isc, Imp, I, Voc, Vmp, K2)

%      v = getv(Isc, Imp, I, Voc, Vmp, K2)
%
%      THIS IS A SUBROUTINE THAT DETERMINES 'V' EXPLICITLY
%      FROM I GIVEN Isc, Imp, Voc, Vmp, and K2
%

    k1 = 1/(log(1/K2 + 1));
    temp = k1*log((1 + K2 - Imp/Isc)/K2);
    rs = (Voc*temp - Vmp)/Imp;

    l = length(I);

    for n=1:l
        v =
[v;k1*Voc*log((Isc*(1+K2) - I(n))/Isc/K2) - I(n)*rs];
    end

```

---

```

##### THIS PROGRAM IS USED TO PLOT THE I-V CURVES
##### SHOWN IN FIGURE 18.
clc
clear
!del ivc_fg18.met
Isc = 0.319; % Short-circuit current
Voc = 0.605; % Open-circuit voltage
Vmp = 0.500; % Maximum power point voltage
Imp = 0.307; % Maximum power point current
K2 = get_K2b(Imp,Isc,Vmp,Voc);
K1 = 1/(log((1/K2) + 1));
RS = (Voc*((log((1 + K2 - Imp/Isc)/K2))/(log((1/K2) + 1))) -
Vmp)/Imp;
fprintf('K2 = %0.5g\nK1 = %0.5f\nRS = %0.5f\n',K2,K1,RS)
V = [0:0.001:Voc];
I = get_I(Isc,Imp,V,Voc,Vmp,K2);

F_rad_I = 0.978; % Radiation degradation factor for
current
F_rad_V = 0.965; % Radiation degradation factor for
voltage
Fc = 0.99; % Cover installation factor
Fcmm = 0.99; % Cell mismatch factor
F_tau = 0.99; % Optical transmission factor
FMM = 0.99; % Micrometeorite degradation factor
delta_V3 = 5e-3; % Series resistance due to assembly
beta_I = 2.188e-5*1.92*4; % Temperature coefficient for
current
beta_V = -2.1e-3; % Temperature coefficient for
voltage
To = 28; % Standard condition test temperature [°K]
Top_min = 16.6;
Top_max = 32.7;
Top = [Top_min,To,Top_max];
Rs = 0.01;
Si = .96896; % Solar intensity at summer solstice
S_eff = Si*F_tau;
S = 1.0;

for m = 1:3;
    Top_temp = Top(m)
    Iscd =
get_Iscd(Isc,F_rad_I,Fc,Fcmm,FMM,Top_temp,To,S_eff,S,beta_I)
    Impd =
get_Impd(Imp,Isc,F_rad_I,Fc,Fcmm,FMM,Top_temp,To,S_eff,S,bet
a_I)
    Vocd =
get_Vocd(Voc,Isc,F_rad_I,F_rad_V,Fc,Rs,Top_temp,To,S_eff,S,b
eta_V,delta_V3)
    Vmpd =
= get_Vmpd(Vmp,Isc,F_rad_I,F_rad_V,Fc,Rs,Top_temp,To,S_eff,S,
beta_V,delta_V3)

```

```

    fprintf('\nm = %0.0f\nIscd = %0.5g\nImpd
    =%0.5f\n',m,Iscd,Impd)
    fprintf('Vmpd = %0.5f\nVocd = %0.5f\n',Vmpd,Vocd)
    K2 = get_K2b(Impd,Iscd,Vmpd,Vocd);
    fprintf('K2 = %0.5g\nK1 = %0.5f\nRS = %0.5f\n',K2,K1,RS)

    V_temp = [0:0.001:Vocd];
    I_temp = get_I(Iscd,Impd,V_temp,Vocd,Vmpd,K2);
    L = length(V_temp);
%    I_temp(L+1) = Iscd;
%    V_temp(L+1) = 0;
    if m == 1;
        I_d1 = I_temp;
        V_d1 = V_temp;
    elseif m == 2;
        I_d2 = I_temp;
        V_d2 = V_temp;
    elseif m == 3;
        I_d3 = I_temp;
        V_d3 = V_temp;
    end

end

axis([0,1.01*Voc,0,1.1*Isc])
x1 = [0 Vmp Vmp];
y1 = [Imp Imp 0];
plot(V,I,'-',x1,y1,'-',V_d1,I_d1,'-',V_d2,I_d2,'-',V_d3,I_
d3,':'),xlabel('Voltage [V]'),ylabel('Current [A]'), grid
gtext('solid: BOL, Standard Test Conditions')
gtext('dash: EOL, Top = 16.6°C')
gtext('dash/dot: EOL, Top = 28°C')
gtext('dot: EOL, Top = 32.7°C')
meta ivc_fg18
pause
axis

```

---

```

function Impd =
get_Impd(Imp,Isc,F_rad_I,Fc,Fg,FMM,Top,To,S_eff,S,beta_I)

% Impd =
get_Impd(Imp,Isc,F_rad_I,Fc,Fg,FMM,Top,To,S_eff,S,beta_I)
%
% THIS SUBROUTINE IS USED TO DETERMINE THE DEGRADED MAX
% POWER POINT CURRENT, GIVEN THE LOSS FACTORS AND %
PARAMETERS SHOWN ABOVE

Impu = Imp*F_rad_I;
Impg = Impu + Isc*F_rad_I*(Fc - 1);
Imps = Impg + (S_eff - S)*Isc*F_rad_I*Fc;
ImpT = Imps + beta_I*Isc*(Top - To);
Impd = ImpT*Fg*FMM;

```



---

```

function Iscd =
get_iscd(Isc, F_rad_I, Fc, Fg, FMM, Top, To, S_eff, S, beta_I)

% Iscd =
get_iscd(Isc, F_rad_I, Fc, Fg, FMM, Top, To, S_eff, S, beta_I) ....
%
% THIS SUBROUTINE IS USED TO DETERMINE THE DEGRADED %
% SHORT-CIRCUIT CURRENT, GIVEN THE LOSS FACTORS AND %
% PARAMETERS SHOWN ABOVE

Iscu = Isc*F_rad_I;
Iscg = Iscu*Fc;
Iscs = Iscg + (S_eff - S)*Iscg;
Isct = Iscs + beta_I*Isc*(Top - To);
Iscd = Isct*Fg*FMM;

```

---

```

function Vmpd =
get_Vmpd(Vmp, Isc, F_rad_I, F_rad_V, Fc, Rs, Top, To, S_eff, S, beta_V,
delta_V3)

% Vmpd =
get_Vmpd(Vmp, Isc, F_rad_I, F_rad_V, Fc, Rs, Top, To, S_eff, S, beta_V,
delta_V3)
%
% THIS SUBROUTINE IS USED TO DETERMINE THE DEGRADED MAX
% POWER POINT VOLTAGE, GIVEN THE LOSS FACTORS AND %
% PARAMETERS SHOWN ABOVE

Vmpg = Vmp*F_rad_V;
Vmgs = Vmpg - (S_eff - S)*Isc*F_rad_I*Fc*Rs +
0.01*log10(S_eff/S);
Vmpt = Vmgs + beta_V*(Top - To);
Vmpd = Vmpt*delta_V3;

```

---

## APPENDIX C - PANSAM AND RELATED PROGRAMS

The first program given below was used to determine the maximum, minimum, and average effective area of PANSAT. The **A** and **B** frame are considered coincident upon PANSAT exiting eclipse. Each time the **B** frame is rotated about one of the axes, it is done so in increments of 0.1 RAD/sec. At this rotation rate it will take  $20\pi$  steps to make a complete revolution about any given axis. In order to investigate all possible orientations, the code is implemented with three nested 'for loops'. The inner 'for loop' rotates the **B** frame through an entire revolution in intervals of 0.1 radian about the **o**-axis for each increment of 0.1 radian about the **q**-axis. Likewise, the middle 'for loop' rotates the **B** frame through an entire revolution in intervals of 0.1 radian about the **q**-axis for each increment of 0.1 radian about the **p**-axis. Finally, the outer 'for loop' rotates the **B** frame through an entire revolution in intervals about the **p**-axis. Assuming the change in effective area is inconsequential for a change of 0.1 radian, the results are considered acceptable. The resulting values for the effective area are a minimum of 696.37 cm<sup>2</sup>, a maximum of 1139.2 cm<sup>2</sup>, and an average of 1036.9 cm<sup>2</sup>.

---

```

clear
clg
%!del effarea1.met
%!del effarea2.met
%!del output_P
%!del eff_area.fil
delta = 23      % DECLINATION OF ECLIPTIC PLANE RELATIVE TO
                % THE EQUATORIAL PLANE
del_rad = delta*pi/180;

%%%%%%%%%      DEFINE PARAMETERS      %%%%%%%%%%%%%%%

inclnatn = 28;  % INCLINATION OF THE ORBIT IN DEGREES
gamma = 0;

                % THE INCLINATION AND THE
                % DECLINATION IN RADIANS
%      THE i, j, k-AXES DESCRIBE THE BODY FRAME OF
REFERENCE

phi      = 0;    % INITIAL ANGLE OF ROTATION ABOUT i-AXIS
theta    = 0;    % INITIAL ANGLE OF ROTATION ABOUT j-AXIS
psi      = 0;    % INITIAL ANGLE OF ROTATION ABOUT k-AXIS

phi_dot  = 0.1;  % ANGULAR RATE OF CHANGE ABOUT i-AXIS
thta_dot = 0.1;  % ANGULAR RATE OF CHANGE ABOUT j-AXIS
psi_dot  = 0.1;  % ANGULAR RATE OF CHANGE ABOUT k-AXIS

PSA = 32*0.04*0.0192  % PANEL SUFACE AREA FOR EACH PANEL

%      DEFINE THE SURFACE AREA VECTOR, SAV, WITH MAGNITUDE
PSA,
%      FOR EACH PANEL, RELATIVE TO THE BODY FRAME OF
REFERENCE

comp_PSA = PSA/(sqrt(2)) % COMPONENT OF PSA

SAV_B(1,1:3) = [PSA 0 0];
SAV_B(2,1:3) = [comp_PSA comp_PSA 0];
SAV_B(3,1:3) = [comp_PSA 0 comp_PSA];
SAV_B(4,1:3) = [comp_PSA -comp_PSA 0];
SAV_B(5,1:3) = [comp_PSA 0 -comp_PSA];
SAV_B(6,1:3) = [0 0 0];
SAV_B(7,1:3) = [0 comp_PSA -comp_PSA];
SAV_B(8,1:3) = [0 PSA 0];
SAV_B(9,1:3) = [0 comp_PSA comp_PSA];
SAV_B(10,1:3) = [0 0 PSA];
SAV_B(11,1:3) = [0 -comp_PSA comp_PSA];

```

```

SAV_B(12,1:3) = [0 -PSA 0];
SAV_B(13,1:3) = [0 -comp_PSA -comp_PSA];
SAV_B(14,1:3) = [-PSA 0 0];
SAV_B(15,1:3) = [-comp_PSA -comp_PSA 0];
SAV_B(16,1:3) = [-comp_PSA 0 comp_PSA];
SAV_B(17,1:3) = [-comp_PSA comp_PSA 0];
SAV_B(18,1:3) = [-comp_PSA 0 -comp_PSA];

%      DEFINE TRANSFORMATION MATRIX M, WHICH TRANSLATES A
VECTOR
%      DESCRIBED IN B INTO A VECTOR DESCRIBED IN A.

rot_amnt = input('Enter desired amount of rotation ');

for L = 1:rot_amnt;
    for M = 1:rot_amnt;
        for N = 1:rot_amnt;

            c_phi = cos(phi);
            c_psi = cos(psi);
            c_theta = cos(theta);
            s_phi = sin(phi);
            s_psi = sin(psi);
            s_theta = sin(theta);

            DCM(1,1) = c_psi*c_theta;
            DCM(1,2) = c_psi*s_theta*s_phi - s_psi*c_phi;
            DCM(1,3) = c_psi*s_theta*c_phi + s_psi*s_phi;
            DCM(2,1) = s_psi*c_theta;
            DCM(2,2) = s_psi*s_theta*s_phi + c_psi*c_phi;
            DCM(2,3) = s_psi*s_theta*c_phi - c_psi*s_phi;
            DCM(3,1) = -s_theta;
            DCM(3,2) = c_theta*s_phi;
            DCM(3,3) = c_theta*c_phi;

            % TRANSLATE EACH SAV IN FRAME 'B' INTO FRAME 'A'
            for l = 1:18;
                temp = DCM*SAV_B(l,1:3)';
                for m = 1:3;
                    SAV_A(l,m) = temp(m);
                end
                % TRANSFORMATION VECTOR TO FIND SAV
                % RELATIVE TO THE SUN VECTOR
                a_I = [-cos(gamma) 0 sin(gamma)];

                % DETERMINE COMPONET OF EACH SAV
                % IN FRAME 'A' POINTING TOWARD THE SUN

```

```

        PARALLEL = a_I*SAV_A(1,1:3)';
        if PARALLEL >= 0;
            PSA_2_SUN(1) = 0;
        else
            PSA_2_SUN(1) = abs(PARALLEL);
        end
    end
    A_eff(N) = sum(PSA_2_SUN)*100^2; % TOTAL
EFFECTIVE AREA IN cm^2
    phi = phi + phi_dot;
end
tmp_minN(M) = min(A_eff);
tmp_maxN(M) = max(A_eff);
tmp_menN(M) = mean(A_eff);

    psi = psi + psi_dot;
end
tmp_minM(L) = min(tmp_minN);
tmp_maxM(L) = max(tmp_maxN);
tmp_menM(L) = mean(tmp_menN);
theta = theta + theta_dot;
end
minA_eff = min(tmp_minM);
maxA_eff = max(tmp_maxM);

fprintf('a_e_mxmN.fil','The maximum effective area is %0.1f
[cm^2]\n',maxA_eff)
fprintf('a_e_mxmN.fil','\n\nThe minimum effective area is
%0.5f [cm^2]\n',minA_eff)
fprintf('a_e_mxmN.fil','\n\nThe average effective area is
%0.1f [cm^2]\n',mean(tmp_menM))
fprintf('The maximum effective area is %0.1f
[cm^2]\n',maxA_eff)
fprintf('\n\nThe minimum effective area is %0.5f
[cm^2]\n',minA_eff)
fprintf('\n\nThe average effective area is %0.1f
[cm^2]\n',mean(tmp_menM))

axis([0 rot_amnt 0.99*min(A_eff) 1.01*max(A_eff)])
plot(A_eff),xlabel('Time'),...
ylabel('Effective Area [cm^2]'),...
meta effareal
pause
axis([0 0.25*rot_amnt 0.99*min(A_eff) 1.01*max(A_eff)])
plot(A_eff([1:0.25*rot_amnt])),xlabel('Time in Sunlight for
One Revolution [s]'),...
ylabel('Effective Area [cm^2]'),...
meta effarea2
pause

```

axis

---

The next program is user interactive, allowing the user to define the initial orientation and the rate of rotation about each axis.

---

```
clear
clg
!del effareal.met
!del eff_area.fil
%      DETERMINE SATELLITE PERIOD, TIME IN ECLIPSE AND TIME
IN SUNLIGHT

mu = 398866.0;    % Gravitational parameter [Km^3/s^2]
Re = 6371.2;      % Earth's radius (average) [Km]
%      h = input('Enter altitude of satellite in Km: ');
h = 480;
%      delta = input('Enter declination of sun in degrees:
');
delta = 23.44      % DECLINATION OF ECLIPTIC PLANE RELATIVE
TO
                  % THE EQUATORIAL PLANE
del_rad = delta*pi/180;
tau = 2*pi*(sqrt(((h + Re)^3)/mu))/60;      % Period in
minutes
tau_E = (tau/pi)*acos(sqrt(1 - (Re^2)/(h +
Re)^2)/cos(del_rad)) %Eclipse period
tau_S = (tau - tau_E)*60    % Portion of period in sun IN
SECONDS

          pause
%%%%%%%%%      DEFINE PARAMETERS      %%%%%%%%%%%%%%%

P = 17.94;      % POWER IN mW/cm^2
inclnatn = 28;  % INCLINATION OF THE ORBIT IN DEGREES
gamma = (inclnatn - delta)*pi/180; % THE DIFFERENCE BETWEEN
                                     % THE INCLINATION AND THE
                                     % DECLINATION IN RADIANS
%      THE i, j, k-AXES DESCRIBE THE BODY FRAME OF
REFERENCE

X = input('Enter angular rate of change about i-axis in
deg/s ');
```

```

Y = input('Enter angular rate of change about j-axis in
deg/s ');
Z = input('Enter angular rate of change about k-axis in
deg/s ');
phi_dot = X*pi/180;    % ANGULAR RATE OF CHANGE ABOUT i-AXIS
thta_dot = Y*pi/180;    % ANGULAR RATE OF CHANGE ABOUT j-AXIS
psi_dot = Z*pi/180;    % ANGULAR RATE OF CHANGE ABOUT k-AXIS

phi_init = input('Enter initial angle for phi in radians ');
thta_int = input('Enter initial angle for theta in radians
');
psi_init = input('Enter initial angle for psi in radians ');

phi = phi_init - phi_dot*tau_S; % INITIAL ANGLE OF
ROTATION ABOUT i-AXIS
theta = thta_int - gamma - thta_dot*tau_S;
                                % INITIAL ANGLE OF ROTATION
ABOUT j-AXIS
psi = psi_init - psi_dot*tau_S; % INITIAL ANGLE OF
ROTATION ABOUT k-AXIS

PSA = 32*0.04*0.0192; % PANEL SUFACE AREA FOR EACH PANEL

%      DEFINE THE SURFACE AREA VECTOR, SAV, WITH MAGNITUDE
PSA,
%      FOR EACH PANEL, RELATIVE TO THE BODY FRAME OF
REFERENCE

comp_PSA = PSA/(sqrt(2)) % COMPONENT OF PSA

SAV_B(1,1:3) = [PSA 0 0]
SAV_B(2,1:3) = [comp_PSA comp_PSA 0];
SAV_B(3,1:3) = [comp_PSA 0 comp_PSA];
SAV_B(4,1:3) = [comp_PSA -comp_PSA 0];
SAV_B(5,1:3) = [comp_PSA 0 -comp_PSA];
SAV_B(6,1:3) = [0 0 0];
SAV_B(7,1:3) = [0 comp_PSA -comp_PSA];
SAV_B(8,1:3) = [0 PSA 0];
SAV_B(9,1:3) = [0 comp_PSA comp_PSA];
SAV_B(10,1:3) = [0 0 PSA];
SAV_B(11,1:3) = [0 -comp_PSA comp_PSA];
SAV_B(12,1:3) = [0 -PSA 0];
SAV_B(13,1:3) = [0 -comp_PSA -comp_PSA];
SAV_B(14,1:3) = [-PSA 0 0];
SAV_B(15,1:3) = [-comp_PSA -comp_PSA 0];
SAV_B(16,1:3) = [-comp_PSA 0 comp_PSA];
SAV_B(17,1:3) = [-comp_PSA comp_PSA 0];
SAV_B(18,1:3) = [-comp_PSA 0 -comp_PSA];

```

```

%      DEFINE TRANSFORMATION MATRIX M, WHICH TRANSLATES A
VECTOR
%      DESCRIBED IN B INTO A VECTOR DESCRIBED IN A.

a_I = [-cos(gamma) 0 sin(gamma)]; % TRANSFORMATION VECTOR TO
FIND SAV                                % RELATIVE TO THE SUN
VECTOR

for t = 1:tau_S;

    c_phi = cos(phi);
    c_psi = cos(psi);
    c_theta = cos(theta);
    s_phi = sin(phi);
    s_psi = sin(psi);
    s_theta = sin(theta);

    M(1,1) = c_psi*c_theta;
    M(1,2) = c_psi*s_theta*s_phi + s_psi*c_phi;
    M(1,3) = -c_psi*s_theta*c_phi + s_psi*s_phi;
    M(2,1) = -s_psi*c_theta;
    M(2,2) = -s_psi*s_theta*s_phi + c_psi*c_phi;
    M(2,3) = s_psi*s_theta*c_phi + c_psi*s_phi;
    M(3,1) = s_theta;
    M(3,2) = -c_theta*s_phi;
    M(3,3) = c_theta*c_phi;

    for l = 1:18;
        temp = M*SAV_B(l,1:3)';
        for m = 1:3;
            SAV_A(l,m) = temp(m);
        end
        PARALLEL = a_I*SAV_A(l,1:3)';
        if PARALLEL >= 0;
            PSA_2_SUN(l) = 0;
        else
            PSA_2_SUN(l) = abs(PARALLEL);
        end
    end

    phi = phi + phi_dot;
    psi = psi + psi_dot;
    theta = theta + theta_dot;
    A_eff(t) = sum(PSA_2_SUN)*100^2; % TOTAL EFFECTIVE AREA IN
    cm^2
end
axis([0 tau_S 0.99*min(A_eff) 1.01*max(A_eff)])

```



```

plot(A_eff),xlabel('Time in Sunlight for a Typical Orbit
[s]'), ...
ylabel('Effective Area [cm^2]'), ...
meta effareal
pause
axis
fprintf('eff_area.fil','The maximum effective area is %0.1f
[cm^2]\n',max(A_eff))
fprintf('eff_area.fil','\n\nThe minimum effective area is
%0.1f [cm^2]\n',min(A_eff))
fprintf('eff_area.fil','\n\nThe average effective area is
%0.1f [cm^2]\n',mean(A_eff))

```

---

## APPENDIX D - BATTERY DESIGN

First, a list defining the variables used in the design:

- $P_c$  = Power required for battery charging
- $P_d$  = Power discharged during eclipse
- $P_{sa}$  = Power provided by solar array
- $P_{sys}$  = Power required by entire system
- $C$  = Battery capacity
- $t_r$  = Time for recharge
- $t_d$  = Time of discharge
- $\eta$  = Charging efficiency
- $V_{bus}$  = Bus voltage (EOL)
- $V_{MinD}$  = Minimum allowable discharge voltage
- $V_{MaxC}$  = Maximum allowable charge voltage
- $V_{DD}$  = Voltage drop across bypass diode
- $V_{SD}$  = Voltage drop across steering diode
- $V_D$  = Minimum allowable discharge voltage of one battery cell
- $V_C$  = Maximum allowable charge voltage of one battery cell
- $R$  = Charge rate
- $I_r$  = Recharge current
- $N$  = Number of battery cells

The battery design investigation will be based on a DOD of 10% and 25% for comparison. The procedure used is in conjunction with the one presented on page 375 of Reference 8.

The design procedure was carried out for a worst case scenario in which only one of the two batteries is operational. It is assumed that in the case where both batteries are in operation, the amount of power discharged from each battery will be half the amount discharged for the case of single battery operation. Furthermore, the sum of the power required to charge both batteries in the two battery case is assumed to be equivalent to the power required to charge one battery in the single battery case.

Assume the minimum discharge voltage of the battery cell,  $V_D$ , is 1.14 V at the end of two years. The number of battery cells in series,  $N$ , is calculated based on the minimum discharge voltage during eclipse. Also, assume the battery is configured as shown in Figure D.1, where each battery cell is connected in parallel with one bypass diode to allow current flow to the bus, and three series-connected diodes to allow current flow from the bus. In the event of an open-circuit failure, the single diode furnishes a path for the remaining cells to supply power to the bus; the three series-connected diodes allow the remaining cells to receive current for charging.

For a design based on the worst case, assume that one cell became an open-circuit failure and that the voltage drop across the bypass diode,  $V_{DD}$ , is approximately 0.38 V. The minimum discharge voltage equation is

$$V_{MinD} = (N - 1)V_D - V_{DD}$$

The minimum input voltage for the DC/DC converter plus the voltage drop across the steering diode,  $V_{SD}$ , restricts  $V_{MinD}$  to 9.4 V (i.e.,  $V_{MinD} = 9 + 0.38$ ). Substituting the appropriate values

$$9.4 \text{ V} = (N - 1) \times 1.14 - 0.38$$

and solving for N yields

$$N = 9.6 \approx 10$$

Now, determining the minimum discharge voltage for 10 cells at EOL

$$V_{MinD} = (10 - 1) \times 1.14 - 0.38 = 9.88 \text{ V}$$

This is above the 9.4 V minimum, therefore, 10 cells supply adequate voltage to compensate for the drop across the steering diode and meet the minimum voltage requirement of the DC/DC converter.

To determine the maximum charge voltage required from the solar array, consider the results of the transient thermal analysis shown in Figure 17. The temperature plot for an internal shelf in PANSAT indicates the temperature will have a nominal variation of  $15 \pm 1^\circ\text{C}$  (approximately  $60^\circ\text{F}$ ). This corresponds to battery charge voltage per cell,  $V_C$ , of 1.47 V [Ref. 24]. Also assuming that an open-circuit failure of one battery cell occurs while charging and that it is accommodated by four series-connected diodes connected in parallel with the failed cell as shown in Figure D.1.

The maximum allowable charge voltage is obtained from the equation

$$V_{MaxC} = V_C \times (N - 1) + 4 \times V_{DD}$$

Substituting the appropriate values

$$V_{MaxC} = 1.47 \times 9 + 4 \times 0.38 = 14.75 \text{ V}$$

Assuming a 0.38 V drop across the isolation diode, the solar array will supply approximately 14.82 V (15.2 - 0.38) to the bus. Additionally, when losses in the BCR circuitry are considered (assume to be approximately 0.7 V) it is apparent that the 14.8 V furnished by the bus is insufficient to meet the charge voltage of 14.43 V determined above. Therefore,

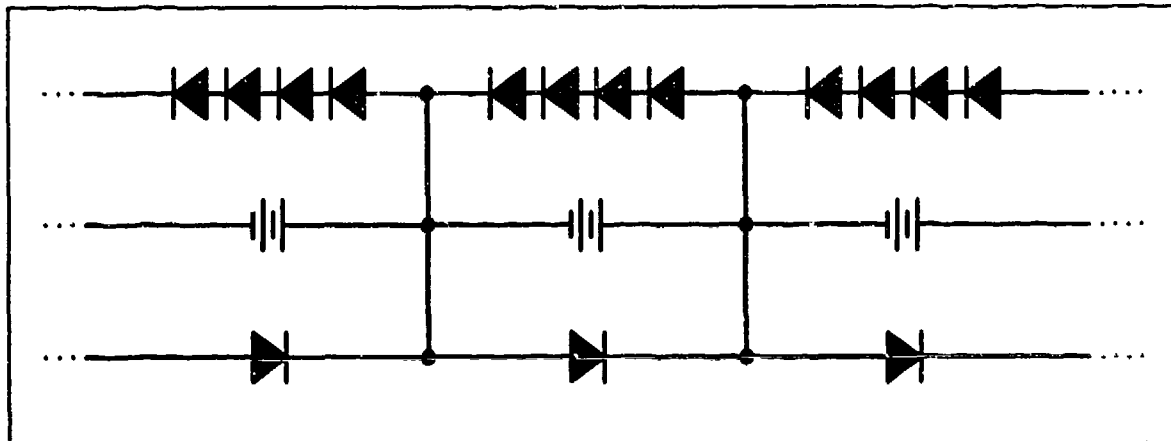


**Figure D.1.** Configuration of Battery Cells within Battery

the design procedure must disregard the case compensating for one open-circuit failure and use nine cells in series at this time, and reevaluate the design once a more thorough transient thermal analysis is complete to determine if an open-circuit failure can be accommodated.

With regard to the latter, consider again the equation

$$V_{\text{MaxC}} = V_C \times (N - 1) + 4 \times V_{\text{DB}}$$

except assume  $V_{\text{MaxC}} = 14.1 \text{ V}$  ( $14.8 - 0.7$ ), while  $N$  and  $V_{\text{DB}}$  remain at 10 and 0.38 V respectfully. Now solving for  $V_C$  yields a charge voltage per cell of 1.40 V, which equates to an internal temperature of  $80^\circ\text{F}$  ( $+26.6^\circ\text{C}$ ) [Ref. 24]. Therefore, the preliminary transient thermal analysis referred to above is well below  $80^\circ\text{F}$ , which is the upper limit on the manufacturer's recommended operating temperature [Ref. 24]. As a result, the design procedure will investigate the case where only nine cells are used and precautions to guard against the open-circuit failure case must be ignored.

#### **BATTERY CAPACITY**

For a battery with nine cells in series and assuming no open-circuit failure and at EOL, the minimum discharge voltage is

$$V_{\text{MinD}} = 9 \times 1.14 = 10.26 \text{ V}$$

As indicated in the proposed power budget, the DC/DC converter must be supplied with roughly 13.8 W of power at its input, to provide adequate dc power to the PANSAT subsystems. The battery must be able to supply power for an eclipse period of approximately 36 minutes (0.6 hours) as shown in Table A-1, Appendix A. The cell capacity of the battery,  $C$ , required for the previously mentioned specifications is given by

$$C = \frac{P \times T_e}{V_{\text{DB}} \times \text{DOD}}$$

Substituting the values  $P = 13.75 \text{ W}$ ,  $T_c = 0.6 \text{ hr}$ , and  $V_{\text{MinD}} = 10.26 \text{ V}$ , the capacity for a 10% and 25% DOD is approximately 8.0 Ah and 3.2 Ah, respectfully.

If adequate overcharge control is provided, charge rates of C/20 to C/2 work well for Ni-Cd batteries. Typical charge rates for Eagle Picher Aerospace Ni-Cd batteries are C/20 to C/6. Additionally, trickle charge rates of C/60 to C/100 are permissible if voltage control is utilized [Ref. 24]. Table D-1 lists the different currents associated with a variety of charge rates for both 10% and 25% DOD. The maximum voltage required to charge the batteries was determined above to be  $V_{\text{MaxC}} = 14.1 \text{ V}$ . Using this value in conjunction with the equation for the power required to charge the batteries

$$P_C = V_{\text{MaxC}} \times C/R$$

$P_C$  is calculated for the various charge rates, and is listed in Table D-1.

For PANSAT, the lengths of time for which the batteries will charge and discharge are essentially fixed such that

$$t_d = T_c$$

and

$$t_r = T - T_c$$

In addition, the amount of power available for charging the batteries is limited by the difference between the average power available from the solar arrays (from Table III, Chapter III) and the power required by the subsystems of PANSAT

$$P_i = P_{\text{sa}} - P_{\text{sys}} = 17.8 - 13.75 = 4.05 \text{ W}$$

As can be seen from Table D-1, there are five situations in which the DOD and charge rate require more power than is available.

**TABLE D-1. THE CURRENT AND POWER OUTPUT ASSOCIATED WITH THE RECOMMENDED CHARGE RATES FOR THE 8.0 AH AND 3.2 AH BATTERIES**

Charge Rate	Current		Power	
	10% DOD (8.0 Ah)	25% DOD (3.2 Ah)	10% DOD (8.0 Ah)	25% DOD (3.2 Ah)
C/100	80.0 mA	32.0 mA	1.13 W	0.45 W
C/60	133.3 mA	53.3 mA	1.88 W	0.75 W
C/20	400.0 mA	160.0 mA	5.64 W	2.26 W
C/6	1.3 A	533.3 mA	18.33 W	7.52 W
C/2	4.0 A	1.6 A	56.40 W	22.56 W

The relationship between the power available during the eclipse phase and the length of time associated with charging and discharging the battery is

$$P_d = \frac{t_r \times P_c \times \eta}{t_d}$$

Substituting the relationships for  $t_r$  and  $t_d$  given above, and conducting some algebraic manipulations leads to

$$P_d = \left( \frac{T}{T_e} - 1 \right) \times P_c \times \eta$$



Assuming a charge efficiency,  $\eta$ , of 90%, the amount of power required from the battery during eclipse, for the altitudes indicated, are given in Table D-2. Table D-2 also provides the ratio between orbital period and eclipse period associated with each altitude, as computed in Table A-1 in Appendix A.

**TABLE D-2. POWER AVAILABLE FROM BATTERY DURING ECLIPSE WITH RESPECT TO ALTITUDE**

Altitude	T/Te		Pc [W]	
	Solstice	Equinox	Solstice	Equinox
160	2.4	2.3	5.1	4.7
200	2.4	2.4	5.1	5.1
300	2.5	2.5	5.5	5.5
400	2.6	2.6	5.8	5.8
480	2.7	2.6	6.2	5.8
600	2.8	2.7	6.6	6.2
700	2.9	2.8	6.9	6.6
800	3	2.9	7.3	6.9

## LIST OF REFERENCES

1. Noble, M.L., *Preliminary Design of the PANSAT Electrical Power System*, Master's Thesis, Naval Postgraduate School, Monterey, California, June 1990.
2. "Petite Amateur Satellite (PANSAT) Preliminary Design Review," collection of view graphs presented at the PANSAT PDR, Naval Postgraduate School, Monterey, California, 27 April 1993.
3. Picholte, R. L., Schilling, D. L., and Milstein, L. B., *Spread-Spectrum Communication - A Tutorial*, v. COM-30, no.5, IEEE Transmission Communications, 1982.
4. Sakoda, D., Code (SP/Sd), (408) 656-2299 to Power Group Meeting Attendees, Subject: Power Group MTG Summary of 4 NOV 92, 4 November 1992.
5. Spectrolab, Inc., Report 629387, *Power Analysis - NPS*, by S. M. Missirian, 21 July 1993.
6. Jet Propulsion Laboratory Publication SP 43-38, *Solar Cell Array Design Handbook*, v.1, October 1976.
7. Rauschenbach, H. S., *Solar Cell Array Design Handbook*, Van Nostrand Reinhold Co., 1980.
8. Agrawal, B. N., *Design of Geosynchronous Spacecraft*, Prentice-Hall, Inc., 1986.
9. Tada, H.Y., Carter, J.R. Jr., Anspaugh, B.E., and Downing, R.E., *Solar Cell Radiation Handbook*, Jet Propulsion Laboratory, 1982.
10. Facsimile sent by Simone Missirian, Spectrolab, Inc., to the author, 8 June 1993.
11. Fahrenbruch, A.L., and Bube, R.H., *Fundamentals of Solar Cells*, Academic Press, Inc., 1983.
12. Bate, R. R., Mueller, D. D., White, J. E., *Fundamentals of Astrodynamics*, Dover Publications, Inc., 1971.
13. Telephone conversation between Craig Tooley, Goddard Space Flight Center, and the author, 1 September 1993.

14. Kraus, A.D., *Transient Thermal Analysis User's Manual*, Intercept Software, October 1985.
15. Missirian, S. M., Spectrolab, Inc., UNCLASSIFIED Letter to author, Subject: Performance Parameters for the K6700 Product, 10 August 1993.
16. Marsden, J. E., and Tromba, A. J., *Vector Calculus*, 3<sup>rd</sup> ed., W. H. Freeman and Co., 1988.
17. Chetty, P. R. K., *Satellite Technology and Its Applications*, TAB Books Inc., 1988.
18. Rashid, M.H., *Power Electronics: Circuits, Devices, and Applications*, Prentice-Hall, Inc., 1988.
19. Chetty, P. R. K., *Switch-Mode Power Supply Design*, TAB Books Inc., 1986.
20. Interview between D. Riggmaiden, System Specialist, Space Systems Academic Group, and the author, 3 November 1992.
21. Gates Energy Products, *Rechargeable Batteries Applications Handbook*, Reed Publishing (USA) Inc., 1992.
22. Barak, M., and others, *Electrochemical Power Sources Primary and Secondary Batteries*, The Institution of Electrical Engineers, 1980.
23. PANSAT Preliminary Design Review, 1992.
24. Facsimile sent by Dale Gordon, Eagle Picher, Electronics Division, to the author, 18 May 1993.
25. Telephone conversation between Jack Brill, Eagle-Picher Industries, Inc., and the author, 4 May 1993.

# INITIAL DISTRIBUTION LIST

	No. Copies
1. Defense Technical Information Center Cameron Station Alexandria, Virginia 22304-6145	2
2. Library, Code 52 Naval Postgraduate School Monterey, California 93943-5101	2
3. Chairman, Code EC Department of Electrical and Computer Engineering Naval Postgraduate School Monterey, California 93943-5121	1
4. Space Systems Academic Group, Code SP Naval Postgraduate School Monterey, California 93943-5110	1
5. Professor Rudolph Panholzer, Code EC/Pz Department of Electrical and Computer Engineering Naval Postgraduate School Monterey, California 93943-5121	1
6. Professor Robert Ashton, Code EC/Ah Department of Electrical and Computer Engineering Naval Postgraduate School Monterey, California 93943-5121	1
7. Professor Sherif Michael, Code EC/Mi Department of Electrical and Computer Engineering Naval Postgraduate School Monterey, California 93943-5121	1
8. LT Gregory F. Hand, USNR 4311 Norwalk Drive #T310 San Jose, California 95129-1756	3